

8-1-2024

# Evaluation of Electrochemical Corrosion, Electrodeposition, and Other Electroanalytical Methods as Investigative Forensic Techniques for Advancing Metal Substrate Analysis

Crystal C. Kitanovski

Follow this and additional works at: <https://digitalscholarship.unlv.edu/thesesdissertations>

 Part of the [Chemistry Commons](#)

---

## Repository Citation

Kitanovski, Crystal C., "Evaluation of Electrochemical Corrosion, Electrodeposition, and Other Electroanalytical Methods as Investigative Forensic Techniques for Advancing Metal Substrate Analysis" (2024). *UNLV Theses, Dissertations, Professional Papers, and Capstones*. 5130.  
<https://digitalscholarship.unlv.edu/thesesdissertations/5130>

This Dissertation is protected by copyright and/or related rights. It has been brought to you by Digital Scholarship@UNLV with permission from the rights-holder(s). You are free to use this Dissertation in any way that is permitted by the copyright and related rights legislation that applies to your use. For other uses you need to obtain permission from the rights-holder(s) directly, unless additional rights are indicated by a Creative Commons license in the record and/or on the work itself.

This Dissertation has been accepted for inclusion in UNLV Theses, Dissertations, Professional Papers, and Capstones by an authorized administrator of Digital Scholarship@UNLV. For more information, please contact [digitalscholarship@unlv.edu](mailto:digitalscholarship@unlv.edu).

EVALUATION OF ELECTROCHEMICAL CORROSION, ELECTRODEPOSITION AND  
OTHER ELECTROANALYTICAL METHODS AS INVESTIGATIVE FORENSIC  
TECHNIQUES FOR ADVANCING METAL SUBSTRATE ANALYSIS

By

Crystal C. Kitanovski

Bachelor of Science – Biochemistry  
University of Nevada, Las Vegas  
2020

A dissertation submitted in partial fulfillment  
of the requirements for the

Doctor of Philosophy – Chemistry

Department of Chemistry and Biochemistry  
College of Sciences  
The Graduate College

University of Nevada, Las Vegas  
August 2024

Copyright by Crystal C. Kitanovski, 2024

All Rights Reserved

**Dissertation Approval**

The Graduate College  
The University of Nevada, Las Vegas

June 6, 2024

This dissertation prepared by

Crystal C. Kitanovski

entitled

Evaluation of Electrochemical Corrosion, Electrodeposition, and Other Electroanalytical  
Methods as Investigative Forensic Techniques for Advancing Metal Substrate Analysis

is approved in partial fulfillment of the requirements for the degree of

Doctor of Philosophy – Chemistry  
Department of Chemistry and Biochemistry

David Hatchett, Ph.D.  
*Examination Committee Chair*

Clemens Heske, Ph.D.  
*Examination Committee Member*

Kenneth Czerwinski, Ph.D.  
*Examination Committee Member*

Cory Rusinek, Ph.D.  
Examination Committee Member

Dustin Hines, Ph.D.  
*Graduate College Faculty Representative*

Alyssa Crittenden, Ph.D.  
*Vice Provost for Graduate Education &  
Dean of the Graduate College*

## **Abstract**

Evaluation of Electrochemical Corrosion, Electrodeposition and  
Other Electroanalytical Methods as Investigative Forensic  
Techniques for Advancing Metal Substrate Analysis

By  
Crystal C. Kitanovski

Dr. David Hatchett, Examination Committee Chair  
Vice President of Research, Professor of Chemistry and Radiochemistry  
University of Nevada, Las Vegas

Friction ridge skin, bearing unique patterns of epidermal ridges commonly known as fingerprints, has served as a crucial tool for identification since ancient times, with its utilization dating back to Chinese culture around 221 B.C. Today, friction ridge skin impressions remain vital evidence in forensic investigations, aiding in the identification of suspects. While fingerprints, palm prints, and footprints can all serve as identifying markers, this dissertation focuses specifically on fingerprints, broadly classified as visible or latent. Latent fingerprints, though invisible to the naked eye, constitute the majority of prints collected from crime scenes, necessitating physical, chemical, or physicochemical processing for visualization.

Despite significant advancements in fingerprint development techniques, current methods often falter when applied to challenging substrates such as fired shell casings or submerged weapons. Electroanalytical methods, an underexplored avenue in latent fingerprint development, present a promising opportunity for innovative forensic investigation techniques. This dissertation surveys novel electroanalytical approaches aimed at enhancing the reliability and efficacy of latent fingerprint development.

The research begins by elucidating optimal electrolyte solutions through soak tests and open circuit potential (OCP) experiments. OCP measurements further provide corrosion potential values for various metal alloys, contributing to a comprehensive understanding of fingerprint resolution enhancement while preserving fingerprint integrity. Subsequent investigations employ potentiodynamic, potentiostatic, and galvanostatic corrosion methods to exploit the corrosion caused by components of eccrine secretions for targeted fingerprint enhancement. Experimental results are systematically analyzed and compared to determine the efficacy of each method in enhancing fingerprint resolution while preserving the integrity of the fingerprint itself. Additionally, inductively coupled plasma-optical emission spectroscopy (ICP-OES) is employed alongside linear sweep voltammetry (LSV) measurements to provide real-time corrosion analysis, enhancing the understanding of targeted corrosion enhancement.

Further exploration includes the investigation of electrodeposition and electroless deposition techniques for latent fingerprint enhancement, comparing their efficacy and preservation capabilities. Finally, a section in Chapter 6 discusses the potential reasons for the challenges in adopting these novel methods within forensic laboratories, such as budget constraints, staffing limitations, and rigorous quality assurance and legal admissibility standards.

This dissertation offers insights into novel electroanalytical methods for latent fingerprint development, addressing critical challenges faced by current forensic techniques. The findings hold significant implications for forensic science, paving the way for more efficient and accurate identification processes in forensic laboratories.

## Acknowledgements

To three people who have happily, selflessly, and without reservation, donated a substantial portion of their childhoods to science. It has been the greatest honor and privilege of my life to grow up raising you. Isaiah, you have spent 12 years holding me together with your tiny, and now quite large, hands. You raised me just as much as I raised you, teaching me more than I could ever teach you. You are my joy and my forever light, mój Sunshine, my permanent reminder that the best is yet to come. The four of us wouldn't have made it here without you. Genesis, you are my excitement, my enthusiasm, and the unrelenting love of science and learning I desperately needed to keep me going on the days I didn't think I could. I see the best parts of me in you, Princeska. The tenacity, the fire... and the stubbornness. Don't worry, you'll make good use of all three in this world. Jeremiah, my fearlessly wild child, my autistic superhero... everyone has disabilities, they're things we're not good at yet. Never let them outshine your *abilities*. You have taught me bravery in the face of absolutely every battle and how to last five years without sleep and not die (a superpower in and of itself).

I promise you all that everything you've so freely given up in helping your mama pursue this crazy dream of ours will be returned to you as limitless opportunities for happiness, fulfillment, and success in each of your futures. Every minute spent earning a doctorate was all for the three of you. You've all permanently lost the right to look at me and say "Mom, I can't do it."

Always remember... nothing worth having comes easy.

It always seems impossible until it's done.

## Table of Contents

|   |     |
|---|-----|
| Abstract .....  | iii |
| Acknowledgements .....  | v   |
| Table of Contents .....   | vi  |
| List of Tables .....  | ix  |
| List of Figures .....   | xi  |
| List of Equations .....   | xvi |
| Chapter 1: Introduction .....                                   | 1   |
| 1.1 Background and Literature Review .....                      | 2   |
| 1.2 Fingerprints and Their Role in Identification .....         | 6   |
| 1.3 Corrosion and Electroanalytical Chemistry in Forensics..... | 10  |
| 1.4 Research Hypothesis and Project Description .....           | 14  |
| Chapter 2: Experimental Methods .....                           | 17  |
| 2.1 Materials .....   | 17  |
| 2.2 Sample Preparation .....                                    | 21  |
| 2.3 Electrochemical Methods and Instrumentation .....           | 23  |
| 2.3.1 Open Circuit Potential.....                               | 27  |
| 2.3.2 Linear Sweep Voltammetry (LSV).....                       | 31  |
| 2.3.3 Tafel Analysis .....                                      | 33  |
| 2.3.4 Electrodeposition .....                                   | 40  |
| 2.3.5 Electroless Deposition .....                              | 43  |



|   |     |
|---|-----|
| 2.4 Inductively Coupled Plasma – Optical Emission Spectroscopy .....  | 44  |
| 2.5 Grading Fingerprint Development .....   | 46  |
| Chapter 3: Targeted Corrosion Enhancement of Latent Fingerprints.....   | 48  |
| 3.1 Introduction.....   | 48  |
| 3.2 Materials and Methods.....  | 50  |
| 3.3 Results and Discussion .....  | 52  |
| 3.3.1 Electrolyte Solution Soak Tests .....   | 53  |
| 3.3.2 Open Circuit Potential Studies.....   | 61  |
| 3.3.3 Dissolved Oxygen Study.....   | 66  |
| 3.3.4 Potentiodynamic Corrosion Studies.....  | 68  |
| 3.3.5 Potentiostatic Corrosion Studies .....  | 82  |
| 3.3.6 Galvanostatic Corrosion Studies.....  | 85  |
| 3.4 Conclusion and Future Work .....  | 88  |
| Chapter 4: A Qualitative Analysis of Corrosion Processes in Alloys Commonly Encountered in<br>Forensic Investigations Using Inductively Coupled Plasma–Optical Emission Spectroscopy .... | 98  |
| 4.1 Introduction.....   | 98  |
| 4.2 Materials and Methods.....  | 110 |
| 4.3 Results and Analysis .....  | 113 |
| 4.3.1 6061-Aluminum Alloy ICP-OES Results .....   | 113 |
| 4.3.2 C260 Brass ICP-OES Results .....  | 122 |
| 4.3.3 Low-carbon Steel ICP-OES Results .....  | 128 |

|  |     |
|--|-----|
| 4.3.4 400-Nickel alloy ICP-OES Results.....  | 134 |
| 4.4 Conclusions and Future Work .....  | 143 |
| Chapter 5: Electrodeposition and Other Electroanalytical Methods as Forensic Investigative<br>Techniques ..... | 146 |
| 5.1 Introduction.....  | 146 |
| 5.2 Materials and Methods.....   | 147 |
| 5.3 Results and Analysis .....   | 149 |
| 5.3.1 Electrodeposition of Gold .....  | 149 |
| 5.3.2 Electrodeposition of Silver .....  | 155 |
| 5.3.3 Electroless Deposition .....   | 163 |
| 5.4 Conclusions and Future Work .....  | 165 |
| Chapter 6: Comprehensive Conclusions and Synthesis of Research Findings.....                                   | 168 |
| 6.1 Overview.....  | 168 |
| 6.2 Analysis of Methods and Results.....   | 168 |
| 6.3 Summary of Novel Contributions.....  | 170 |
| 6.4 Integration of Forensic Education and Research .....   | 173 |
| 6.5 Future Work .....  | 178 |
| References.....  | 180 |
| Curriculum Vitae .....   | 188 |

## List of Tables

|  |     |
|--|-----|
| Table 1: Percentage compositions for all metal substrates purchased through McMaster-Carr...   | 18  |
| Table 2: Standard element solutions utilized in calibration curves for each metal substrate .....  | 20  |
| Table 3: Bandey grading system for fingerprint development .....   | 47  |
| Table 4: Electrolyte solution soak test results.....   | 60  |
| Table 5: Electrolyte solution and electrolyte concentration effects on corrosion potential with potentials measured versus Ag/AgCl reference electrode .....   | 65  |
| Table 6: Results of dissolved oxygen study where metal substrates exposed to ambient air, and those kept in an environment free of dissolved oxygen, were compared to elucidate the effects on standard deviation amongst trials. Potentials measured versus Ag/AgCl reference electrode ..... | 67  |
| Table 7: Average fingerprint development grades on four substrates .....   | 74  |
| Table 8: Tafel analysis yielding corrosion potential, corrosion current, cathodic tafel coefficient, and anodic tafel coefficient for both C260 brass and low-carbon steel substrates .....  | 81  |
| Table 9: Average development grades of ultra-formable C260 brass and low-carbon steel after potentiostatic corrosion. Each sample was held at the listed potential for 5 minutes.....  | 84  |
| Table 10: Average development grades of ultra-formable C260 brass and low-carbon steel after galvanostatic corrosion. Each sample was held at the listed potential for 5 minutes .....   | 87  |
| Table 11: List of reduction potentials relevant to the most abundant elements in each alloy ....   | 100 |
| Table 12: Expected ions in TEA experiments based on standard reduction potentials and Pourbaix diagrams .....  | 109 |
| Table 13: ICP-OES measurement results of three trials of fingerprinted 6061-Aluminum alloy samples.....  | 114 |

|   |     |
|---|-----|
| Table 14: ICP-OES measurement results of three trials of non-fingerprinted 6061-Aluminum alloy samples.....   | 117 |
| Table 15: ICP-OES measurement results of three trials of fingerprinted C260 brass samples ..  | 122 |
| Table 16: ICP-OES measurement results of three trials of non-fingerprinted C260 brass samples .....   | 124 |
| Table 17: ICP-OES measurement results of three trials of fingerprinted low-carbon steel samples .....   | 128 |
| Table 18: ICP-OES measurement results of three trials of non-fingerprinted low-carbon steel samples.....  | 131 |
| Table 19: ICP-OES measurement results of three trials of fingerprinted 400-Nickel alloy samples .....   | 135 |
| Table 20: ICP-OES measurement results of three trials of non-fingerprinted 400-Nickel alloy samples.....  | 138 |
| Table 21: Electrodeposition of gold onto C260 brass substrates and the average change in fingerprint grade for various applied potentials and time frames .....                   | 150 |
| Table 22: Electrodeposition of gold onto low-carbon steel substrates and the average change in fingerprint grade for various applied potentials and time frames .....             | 153 |
| Table 23: Electrodeposition of silver onto C260 brass substrates and the average change in fingerprint grade for various applied potentials and time frames .....                 | 158 |
| Table 24: Average change in fingerprint grade resulting from electrodeposition of silver onto low-carbon steel substrates for various applied potentials and lengths of time..... | 161 |

## List of Figures

|   |    |
|---|----|
| Figure 1: Flow chart for processing a latent fingerprint on a porous surface. Note that visual inspection, laser or alternate light source, and iodine fuming are all classified as non-destructive processing methods and come first in the sequence ..... | 8  |
| Figure 2: Flow chart for processing a latent fingerprint on a non-porous surface. Note that Vacuum Metal Deposition is not widely used .....  | 9  |
| Figure 3: Image of Metrohm flat platform electrochemical cell (left) and schematic of the orientation of three electrodes within the Metrohm flat platform cell (right).....  | 19 |
| Figure 4: Image of metal samples inside infrared sauna immediately after application of eccrine fingerprint by donor .....  | 22 |
| Figure 5: Flow chart illustrating all procedural steps in preparing, generating, applying, containing, and aging samples .....  | 23 |
| Figure 6: Generic diagram of potential vs time obtained during open circuit potential measurements. This diagram also displays what would be considered capacitive current generated during equilibration of substrate and electrolyte solution .....       | 29 |
| Figure 7: Generic diagram of current vs potential obtained during LSV measurements .....  | 32 |
| Figure 8: Resulting Tafel plot after the logarithm of the y-axis of the LSV voltammogram is taken .....   | 34 |
| Figure 9: Images of each of the four substrates, without fingerprints applied, after soaking for 24 hours in each of the four listed electrolyte solutions. Note that Ultrapure H <sub>2</sub> O is the control for this experiment.....                    | 54 |

Figure 10: Images of each of the four substrates, with eccrine fingerprints applied, after soaking for 24 hours in each of the four listed electrolyte solutions. Note that Ultrapure H<sub>2</sub>O is the control for this experiment..... 56

Figure 11: Images of each of the four substrates, with sebaceous fingerprints applied, after soaking for 24 hours in each of the four listed electrolyte solutions. Note that Ultrapure H<sub>2</sub>O is the control for this experiment..... 57

Figure 12: Open circuit potential graph with each line representing the average of 10 trials of each respective substrate in varying concentrations (0.1M H<sub>2</sub>SO<sub>4</sub> and 0.5M H<sub>2</sub>SO<sub>4</sub>) of sulfuric acid..... 63

Figure 13: Open circuit potential graph with each line representing the average of 10 trials of each respective substrate in either 0.1M KCl or 0.1M Na<sub>2</sub>SO<sub>4</sub>..... 63

Figure 14: Before and after images of three out of five 6061-Aluminum alloy samples subject to potentiodynamic corrosion via linear sweep voltammetry ranging from + 250 mV to – 250 mV versus the open circuit potential of the substrate ..... 69

Figure 15: Before and after images of three out of five C260 brass samples subject to potentiodynamic corrosion via linear sweep voltammetry ranging from + 250 mV to – 250 mV versus the open circuit potential of the substrate ..... 70

Figure 16: Before and after images of three out of five low-carbon steel samples subject to potentiodynamic corrosion via linear sweep voltammetry ranging from + 250 mV to – 250 mV versus the open circuit potential of the substrate ..... 71

Figure 17: Before and after images of three out of five 400-Nickel alloy samples subject to potentiodynamic corrosion via linear sweep voltammetry ranging from + 250 mV to – 250 mV versus the open circuit potential of the substrate ..... 72

Figure 18: Linear sweep voltammogram and resulting Tafel plot overlay for three trials of 6061-Aluminum alloy in 0.1M H<sub>2</sub>SO<sub>4</sub> electrolyte solution for the commencement of potentiodynamic corrosion ..... 75

Figure 19: Linear sweep voltammograms and resulting Tafel plot overlay for three trials of C260 brass in 0.1M H<sub>2</sub>SO<sub>4</sub> electrolyte solution for the commencement of potentiodynamic corrosion 76

Figure 20: Linear sweep voltammograms and resulting Tafel plot overlay for three trials of low-carbon steel in 0.1M Na<sub>2</sub>SO<sub>4</sub> electrolyte solution for the commencement of potentiodynamic corrosion ..... 77

Figure 21: Linear sweep voltammogram and resulting Tafel plot overlay for three trials of 400-Nickel alloy in 0.1M H<sub>2</sub>SO<sub>4</sub> electrolyte solution for the commencement of potentiodynamic corrosion ..... 79

Figure 22: Pourbaix diagram for aluminum corresponding to 6061-Aluminum alloy ..... 106

Figure 23: Pourbaix diagram for copper and zinc corresponding to ultra formable C260 brass 106

Figure 24: Pourbaix diagram for iron corresponding to low-carbon steel..... 107

Figure 25: Pourbaix diagram for nickel and copper corresponding to 400-Nickel alloy ..... 107

Figure 26: Tafel plot schematic with labeled aliquot removal points. The first 5mL aliquot is removed at point one, the second at point two, the third at point three, the fourth at point four, and the fifth at point five on the diagram..... 112

Figure 27: A graph displaying the ICP-OES results of fingerprinted 6061-Aluminum alloy samples. The concentrations of Cu, Fe, Al, and Cr are displayed for each corresponding aliquot taken from the bulk solution over the course of the applied linear potential sweep..... 116

Figure 28: A graph displaying the ICP-OES results of non-fingerprinted 6061-Aluminum alloy samples. The concentrations of Cu, Fe, Al, and Cr are displayed for each corresponding aliquot taken from the bulk solution over the course of the applied linear potential..... 118

Figure 29: A graph displaying the ICP-OES results of fingerprinted C260 Brass samples. The concentrations of Cu, Zn, and Fe are displayed for each corresponding aliquot taken from the bulk solution over the course of the applied linear potential sweep ..... 123

Figure 30: A graph displaying the ICP-OES results of non-fingerprinted C260 Brass samples. The concentrations of Cu, Zn, and Fe are displayed for each corresponding aliquot taken from the bulk solution over the course of the applied linear potential sweep ..... 126

Figure 31: A graph displaying the ICP-OES results of fingerprinted low-carbon samples. The concentrations of Fe and Mn are displayed for each corresponding aliquot taken from the bulk solution over the course of the applied linear potential sweep ..... 129

Figure 32: A graph displaying the ICP-OES results of non-fingerprinted low-carbon samples. The concentrations of Fe and Mn are displayed for each corresponding aliquot taken from the bulk solution over the course of the applied linear potential sweep ..... 132

Figure 33: A graph displaying the ICP-OES results of fingerprinted 400-Nickel alloy samples. The concentration of Ni is displayed for each corresponding aliquot taken from the bulk solution over the course of the applied linear potential sweep ..... 136

Figure 34: A graph displaying the ICP-OES results of fingerprinted 400-Nickel alloy samples. The concentrations of Cu, Fe, and Mn are displayed for each corresponding aliquot taken from the bulk solution over the course of the applied linear potential sweep ..... 137



Figure 35: A graph displaying the ICP-OES results of non-fingerprinted 400-Nickel alloy samples. The concentration of Ni is displayed for each corresponding aliquot taken from the bulk solution over the course of the applied linear potential sweep ..... 139

Figure 36: A graph displaying the ICP-OES results of non-fingerprinted 400-Nickel alloy samples. The concentrations of Cu, Fe, and Mn are displayed for each corresponding aliquot taken from the bulk solution over the course of the applied linear potential sweep..... 140

Figure 37: One of three trials of gold electrodeposited onto C260 brass using an applied potential of 4V for a total of 20 seconds..... 151

Figure 38: One of three trials of Au electrodeposited onto C260 brass using an applied potential of 4V for a total of 20 seconds. Images are taken before electrodeposition, after electrodeposition whilst still in solution, after electrodeposition solution has been poured off and the sample rinsed with ultrapure water, and lastly, after the sample has been removed from the flat platform cell and dried with a KimWipe..... 152

Figure 39: A and B represent before and after images of two of three trials of low-carbon steel samples subjected to electrodeposition of gold with an applied potential of 3V for 60 seconds. C represents before and after images of one of three trials subjected to an applied potential of 3V for 90 seconds ..... 154

Figure 40: One of three trials of silver electrodeposited onto C260 brass held at an applied potential of 1V for 30 seconds ..... 159

Figure 41: Images from two separate low-carbon steel trials subjected to electrodeposition of silver. Image A was taken looking down into the cell after 5 seconds of the measurement with the sample still submerged in solution. Image B is a separate trial that was completed, the sample was removed from the cell, rinsed and dried with a KimWipe ..... 162

## List of Equations

|   |    |
|---|----|
| Equation 1: Anodic oxidation reactions where M represents a metal and z represents the number of electrons.....                               | 3  |
| Equation 2: Corresponding cathodic reduction reaction.....  | 3  |
| Equation 3: Hydrochloric acid formed through the ion products of equations 1 and 2.....   | 3  |
| Equation 4: Electrochemical potential energy of an electron .....   | 4  |
| Equation 5: Work function of the metal substrate being examined by Scanning Kelvin Probe.<br>Also referred to as the electric potential ..... | 5  |
| Equation 6: Volta potential, or contact potential difference, measured by the capacitor .....   | 5  |
| Equation 7: Gibbs free energy equation.....   | 11 |
| Equation 8: Gibbs free energy equation under standard conditions .....  | 24 |
| Equation 9: Relating Gibbs free energy across conditions .....  | 24 |
| Equation 10: Integration of Gibbs free energy equations .....   | 24 |
| Equation 11: Nernst equation.....   | 24 |
| Equation 12: Nernst equation at standard temperature (298K) .....   | 25 |
| Equation 13: Oxidation reaction of iron .....   | 25 |
| Equation 14: Reduction of dissolved oxygen .....  | 26 |
| Equation 15: Formation of iron hydroxide .....  | 26 |
| Equation 16: Overpotential equation .....   | 26 |
| Equation 17: Butler-Volmer equation.....  | 35 |
| Equation 18: Total current density is equal to the sum of the anodic and cathodic current densities.....                                      | 36 |

|  |     |
|--|-----|
| Equation 19: Corrosion current density equation representing the corrosion rate per unit area of the metal surface .....   | 37  |
| Equation 20: Butler-Volmer equation (anodic reaction dominant) .....   | 38  |
| Equation 21: Tafel equation (anodic dominant) .....  | 38  |
| Equation 22: Tafel coefficient (anodic dominant) .....   | 38  |
| Equation 23: Wagner-Traud equation.....  | 39  |
| Equation 24: Wagner-Traud anodic tafel coefficient.....  | 39  |
| Equation 25: Wagner-Traud Cathodic Tafel Coefficient.....  | 40  |
| Equation 26: Faraday's first law of electrolysis where Q represents electric charge, F is Faraday's constant, M is the molar mass of a given material and z represents the electrons transferred per ion ..... | 41  |
| Equation 27: Boltzmann distribution equation describing the ratio of the number of atoms in an excited state $N_j$ to the number of atoms in the ground state $N_0$ .....                                      | 45  |
| Equation 28: Reduction of aluminum oxide in the formation of a protective passive oxide layer .....  | 102 |
| Equation 29: The formation of iron (III) oxide in aqueous conditions.....  | 103 |
| Equation 30: The dissolution reaction of iron in acidic conditions .....   | 103 |
| Equation 31: The formation of zinc oxide .....   | 103 |
| Equation 32: The dissolution of zinc oxide .....   | 104 |
| Equation 33: The formation of copper (I) oxide or cuprous oxide .....  | 104 |
| Equation 34: The formation of copper (II) oxide or cupric oxide .....  | 104 |
| Equation 35: The formation of nickel (II) oxide.....   | 104 |

Equation 36: Conversion of aluminum corrosion potential vs. SHE to reflect the value vs. Ag/AgCl..... 114

Equation 37: The formation of soluble iron chloride complexes ..... 130

Equation 38: Disruption of nickel (II) oxide layer by exposure to sodium borohydride forming nickel borides on the surface of the metal alloy substrate ..... 141

Equation 39: Corrosion of nickel through the removal of nickel borides formed on the surface.....141

Equation 40: Disruption of nickel (II) oxide layer by exposure to nitric acid ..... 142

Equation 41: Corrosion of nickel after destruction of nickel (II) oxide layer ..... 142

## Chapter 1: Introduction

The recovery of latent fingerprints on fired cartridge casings and other metal substrates subjected to extreme or otherwise harsh conditions is extremely low [1], [2], [3]. Through interviews conducted with leaders from forensic laboratories at both the state and federal levels, the recovery rate for latent fingerprints on fired cartridge cases is less than 1% [4]. The need for novel fingerprint development methods that can yield success in these cases cannot be overstated, which led to three consecutive research fellowships through Oak Ridge Institute for Science and Education (ORISE) with the Department of Homeland Security – United States Secret Service Forensic Services Division (DHS-USSS). This research aims to explore novel approaches, mainly focusing on electrochemical corrosion and other electroanalytical methods, to enhance latent fingerprint visualization on challenging substrates and improve the low recovery rate.

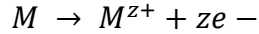
The vast majority of successful, widely used latent fingerprint development techniques today and research in developing novel latent fingerprint development techniques focus on chemical reactions between organic or inorganic fingerprint residue components, the surface it has been deposited on, and a reagent. Naturally, this fails when insufficient residue to initiate and sustain the chemical reaction such that the fingerprint develops. This has created increased interest in latent fingerprint development techniques that exploit corrosion reactions of eccrine secretion components and metal substrates instead of relying solely on the presence of sufficient fingerprint residue [5], [6], [7].

This chapter is structured into four main subcategories to provide a comprehensive overview of the research landscape: background and literature review, fingerprints and their role in identification, corrosion and electroanalytical chemistry in forensics, and finally, research hypothesis and project description.

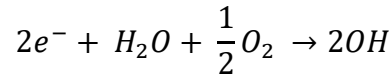
## **1.1 Background and Literature Review**

Recent literature underscores the pressing need for improved fingerprint development techniques, especially in cases involving substrates exposed to harsh conditions. A comprehensive review of existing methods highlights the limitations of traditional approaches and emphasizes the potential of electrochemical and electroanalytical methods in overcoming these challenges. By integrating recent advancements and historical context, this research seeks to contribute to the evolving landscape of forensic fingerprint analysis.

In 2008, Bond and Phil explored the interactions between latent fingerprints and metal substrates, subjecting them to intense heat of 600°C via a propane gas burner to exploit electrochemical corrosion reactions [8]. Successful fingerprint development was achieved through thermal visualization, indicating that the duration between fingerprint deposition and heat exposure did not significantly affect enhancement. Bond proposed that chloride ions in eccrine secretions catalyze two corrosion reactions, leading to fingerprint development via pitting corrosion:

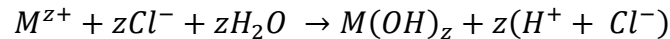


Equation 1: Anodic oxidation reactions where M represents a metal and z represents the number of electrons



Equation 2: Corresponding cathodic reduction reaction

Most commonly, the ion products would combine to form  $M(OH)_z$ , but Bond mentions that current density at the anode can cause an aggregation of metal ions. The positive charge held by such ions then attracts negatively charged chloride ions which can lead to autocatalytic reactions forming hydrochloric acid.



Equation 3: Hydrochloric acid formed through the ion products of equations 1 and 2

Bond states that this leads to pitting corrosion, specifically corresponding to fingerprint residue deposition, and thus, generating a developed fingerprint. Additionally, Bond noted that higher chloride ion concentrations in fingerprint residue correlated with greater enhancement through thermal visualization.

In a subsequent study, Bond et al. (2009) re-examined four spent cartridge casings recovered 14 years prior, heating them to 700°C to reveal faint fingerprint ridge lines [9]. Further experimentation involving an applied potential and conducting carbon powder showed limited improvement, suggesting that heat alone was sufficient for enhancing corrosion and fingerprint visibility.

Wightman and O'Connor explored thermal visualization using an electric furnace to heat brass, aluminum, and stainless-steel samples across various temperatures between 180-600°C, revealing varying degrees of fingerprint development [10]. They suggested that oxidation rates might influence development and questioned the validity of Bond's hydrochloric acid formation model at higher temperatures.

In another study, Wightman et al. investigated thermal oxidation and subsequent oxide film generation using ammonium sulfide, yielding inconclusive results regarding corrosion mechanisms [11]. While confirming the efficacy of heat to catalyze electrochemical corrosion reactions in fingerprint development, this study did not elucidate the precise role of passive oxide layers on different metals.

Williams et al. used a Scanning Kelvin Microprobe for successful fingerprint visualization [12]. This instrument measures changes in the Volta potential difference between a metal substrate and a probe that is slowly moved across its surface. Contact between the metal substrate and probe causes equilibration of Fermi levels via electron drift from the metal with the higher Fermi level to that of the lower Fermi level [13]. The energy requirement for each electron to move from one phase to another, is represented by the equation for the electrochemical potential energy of an electron:

$$\bar{\mu} = \mu + zF\Phi$$

Equation 4: Electrochemical potential energy of an electron

In this equation,  $\bar{\mu}$  represents the electrochemical potential energy of an electron or the work needed to transfer one electron,  $\mu$  represents chemical potential of an electron,  $z$  is the



valence,  $F$  is Faraday's constant and  $\Phi$  represents the work function [14]. The equilibration of electrons, or their movement from higher to lower Fermi levels, creates a difference in the work functions of the metal substrate and probe.

$$\Phi_m = -\mu + eX^m$$

Equation 5: Work function of the metal substrate being examined by Scanning Kelvin Probe. Also referred to as the electric potential

Within the work function of the metal substrate ( $\Phi_m$ ),  $\mu$  represents the same chemical potential of an electron seen in Equation 4,  $e$  the electron, and  $X^m$  is the potential drop between the interface of the metal substrate surface and vacuum air [15]. This equation describes the electric work required to transfer a charge from a reference point to a different point in space. Differences in the work functions, or the electric potentials, of the metal substrate and probe material yield a proportional contact potential difference, the Volta potential, which is measured by the capacitor.

$$\Delta V = \frac{\Phi_m - \Phi_{probe}}{e}$$

Equation 6: Volta potential, or contact potential difference, measured by the capacitor

The moving probe continuously reads the corrosion of the metal substrate and the resulting Volta potential difference to create an image of the fingerprint. Several years later, Dafydd et al. expanded on this work by incorporating Vacuum Metal Deposition (VMD), achieving improved results albeit with increased time and cost requirements [16].

Beyond thermal visualization, electroanalytical methods such as conductive polymer films and microfluidic devices have shown promise in suspect identification. Beresford and Hillman deposited polyaniline films electrochemically onto sebaceous fingerprints, generating negative fingerprints due to repulsion from sebaceous components [17]. However, the study focuses exclusively on fingerprints with sebaceous components constituting the majority where the repulsion from those sebaceous components is responsible for generating the negative fingerprint. Sapstead et al. conducted a study where pyrrole (Py) and 3,4-ethylenedioxythiophene (EDOT) were electrochemically deposited onto stainless steel, forming copolymer films to develop latent fingerprints [18]. Again, this study only focused on fingerprints with sebaceous components comprising the majority, thus generating the negative fingerprints visualized. In 2003, Valussi and Marshall et al. utilized microfluidic systems to analyze amino acids present in fingerprint residue, providing valuable suspect trait information [19], [20].

These examples underscore the potential of electrochemical and electroanalytical methods in forensic science, not only for fingerprint development but also for suspect identification and trait analysis, contributing to the advancement of forensic techniques and their efficacy.

## **1.2 Fingerprints and Their Role in Identification**

Friction ridge skin displays unique patterns of epidermal ridges, affected by growth in utero, on the palms, fingers, and soles of the feet [21]. Epidermal ridge patterning is believed to form near the 10<sup>th</sup> week of pregnancy, with the undulation of the epidermis generating the primary ridges that lead to what is commonly referred to as the fingerprint [22], [23]. Since the

19th century, fingerprints have been accepted as an appropriate means of positively identifying those suspected of committing a crime [24]. This logic rests entirely on the persistence and uniqueness of friction ridge skin, which solidifies the understanding that no two can ever be the same [25], [26], [27].

Fingerprints, in the form of residue attached to the outermost layer of the epidermis at a given time, are deposited when contact is made between friction ridge skin and a substrate. At the crime scene, fingerprints may be found on various pieces of evidence. These fingerprints come in two forms: visible and latent. Visible fingerprints are imaged and used for comparison purposes. In forensic fingerprint analysis, "comparison" refers to the systematic process of scrutinizing a recovered fingerprint (latent print) and comparing it to a known set of fingerprints (exemplars) to determine if there is a match or correspondence between them. This process is crucial for identifying individuals associated with a crime scene or piece of evidence.

Latent fingerprints, however, require additional processing steps before visualization and comparison are possible. Fingerprint residue composition and substrate surface dictate appropriate processing methods. Fingerprint residue composition can be broadly classified as either eccrine (aqueous-based) or sebaceous (organic-based). Surfaces are typically classified as either porous or non-porous.

Processing of latent fingerprints begins with a visual inspection to discern surface type and fingerprint composition which are the cornerstones of the decision-making process in terms of what steps will come next. This is followed by inspection with an appropriate light source or laser. Both visual inspection and inspection with light sources and lasers constitute non-destructive methods, which can be defined as methods that do not change the fingerprint residue, thus allowing for other processing methods to be conducted as well. Non-destructive methods

will always come before destructive methods, or those that do damage or cause a chemical change in the fingerprint residue, in any latent fingerprint processing sequence [28].

When presented with a porous surface, Ninhydrin has been successfully used to develop eccrine fingerprints since 1954 [29], [30]. Because of its success, several analogs were created and explored. 1,8-diazafluoren-9-one (DFO), though first synthesized in 1950, was not used as a fingerprint reagent until 1990. Two unique advantages of DFO are its higher sensitivity and its ability to be used sequentially with Ninhydrin to yield an even larger number of developed fingerprints than either compound alone [28]. These compounds react with amino acids in the aqueous, or water-soluble, portions of fingerprint residue [31], [32]. Physical developers have been successfully used since the 1970s, reacting with proteins in the fingerprint residue [28]. Other compounds like Oil Red O react with fatty acids in the organic, non-aqueous residue components [33]. According to the Processing Guide for Developing Latent Prints, published by the Federal Bureau of Investigation, the flow chart for processing a latent fingerprint on a porous surface is as follows [34]:



Figure 1: Flow chart for processing a latent fingerprint on a porous surface. Note that visual inspection, laser or alternate light source, and iodine fuming are all classified as non-destructive processing methods and come first in the sequence

For non-porous surfaces, the staple in many forensic laboratories has been cyanoacrylate “superglue” fuming since it was found to develop latent fingerprints in the 1970s successfully [35]. Cyanoacrylate fuming can utilize amines and carboxylic groups as initiators in its chemical reaction making it effective for eccrine and sebaceous fingerprint residue components [36]. Cyanoacrylate ester monomers bond to either residue component as an initiator, then bond with another monomer. The dimer then bonds with another monomer, and thus, polymerization occurs. This generates a white, opaque three-dimensional fingerprint on the substrate surface. Cyanoacrylate fuming can be reinitiated again to develop fingerprints further if necessary. It is worth mentioning that the generated fingerprints are subject to degradation as they age, with eccrine fingerprints degrading more rapidly than sebaceous [28]. The Processing Guide for Developing Latent Prints provides the following flow chart for processing a latent fingerprint on a porous surface [34]:

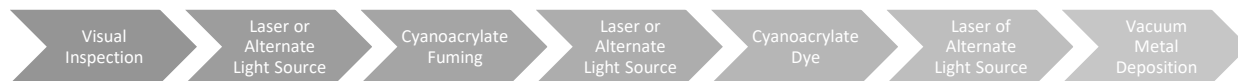


Figure 2: Flow chart for processing a latent fingerprint on a non-porous surface. Note that Vacuum Metal Deposition is not widely used

Vacuum metal deposition (VMD) was first investigated as a fingerprint development technique in the 1960s, implemented as a fingerprint development technique in the United Kingdom during the 1970s and about 20 years later in the United States [37], [38]. Deposition of

a thin gold film is the first step in the process. However, uniformity of the thin gold film is subject to the composition of fingerprint residue. Higher levels of stearic acid and other fatty acids cause the gold atoms to be absorbed into the residue, thus leaving a discontinuous layer of gold that covers the substrate surface and not the fingerprint itself [28], [39]. Following the deposition of gold, a thin layer of zinc is added which preferentially deposits on the previously formed agglomerates of gold. Due to variations in residue composition, both regularly developed and reverse-developed, or negative, fingerprints have been generated with this technique. Other development methods were found to be more successful on porous substrates, but VMD yielded superior fingerprint development on non-porous substrates, especially plastic bags and evidence subjected to water or moisture [28], [40]. VMD faces difficulties with widespread implementation due to the cost associated with instrumentation, operation, and staff training.

### **1.3 Corrosion and Electroanalytical Chemistry in Forensics**

The exploration of corrosion-based methods in forensic fingerprint analysis arises from the necessity to address cases where traditional fingerprint development techniques fail due to the absence of residue. Particularly challenging are scenarios involving firearms, weapons, shell casings, or explosive device components, which endure harsh conditions rendering conventional development and visualization methods ineffective [41]. The fingerprint residue that is necessary for Ninhydrin, cyanoacrylate fuming, VMD and most other processing methods to be successful is almost absent or absent entirely in these cases. What is not absent, however, is the corrosion caused by electrochemical reactions between eccrine sweat components and the metal substrates.

Corrosion is the deterioration of a metal due to interactions with its environment that cause thermodynamic instability [42]. This occurs under oxidizing conditions. Corrosion occurs through electrochemical reactions where at least one species present undergoes a change in valence electrons through oxidation reduction reactions. There are four basic requirements for corrosion of a metal to take place. There must be an anodic site, a cathodic site, ionic conduction between the anode and cathode, and electron conduction between the anode and cathode [42]. For the purposes of this dissertation, the four types of metal substrates being characterized constitute the anodic site, cathodic site, and the electron conduction between the anode and cathode. The only remaining requirement, ionic conduction between the anode and cathode, is accomplished by an electrolyte, often water. If the metal substrate in question is either submerged in water or exposed to air, which contains some level of humidity, these two environments would constitute oxidizing conditions whereby the standard reduction potential of the material, governed by thermodynamics, is exceeded.

Alternatively, if a small amount of eccrine sweat, largely comprised of water, is deposited on a metal substrate, these droplets would constitute the electrolyte and corrosion has been shown to occur under these oxidizing conditions [43]. The spontaneity of the corrosion reaction between eccrine sweat components and a metal substrate is dictated by the change in Gibbs free energy of the reaction:

$$\Delta G = -nFE$$

Equation 7: Gibbs free energy equation

In this reaction,  $\Delta G$  represents the change in free energy in Joules per mole,  $n$  represents the number of moles of electrons,  $F$  is Faraday's constant ( $\cong 96,485 \text{ J}/(\text{V} \cdot \text{mol } e^-)$ ), and  $E_{cell}$  is the cell potential in Volts. For a reaction to spontaneously occur, the value of  $E$  must be positive, and thus the value for  $\Delta G$  negative, indicating that energy, or work, is able to be done by the system. In this case, a negative value of  $\Delta G$  would indicate a spontaneous corrosion reaction between the eccrine sweat components and the metal substrate. The magnitude of  $\Delta G$  corresponds to the magnitude of the expected electrochemical corrosion reaction.

Eccrine droplets in fingerprint residue deposited on metal surfaces create small, discrete areas where electrochemical corrosion reactions begin to occur. The metal substrate constitutes the anode, cathode, and electronic conduction required for corrosion to occur. The fourth requirement, ionic conduction, is established by the fingerprint residue [42]. It has been well-documented that fingerprint residue corrodes metal surfaces [43]. The aggressive nature of chloride ions in fingerprint residue breaks down passivation layers and triggers pitting corrosion, a type of localized corrosion [44], [45]. Pitting corrosion is aptly named for the autocatalytic pits that continue to grow downward underneath fingerprint residue droplets where the local concentration of chloride ions is high [46]. The downward growth of these pits etches the fingerprint into the surface which makes pitting corrosion beneficial in this case. Friction remains problematic as it can disturb the high chloride concentration of these pits, but it remains a much larger threat to fragile fingerprint residue one would find on the substrate surface as opposed to the corrosive etching of pitting corrosion.

Fingerprint residue, local solution chemistry, and charge variations within the corroded pits of the etched fingerprint create non-uniform surface chemistry on the substrate that can be



exploited. This non-uniformity caused by fingerprint residue deposited on substrate surfaces has been exploited previously in several different ways. In examples where fingerprint residue is primarily sebaceous in composition, gun-bluing solution applied on the surface of the metal substrate was found to work as a fingerprint enhancement technique. Fingerprint residue acts as a passivation layer on the metal, preventing the gun-bluing solution from reacting with the metal substrate in that area [47], [48], [49]. This creates what is commonly referred to as a negative fingerprint and is used in identification just as other fingerprint images would be.

As it was described previously, the entire basis of VMD in latent fingerprint development rests on the non-uniformity of the thin gold film deposited, not dissimilar to electrodeposition, in the first step of the process. Increased amounts of fatty acids, or sebaceous residue constituents, absorb the gold which would ultimately generate a negative fingerprint like those enhanced with gun blue solution. However, fingerprints with largely aqueous residue constituents are less likely to absorb the gold atoms, thus generating a regularly developed fingerprint.

Electrodeposition of other metal species onto the metal substrate for development offers another way to enhance and visualize any surface corrosion caused by residue constituents of latent fingerprints, thus contributing another possibility in the realm of corrosion-based latent fingerprint development methods. Fundamentally, electrodeposition is a means to modify substrate surface properties. This dissertation focuses on electrodeposition as it pertains to the application of thin films or coatings to a metal or alloyed substrate to enhance the resolution of fingerprint ridges on the metal substrate surface. This is accomplished with the application of current to an electrode submerged in an aqueous electrolyte solution within an electrochemical cell.

The exploration of corrosion-based methods and electroanalytical chemistry in forensic fingerprint analysis represents a crucial advancement in overcoming the challenges posed by difficult substrates and harsh environmental conditions. By exploring the mechanisms of corrosion and leveraging electrochemical reactions, this research not only illuminates the complex interactions between fingerprint residue and metal substrates which may be applicable to previous techniques but also offers novel strategies for latent fingerprint development and visualization. Through innovative approaches such as electrodeposition and the exploitation of non-uniform surface chemistry, this study paves the way for novel forensic analysis techniques, contributing to more effective crime scene investigations.

#### **1.4 Research Hypothesis and Project Description**

This dissertation examines the hypothesis that induced electrochemical corrosion and electrodeposition techniques can serve as effective corrosion-based methods for developing latent fingerprints where traditional residue-based methods may falter. Coined as 'targeted corrosion enhancement' within this study, the approach diverges from conventional methods by focusing on exploiting and enhancing the corrosion caused by aqueous residue constituents rather than relying solely on the visualization of fingerprint residue itself. The primary objective is to develop a method that can effectively target corroded fingerprint ridges, enhancing them to the point of discernibility for imaging, mapping, and, ultimately, positive suspect identification.

The initial phase of the research involves identifying suitable electrolyte solutions for each metal alloy. This is achieved through extensive 24-hour soak tests and open circuit potential

measurements, supplemented by a detailed investigation into the effects of sulfuric acid concentrations, hydrogen evolution, and dissolved oxygen levels. Potentiodynamic corrosion, conducted via Linear Sweep Voltammetry (LSV), establishes a baseline for the level of development achievable through targeted corrosion enhancement. This method is then compared with two alternative approaches: potentiostatic and galvanostatic corrosion experiments. These variations allow us to assess the efficacy of holding metal substrates at constant potentials or currents for different durations, potentially streamlining evidence processing throughput.

To quantify the corrosion process and its progression overtime on the substrate surface during LSV measurements, we employ Inductively Coupled Plasma – Optical Emission Spectroscopy (ICP-OES) analysis. This method offers a detailed characterization of substrate corrosion, facilitating further optimization of targeted corrosion enhancement methods and enhancing our understanding of the interactions between metal substrates and electrolyte solutions, with and without latent fingerprints.

Furthermore, electrodeposition experiments are conducted with gold and silver at various applied potentials and durations to determine the parameters yielding optimal latent fingerprint development. Additionally, electroless deposition, employing heat as a catalyst, is explored, and its efficacy is compared with electrodeposition in terms of latent fingerprint visualization. The resulting images are analyzed, graded, and compared to identify the most effective fingerprint development method.

The core focus of this dissertation centers on the thorough imaging, grading, and comparison of all corrosion-based fingerprint development techniques regarding their capacity to reveal discernible fingerprint ridges. Ultimately, each method of corrosion (potentiodynamic, potentiostatic, galvanostatic) will be compared with both forms of deposition to evaluate their

individual strengths and weaknesses, thus identifying the most effective corrosion-based fingerprint development approach. Additionally, practical considerations such as cost and time implications are taken into account to address barriers to implementation and facilitate widespread adoption.

## **Chapter 2: Experimental Methods**

Chapter Two provides a detailed account of the materials, sample preparation techniques, methods, instrumentation, and characterization processes applied to all substrate samples during this research. These methodologies were carefully selected to ensure rigorous testing and reproducibility, critical for validating the results within the broader context of forensic science.

### **2.1 Materials**

The materials selected for this study included 6061-Aluminum alloy, ultra-formable C260 brass, low-carbon steel, and multipurpose 400-Nickel alloy. These metals and alloys, commonly encountered in forensic evidence, were sourced from McMaster-Carr. The percentage compositions of these materials are detailed in Table 1 below.

Table 1: Percentage compositions for all metal substrates purchased through McMaster-Carr

| <b>Substrate</b>        | <b>Composition</b>   |
|-------------------------|--|
| <b>6061-Aluminum</b>    | 95.1-98.2% Al, 0.8-1.2% Mg, 0.4-0.8% Cr, 0.4-0.8% Si,<br>0.05-0.4% Cu, 0-0.7% Fe, 0-0.15% Mn, 0-0.05% Ni,<br>0-0.15% Ti, 0-0.25% Zn, 0-0.25% Zr, 0.15% Other |
| <b>C260 Brass</b>       | 68.5%-71.5% Cu, 28.38-31.38% Zn, 0-0.07% Pb, 0-0.05% Fe  |
| <b>Low-carbon Steel</b> | > 99% Fe, 0.5% Max Mn, 0.03% Max P,<br>0.1% Max Si, 0.01-0.13% C, 0.035% Max S   |
| <b>400-Nickel</b>       | 60.7-72.0% Ni, 28-34% Cu, 2.5% Max Fe,<br>2% Max Mn, 0.5% Max Si, 0.3% Max C   |

The electrochemical measurements were performed using an HP laptop computer and an SP-300 (BioLogic, Seyssinet-Pariset, France) with a connected 2A/30V booster (BioLogic, Seyssinet-Pariset, France), an Autolab PGSTAT302N (Metrohm, Herisau, Switzerland), or an Emstat Blue (PalmSens, Houten, The Netherlands).

Measurements were performed in an Autolab Flat Sample Platform Cell (Metrohm, Herisau, Switzerland) consisting of a flat cell glass vessel clamped to a PVC holder with a Viton O-ring at the interface. The exposed surface area of the sample is 16.9 cm<sup>2</sup> and the cell can accommodate a thickness of up to 5 mm.

Reference electrode 6.0733.100 (Metrohm, Herisau, Switzerland) was used for all experiments and is filled with 3 M KCl solution. Metrohm literature provides a standard reference electrode potential of 210 mV ± 5 mV with respect to the Standard Hydrogen

Electrode (SHE). Electrochemical measurements in this dissertation are conducted and reported against the Ag/AgCl reference electrode potential value.

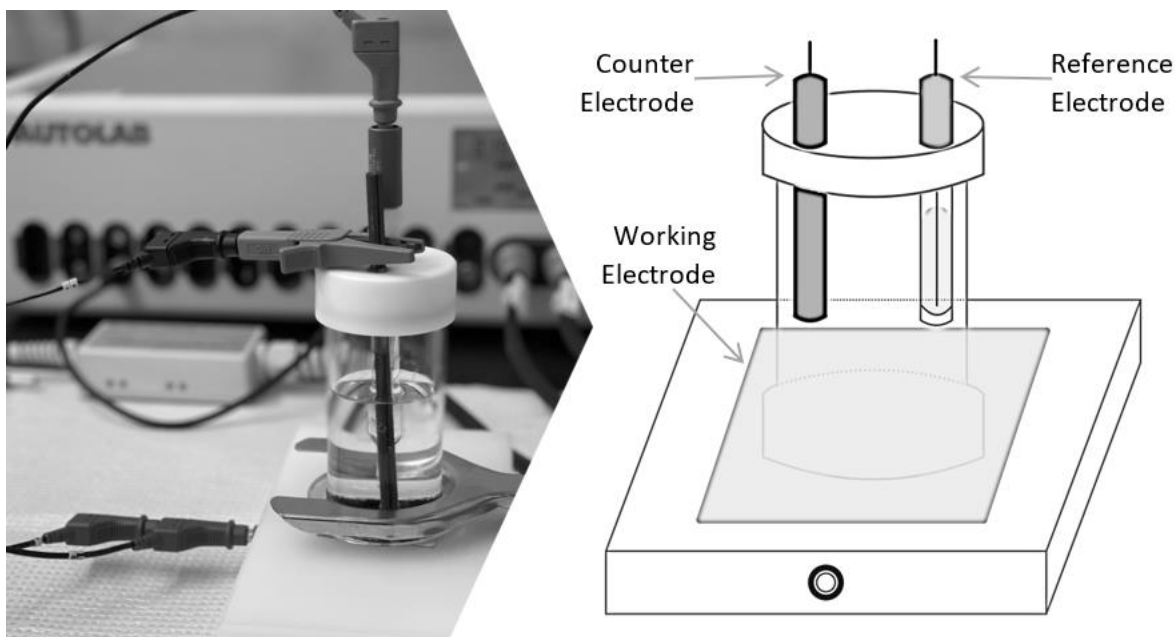


Figure 3: Image of Metrohm flat platform electrochemical cell (left) and schematic of the orientation of three electrodes within the Metrohm flat platform cell (right)

Acetone ( $C_3H_6O$ , VWR Chemicals, 99.6%) was used to thoroughly cleanse all metal samples. To prepare 0.1M solutions, sulfuric acid ( $H_2SO_4$ , 93-98%, Fisher Chemical), potassium chloride (KCl, 99.0-100.5%, VWR Chemicals), and sodium sulfate ( $Na_2SO_4$ , 99%, EM Science) were dissolved or diluted in ultrapure water ( $H_2O$ , Barnstead E-Pure D4641, 18  $M\Omega$ ). Alconox anionic detergent, mixed with ultrapure water, was an additional cleaning agent. Nitrogen ( $N_2$ , Ultra High Purity – Pure, Airgas) was used for degassing solutions for dissolved oxygen studies.

Inductively Coupled Plasma - Optical Emission Spectroscopy (ICP-OES) analysis incorporated various standard solutions: chromium (Cr – 1,000 µg/mL in 5% HNO<sub>3</sub>, LGC Standards, VHG Labs, Lot 76794R-25), nickel (Ni – 10 µg/mL in 2% HNO<sub>3</sub>, LGC Standards, VHG Labs), manganese (Mn – 1,000 µg/mL in 2% HNO<sub>3</sub>, PerkinElmer Pure), iron (Fe – 1,000 µg/mL in 2% HNO<sub>3</sub>, SPEX CertiPrep), copper (Cu – 1,000 µg/mL in 3% HNO<sub>3</sub>, Ricca Chemical), and zinc (Zn – 1,000 µg/mL in 2% HNO<sub>3</sub>, SPEX CertiPrep). Table 2 displays which standard solutions were utilized for each metal and in which concentrations to construct their respective calibration curves is shown below:

Table 2: Standard element solutions utilized in calibration curves for each metal substrate

| <b>Substrate</b>        | <b>Elements Tested</b> | <b>Concentrations</b>                      |
|-------------------------|------------------------|--|
| <b>6061-Aluminum</b>    | Cu, Fe, Al, Cr         | 50ppm, 20ppm, 10ppm,<br>5ppm, 1ppm, 0.1ppm |
| <b>C260 Brass</b>       | Cu, Fe, Zn             | 100ppm, 50ppm, 20ppm,<br>10ppm, 5ppm, 1ppm |
| <b>Low-carbon Steel</b> | Fe, Mn                 | 50ppm, 20ppm, 10ppm,<br>5ppm, 1ppm, 0.1ppm |
| <b>400-Nickel</b>       | Fe, Mn, Ni             | 50ppm, 20ppm, 10ppm,<br>5ppm, 1ppm, 0.1ppm |



A dilute rinsing solution of nitric acid ( $\text{HNO}_3$ , 69.0-70.0%, J.T. Baker) and ultrapure water was also prepared at a concentration of 2%  $\text{HNO}_3$ .

For the electroplating experiments, Krohn 24K gold and silver electroplating solutions were used to deposit layers of gold and silver, respectively. Electroless deposition of gold, silver, and zinc was also conducted using Transene bright electroless gold, electroless silver, and zincate immersion zinc plating solutions. A Cimarec+ HP88854100 (Thermo Scientific, Waltham, Massachusetts) hot plate was used to maintain the temperature of the solution baths in the electrodeposition and electroless deposition experiments. Electroless deposition experiments utilized a Pyrex Griffin Low Form 250 mL beaker (Corning, Corning, New York) as a bath container. Three different materials were used as counter electrodes throughout all electrodeposition and electroless deposition experiments: a graphite bar with dimensions 76mm by 12mm by 6mm, a boron-doped diamond-coated tantalum rod with dimensions 2mm by 152mm, and the 304 stainless-steel counter electrode included with the Autolab Flat Sample Platform Cell.

## **2.2 Sample Preparation**

Ultra-formable C260 Brass and Low-Carbon Steel were shaped into 2" x 2" squares using a metal table shear, and their edges were subsequently smoothed with a belt sander. These square metal samples served as the working electrodes. The metal squares were initially rinsed with acetone, followed by a wash with warm water and Alconox solution (anionic detergent), another rinse with ultrapure water, and drying with KimWipes.



interact with the metal surfaces. After aging, the samples were rinsed with ultrapure water, dried with KimWipes, and placed into the flat platform cell for experimentation.



Figure 5: Flow chart illustrating all procedural steps in preparing, generating, applying, containing, and aging samples

Samples not subjected to fingerprint application underwent the same preparation, containment, and aging steps to ensure consistency in forming passive-oxide layers on the substrate surfaces. Samples intended for sebaceous fingerprint application followed the same initial preparation. The fingerprint donor swiped across their forehead to collect sebaceous residue on their fingertip, then applied it to each metal substrate with consistent force. These samples were then aged in Petri dishes, similar to the eccrine-treated samples, before being rinsed and readied for experimentation.

### **2.3 Electrochemical Methods and Instrumentation**

Electrochemistry is the study of electrical influence on chemical change, particularly the transfer of electrons across species in oxidation-reduction (redox) reactions [50]. It encompasses

reactions where electrons are transferred between species, typically involving oxidation-reduction (redox) reactions. This field is crucial for understanding how the polarization of a working electrode, sufficient to overcome the energy barrier, facilitates charge transfer at the electrode-electrolyte interface, resulting in a chemical transformation of the electrode surface.

The fundamental behavior of these reactions is governed by the Nernst equation, derived from the Gibbs free energy equation:

$$\Delta G^\circ = -nFE^0$$

Equation 8: Gibbs free energy equation under standard conditions

Under both standard and non-standard conditions, Gibbs free energy is related by:

$$\Delta G = \Delta G^\circ + RT \cdot \ln(Q)$$

Equation 9: Relating Gibbs free energy across conditions

Substituting the standard and non-standard Gibbs energies into the combined form yields:

$$-nFE = -nFE^0 + RT \cdot \ln(Q)$$

Equation 10: Integration of Gibbs free energy equations

Dividing through by  $-nF$  simplifies to the Nernst equation which assumes that the reaction studied is not at equilibrium but driven by the potential difference given by  $E - E^0$ :

$$E = E^0 - \frac{RT}{nF} \cdot \ln(Q)$$

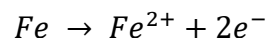
Equation 11: Nernst equation

Here,  $E$  represents the cell potential under non-standard conditions,  $E^0$  is the standard cell potential,  $R$  is the universal gas constant ( $8.314 \text{ J/mol} \cdot \text{K}$ ),  $T$  is the temperature in Kelvin,  $n$  is the moles of electrons, and  $F$  is Faraday's constant ( $\cong 96,485 \text{ J/(V} \cdot \text{mol } e^-)$ ). Applying these constants at 298K simplifies the Nernst equation to:

$$E = E^0 - \frac{0.591 \text{ V}}{n} \cdot \log(Q)$$

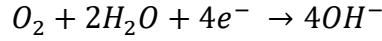
Equation 12: Nernst equation at standard temperature (298K)

Electroanalytical methods are routinely used in characterizing corrosion because it is an electrochemical process [51]. Electrochemical reactions require that at least one species change its number of valence electrons through oxidation/reduction. This charge transfer happens through coupled oxidation and reduction reactions where one species is an electron donor and the other is an acceptor. Corrosion reactions also involve charge transfer through electrochemical oxidation-reduction reactions. Electrochemical reactions and chemical reactions are often coupled, as is the case in corrosion. However, oxidation and reduction reactions often generate products that proceed to undergo chemical reactions. For example, the oxidation reaction of iron is as follows:



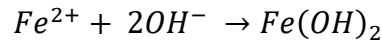
Equation 13: Oxidation reaction of iron

Oxygen, conversely, undergoes reduction by gaining electrons lost by iron:



Equation 14: Reduction of dissolved oxygen

These reactions produce  $Fe^{2+}$  and  $4OH^-$  ions, which can react to form iron hydroxide, a typical corrosion product:



Equation 15: Formation of iron hydroxide

While chemical processes like rust formation are visible outcomes, the initial electrochemical reactions are vital for generating the necessary reactants. This understanding emphasizes the role of electrochemical studies in assessing corrosion rates and mechanisms.

One common approach in such studies involves applying an overpotential using a potentiostat to induce oxidation at the electrode surface. In the context of this dissertation, metals and alloys frequently encountered in the processing of latent fingerprint evidence are utilized as the electrodes undergoing polarization. The potentiostat applies an overpotential, which is the disparity between the potential applied to the working electrode and the corrosion potential of the material [52]. This overpotential enhances any existing corrosion on the substrate, allowing for detailed analysis and characterization.

$$\eta = E - E_{corr}$$

Equation 16: Overpotential equation

The overpotential ( $\eta$ ) is calculated using Equation 16, where  $E$  represents the potential applied to the working electrode and  $E_{corr}$  denotes the corrosion potential. This overpotential manipulation is central to the experimental design, allowing for precise control over the electrochemical processes occurring at the electrode-electrolyte interface. By systematically varying the overpotential, the effects on corrosion behavior can be thoroughly investigated, providing insights into the underlying mechanisms. Additionally, the corrosion potential values obtained serve as pivotal reference points for optimizing experimental conditions and interpreting corrosion rate data. Through these methodologies, this dissertation aims to advance our understanding of corrosion processes and contribute to developing novel forensic methods.

### **2.3.1 Open Circuit Potential**

Open circuit potential (OCP) is a crucial parameter in electrochemical studies, particularly in corrosion research. It refers to the potential difference between a working electrode and a reference electrode when no current flows between them. Essentially, it represents the equilibrium potential of the electrode-electrolyte interface under the given experimental conditions [50]. For this reason, these measurements fall under the umbrella of passive techniques. The OCP provides valuable information about the corrosion behavior of a material in its natural environment without applying any external potential. By measuring the OCP over time, researchers can observe changes in the electrochemical state of the material, such as the initiation and progression of corrosion processes. Moreover, deviations from the expected OCP value can indicate the onset of corrosion or other electrochemical reactions.

Moving the potential in more positive directions would result in oxidative current, and conversely, potentials at more negative potential would be reductive.

Notably, although no external current is applied during OCP measurements, introducing an acidic electrolyte solution can lead to current flow between the working and counter electrodes, triggering electrochemical reactions until equilibrium is attained. Consequently, the OCP value precisely corresponds to the electrical potential required to initiate corrosion reactions on the substrate surface. This is why, and how, the open circuit potential value correlates precisely to the electrical potential needed to initiate corrosion reactions on the surface of a given substrate [53]. Thus,  $E_{OCP} = E_{corr}$ . The value of OCP is influenced by the kinetics of anodic oxidation, which entails the material's degradation and the cathodic reduction of any oxidants present within the electrochemical cell. The OCP value dictates the material's susceptibility to oxidation and its thermodynamic stability within the environment [54]. A generic diagram representing data that would be obtained in open circuit potential measurements is displayed below for clarity. A larger initial potential and subsequent drop correspond to the initial capacitive current generated during the equilibration of the metal substrate in acidic electrolyte solutions used in this dissertation.



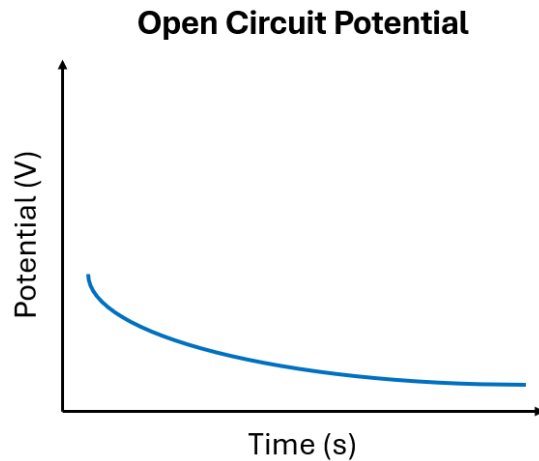


Figure 6: Generic diagram of potential vs time obtained during open circuit potential measurements. This diagram also displays what would be considered capacitive current generated during equilibration of substrate and electrolyte solution

Platinum, ruthenium, rhodium, palladium, osmium, iridium, platinum, gold, and sometimes silver are regarded as the “noble metals.” This is due to their intrinsic corrosion resistance and chemical inertness [55], [56]. Open circuit potentials are considered more noble if they have a more positive value and more active if they have a more negative value. More noble open circuit potentials correlate to higher corrosion resistance of the material, meaning that they reduce more readily and prefer existing in a pure element form or passive readily by forming a thin layer of oxide. Conversely, more active corrosion potentials represent materials that corrode more readily, are more prone to oxidation, and prefer to exist as ions. These initial open circuit potential measurements are essential to provide the exact potential at which the metal begins to corrode. This prohibits the substrate from undergoing rapid corrosion that would likely destroy any fingerprints present on the substrate surface.

The working electrodes (referenced in 2.1 and 2.2) employed in these studies are relatively large 2" x 2" flat metal squares. It is important to recognize that potential drop within the electrolyte solution, resulting from solution resistance, can introduce inaccuracies into measurements [50], [57], [58]. A three-electrode system was chosen to provide the most control and the ability to measure both potential and current accurately. In a three-electrode system, current flows between the working and counter electrode, which is in place to complete the electrical circuit. The use of a reference electrode, as well as its placement, can minimize the effects of the potential drop associated with the junction potential, which is the difference in electric potential that develops at the interface between two different conductive phases. The reference electrode acts as the reference point to which the potential at the working electrode is measured. Designed to be ideally non-polarizable, reference electrodes do not react under electrical stimulation and maintain their designated open circuit potential value without drifting, thus providing a stable electrochemical potential relative to the working electrode and not reacting to change the chemical composition or overall potential of the cell. Furthermore, the three-electrode configuration allows for precise control of experimental conditions. For instance, it enables the application of specific potentials to the working electrode using a potentiostat while simultaneously measuring the resulting current flow. This capability is crucial for performing various electrochemical techniques, such as cyclic voltammetry, potentiodynamic polarization, and electrochemical impedance spectroscopy, which are commonly used in corrosion studies. The counter electrode, functioning as an electron donor and sink, maintains its role without affecting the reference electrode, which remains unreacted despite potential changes.

These initial OCP measurements are indispensable for determining the potential at which the metal substrate initiates corrosion. This knowledge prevents rapid substrate corrosion that could obliterate any fingerprint on the surface.

### **2.3.2 Linear Sweep Voltammetry (LSV)**

Linear sweep voltammetry (LSV) is an electrochemical technique used to study the behavior of electrochemical systems by measuring the current response as a function of applied potential. These measurements generally provide details regarding the thermodynamics of oxidation-reduction reactions and electron transfer kinetics [59]. LSV involves applying a sweeping range of electrical potentials to the working electrode relative to the reference electrode. The generated current response is measured. For these reasons, a three-electrode system is required for these measurements. Potentiodynamic corrosion, the first method being studied for targeted corrosion enhancement of latent fingerprints, is induced by applying a sweeping range of electrical potentials. Thus, LSV measurements constitute potentiodynamic corrosion of the four metal alloy substrates being studied [60], [61]. A generic voltammogram representing data obtained in LSV measurements is displayed below for clarity.

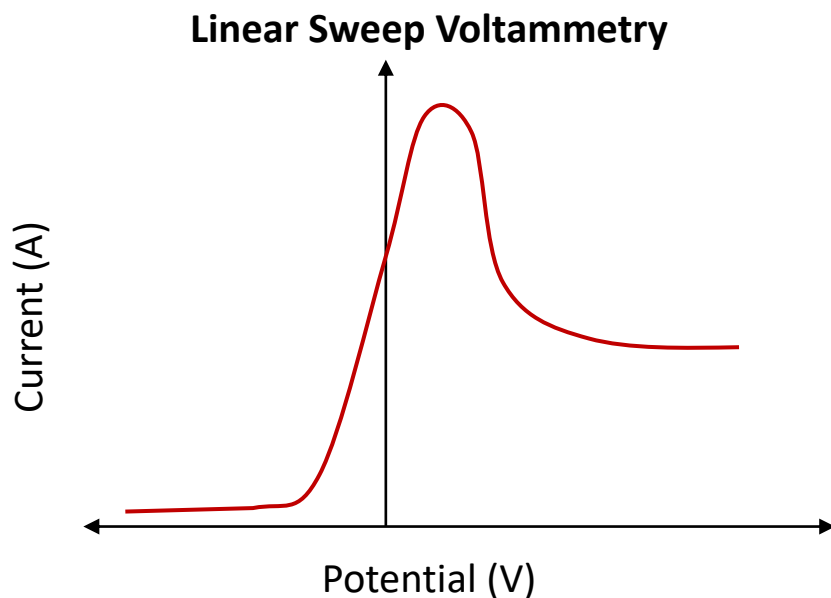


Figure 7: Generic diagram of current vs potential obtained during LSV measurements

Secondly, in LSV measurements, the corrosion potential ( $E_{corr}$ ) and corrosion current ( $I_{corr}$ ) can be obtained by analyzing the resulting voltammogram.

The corrosion potential represents the point at which the current response suddenly changes, indicating the onset of corrosion processes. In LSV,  $E_{corr}$  corresponds to the potential at which the current starts to increase significantly from its baseline value. This point is typically identified by visual inspection of the voltammogram or by using analytical techniques to determine the inflection point. The corrosion current  $I_{corr}$  represents the rate of corrosion occurring at the electrode surface. It can be calculated from the current value recorded at the corrosion potential. Typically, corrosion current is determined by extrapolating the linear portion of the Tafel plot, which is constructed using the current values obtained at different potentials

during the LSV experiment. The intersection of the extrapolated linear portion with the corrosion potential provides the value of  $I_{corr}$ .

The open circuit potential values obtained in earlier stages act as a validation of the corrosion potential values derived from Tafel analysis. Conversely, the corrosion potential values derived from Tafel analysis validate the open circuit potential values. This reciprocal validation process enhances overall accuracy and precision, ensuring robustness before proceeding with subsequent electrochemical corrosion methods to enhance latent fingerprints. Before conducting potentiostatic and galvanostatic corrosion measurements, potentiodynamic corrosion measurements are performed to establish baseline corrosion potential and corrosion current values. These values are pivotal reference points for optimizing the subsequent electrochemical corrosion methods.

LSV experiments can be conducted over a range of potentials to fully characterize the electrochemical behavior of the system under investigation. By analyzing the resulting voltammogram and constructing Tafel plots, researchers can accurately determine the corrosion potential and current, essential parameters for understanding and quantifying corrosion processes.

### **2.3.3 Tafel Analysis**

Tafel analysis is a technique used to extract valuable electrochemical parameters from the voltametric data obtained during an experiment. Specifically, Tafel analysis focuses on the

behavior of the current-voltage response near the corrosion potential ( $E_{corr}$ ) of a working electrode.

In LSV, the working electrode's potential is swept linearly with time while the current response is recorded. Near the corrosion potential, the current response exhibits a characteristic behavior that can be analyzed using Tafel analysis. This analysis involves plotting the logarithm of the current density versus the electrode potential, producing a semi-logarithmic plot known as a Tafel plot. A generic Tafel plot is shown below.

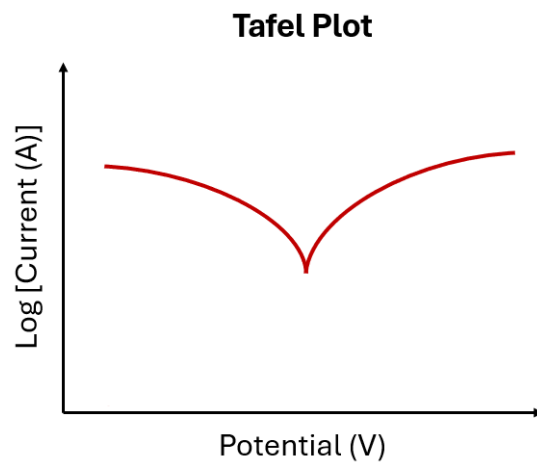


Figure 8: Resulting Tafel plot after the logarithm of the y-axis of the LSV voltammogram is taken

Tafel analysis plays a dual role, furnishing both the corrosion potential and corrosion current values, which directly correlate to the potential and current required to initiate the corrosion process of the metal substrate. Additionally, the Tafel slope emerges as a fundamental parameter, elucidating the required overpotential (described in section 2.3, Equation 16) applied

by the potentiostat, whether in the anodic or cathodic direction, to elevate the reaction rate by a factor of ten [62]. Each half reaction is governed by the kinetics of the Butler-Volmer equation [63]:

$$i = i_0 \exp \left[ \frac{\alpha n F \eta_a}{RT} \right] - i_0 \exp \left[ \frac{-(1 - \alpha) n F \eta_c}{RT} \right]$$

Equation 17: Butler-Volmer equation

In electrochemistry and corrosion, the Butler-Volmer equation is utilized to understand electrode reaction kinetics. It describes the rate of an electrode reaction in terms of the exchange of electrons between the electrode and the electrolyte solution. It's beneficial for understanding processes like corrosion, where metal ions are released into solution due to reactions occurring at the electrode surface. In the Butler-Volmer equation, the applied voltage by the potentiostat is represented by  $E$ , cathodic and anodic overpotentials by  $\eta_c = E - E_{corr}$  and  $\eta_a = E - E_{corr}$ , corrosion potential by  $E_{corr}$ , number of electrons involved in the reaction by  $n$ , total current density at the electrode surface by  $i$ , exchange current density by  $i_0$ , and transfer coefficients by  $\alpha$ .

The alpha transfer coefficient ( $\alpha$ ) represents the extent to which the reaction mechanism follows either an adsorption process ( $\alpha = 0.5$ ) or a charge-transfer process ( $\alpha = 1$ ). An  $\alpha$  value of 0.5 indicates that the reaction rate is primarily influenced by the adsorption of reactants onto the electrode surface. This is typical for responses where the rate-limiting step involves the adsorption of species onto the electrode surface. Conversely, an  $\alpha$  value of 1 indicates that the reaction rate is controlled solely by the transfer of charge across the electrode-electrolyte interface. This is observed in reactions where the electron transfer step is the slowest part of the

process. For most electrode reactions, the value of  $\alpha$  falls somewhere between 0.5 and 1.0, which indicates a combination of both adsorption and charge transfer processes influencing the reaction rate. Understanding the value of  $\alpha$  is crucial because it provides insights into the mechanism of the electrode reaction. In the context of corrosion, it helps us comprehend whether the corrosion process is predominantly controlled by the adsorption of corrosive species onto the metal surface or by the transfer of electrons between the metal and the electrolyte.

Understanding the distinction between the total current density ( $i$ ), exchange current density ( $i_0$ ), corrosion current density ( $i_{corr}$ ), and corrosion current ( $I_{corr}$ ) is important to analyze and predict electrochemical behavior, particularly concerning corrosion studies and materials degradation. The total current density is the sum of the anodic current density ( $i_a$ ) and the cathodic current density ( $i_c$ ) in the equation below:

$$i = i_a + i_c$$

Equation 18: Total current density is equal to the sum of the anodic and cathodic current densities

The total current density ( $i$ ) represents the total current density at the electrode surface under a given set of conditions which would typically be influenced by the applied potential. This term considers both the forward (oxidation or anodic) and reverse (reduction or cathodic) reactions occurring at the electrode-electrolyte interface. This term can be influenced by the overpotential, exchange current density and alpha transfer coefficient.

The exchange current density ( $i_0$ ) represents the hypothetical or expected current density of the system at equilibrium where the forward and reverse reactions are equal, which would be achieved under steady-state conditions. The exchange current density is aptly named as it



represents the current density at which there is some species exchange (e.g. electrons) occurring at the electrode-electrolyte interface but there is no net corrosion (metal dissolution) or reduction (product formation) occurring. It signifies the rate of anodic and cathodic reactions when the system exists in equilibrium. This term can be influenced by the rate constants of the individual electrode reactions and the specific concentrations of both reactants and products.

The corrosion current density ( $i_{corr}$ ) refers explicitly to the rate at which corrosion proceeds on the surface of the metal electrode per unit area and is typically expressed in units of amperes per square meter ( $A/m^2$ ). It is essentially the rate of metal dissolution due to the electrochemical reactions at the electrode-electrolyte interface, often associated with anodic dissolution. This value is crucial for quantifying the corrosion rate of a material under specific conditions, thus providing insights into its susceptibility to corrosion. The corrosion current density ( $i_{corr}$ ) typically equals the exchange current density ( $i_0$ ) for actively corroding systems. Mathematically, it can be obtained by dividing the corrosion current ( $I_{corr}$ ) by the surface area of the electrode ( $A$ ):

$$i_{corr} = \frac{I_{corr}}{A}$$

Equation 19: Corrosion current density equation representing the corrosion rate per unit area of the metal surface

The corrosion current ( $I_{corr}$ ), typically expressed in units of amperes (A), represents the total corrosion current, which is the overall rate of metal dissolution over the entire electrode surface area. This parameter gives the total amount of metal loss due to corrosion, considering the entire electrode surface area.

In summary,  $i$  is the total current density,  $i_0$  is the exchange current density at equilibrium, and  $i_{corr}$  is the corrosion current density representing the rate of metal dissolution. While  $i$  and  $i_0$  are general terms used in electrochemical kinetics,  $i_{corr}$  specifically pertains to corrosion processes where metal degradation is the primary motivation for research.

At large enough overpotentials, the anodic and cathodic half-reactions are de-coupled, with one becoming the dominant reaction. The individual Tafel relationships are determined in this manner. It is important to note that the total current is the sum of the anodic and cathodic current. At anodic overpotentials of more than 50mV ( $\eta_a > 50\text{mV}$ ), the anodic half-reaction, represented by the first term in the equation, is dominant [64]. When this happens, the Butler-Volmer equation can be re-written as:

$$i = i_0 \exp \left[ \frac{\alpha n F \eta_a}{RT} \right]$$

Equation 20: Butler-Volmer equation (anodic reaction dominant)

This is rearranged again to what is commonly known as the Tafel equation with the corresponding anodic Tafel coefficient:

$$\eta_a = \beta_a \log \frac{i}{i_0}$$

Equation 21: Tafel equation (anodic dominant)

$$\text{where } \beta_a = \frac{2.3RT}{\alpha n F}$$

Equation 22: Tafel coefficient (anodic dominant)

The same procedure can be followed for cathodic overpotentials, and the Butler-Volmer equation can be rewritten using the second term to generate the Tafel equation and cathodic Tafel coefficient. In the voltammograms generated by LSV measurements, the regions of larger overpotentials are condensed into two simplified linear polarization curves forming the Tafel plot. The anodic polarization curve, corresponding to the oxidation reaction, has a slope of  $\frac{1}{\beta_a}$ , and the cathodic polarization curve, corresponding to the reduction reaction, has a slope of  $\frac{1}{\beta_c}$ . These slopes intersect at a y-coordinate of  $\log I_{corr}$  and an x-coordinate of  $E_{corr}$ , and thus, values for corrosion current and corrosion potential are obtained in this analysis.

The BioLogic SP-300 instrument used for these measurements calculates corrosion potential and corrosion current values using the Tafel Fit tool based on the Wagner-Traud or Stearn-Geary equation [65]:

$$I = I_{corr} \left( \exp \left( \ln 10 \frac{\eta}{\beta_a} \right) - \exp \left( - \ln 10 \frac{\eta}{\beta_c} \right) \right)$$

Equation 23: Wagner-Traud equation

In this equation, the applied voltage by the potentiostat is represented by  $E$ , the overpotential by  $\eta = E - E_{corr}$ , corrosion potential by  $E_{corr}$ , corrosion current by  $I$  and corrosion current density by  $I_{corr}$ . The Tafel coefficients are expressed as:

$$\beta_a = \frac{RT}{n_1 \alpha_a F}$$

Equation 24: Wagner-Traud anodic tafel coefficient

$$\text{and } \beta_c = \frac{RT}{n_2 \alpha_c F}$$

Equation 25: Wagner-Traud Cathodic Tafel Coefficient

The Butler-Volmer equation and resulting Tafel equations are technically only valid for single electron transfer reactions, and the  $n$  term is often left out entirely for that reason. The key difference with the Wagner-Traud method is that it accounts for the fact that there may be more than a single electron transfer occurring anodically and cathodically. For this reason, it is accepted as the more accurate equation for Tafel analysis and utilized by the potentiostat software to make such calculations [66].

### **2.3.4 Electrodeposition**

Electrodeposition is an electrochemical process that involves the reduction of metal ions in a solution to form a solid metal coating on an electrode surface. This transformation occurs when an electric current is passed through the solution, driving the metal ions towards the oppositely charged electrode, where they gain electrons and are reduced to a metallic state. This technique serves as a method for altering the surface properties of substrates.

The process begins with preparing a solution containing metal ions, typically from soluble salts, and an electrolyte. Next, electrodes are selected based on their conductivity and compatibility with the electrolyte solution. The cathode is the electrode where the metal ions will be deposited, while the electrode connected to the positive terminal of the power supply constitutes the anode. Then, a voltage is applied across the electrodes, generating an electric field

in the solution. This electric field drives the migration of metal ions towards the cathode, where they are reduced and deposited as solid metal. At the cathode, metal ions gain electrons and undergo reduction, forming a solid metal deposit on the electrode surface. The reduction reaction depends on the specific metal ions present in the solution. As the reduction reaction proceeds, the metal deposit grows on the cathode surface, forming a uniform coating if the conditions are appropriately controlled.

Michael Faraday's laws of electrolysis, which originated in 1833, govern the processes by which surface properties are modified during electrodeposition. They describe the quantitative relationship between the amount of substance deposited during electrolysis and the electric charge passed through the electrolytic cell. The first law explains that the amount of mass ( $m$ ) of a metal film deposited onto an electrode is proportional to the amount of electric charge ( $Q$ ), or the number of moles of electrons, being passed through the electrochemical cell [67]. Faraday's Constant, 96,485 Coulombs per mole, represents the electric charge required to cause a chemical change to one equivalent weight unit. Faraday's second law explains that the amounts of chemical changes produced by the same amount of electric charge in different substances are proportional to the equivalent weights of each substance [68]. Both laws can be summarized and written together as follows:

$$m = \left(\frac{Q}{F}\right) \left(\frac{M}{z}\right)$$

Equation 26: Faraday's first law of electrolysis where  $Q$  represents electric charge,  $F$  is Faraday's constant,  $M$  is the molar mass of a given material and  $z$  represents the electrons transferred per ion

This dissertation utilizes electrodeposition to apply a precise and uniform thin film coating of one metal onto the surface of a metal alloy. Through the controlled application of

electric current, facilitated by the potentiostat, the metal alloy is submerged in an electrodeposition solution. Within this solution, electrochemical reactions drive the transfer of electrons between the electrolyte solution and the submerged electrode. Specifically, metal ions present in the electrolyte solution are selectively reduced onto the surface of the electrode material, resulting in the formation of the desired thin film coating [69], [70].

Since the pioneering work of Faraday, who elucidated the laws governing electrolysis in 1833, electrodeposition has evolved significantly, becoming a widely employed technique in various industries. Manufacturers often provide tables detailing the recommended voltage and time parameters to achieve a desired film thickness with specific electrodeposition solutions. While these tables offer valuable starting points, it is essential to recognize that the morphology and composition of the deposited film are influenced by a myriad of factors. These include current density, electrolyte solution composition and concentration, bath temperature, presence of impurities, characteristics of the electrode surface, and more. By meticulously controlling these parameters, electrodeposition emerges as a versatile and indispensable tool for tailored thin film fabrication, with applications ranging from electronics to surface engineering.

Furthermore, electrodeposition finds practical application in the realm of latent fingerprint development. By carefully modulating the electrodeposition parameters such as voltage, time, and electrolyte composition, it becomes possible to deposit metallic coatings onto fingerprint-bearing substrates selectively. This process can enhance the visibility of latent fingerprints by providing a contrast between the ridges and background surface, aiding forensic investigations. Thus, electrodeposition is a versatile technique, offering precise control over film deposition for diverse applications, including forensic science.

### 2.3.5 Electroless Deposition

Electroless deposition, also known as chemical or autocatalytic deposition, is a method of depositing a metal or metal alloy onto a substrate without using an external electrical current [71], [72]. Instead, the reduction of metal ions to metal atoms occurs through chemical reactions catalyzed by the surface of the substrate itself or by a catalyst deposited on the substrate. Electroless deposition was first described in 1846, and although it became widely used, it was not well understood until a US patent was issued to Francois Auguste Roux in 1916 for producing metallic deposits [73], [74].

The process typically involves several steps. First, the substrate surface is activated to provide sites for the subsequent deposition of metal atoms. This can include cleaning the surface to remove contaminants and creating nucleation sites for metal deposition. Then, a catalytic layer is deposited onto the substrate surface. This catalyst initiates the electroless deposition by reducing metal ions from the solution onto the substrate surface [75]. The metal ions in the solution are reduced to metal atoms at the catalytic sites on the substrate surface. This reduction reaction is driven by the chemical potential difference between the metal ions in the solution and the metal atoms on the substrate surface. Lastly, the reduced metal atoms continue to deposit onto the substrate surface, forming a continuous metal film or coating.

Electroless deposition holds promise as a valuable technique in fingerprint development. By leveraging the autocatalytic nature of this process, it becomes possible to deposit a thin layer of metal onto the surface of a substrate without the need for an external electrical current. In the context of fingerprint development, electroless deposition can enhance latent fingerprints on various surfaces, including metals, plastics, and other non-conductive materials. In forensic

applications, the substrate often acts as the catalytic layer required for deposition. This autocatalytic feature enables the substrate to facilitate the reduction of metal ions, effectively amplifying the fingerprint ridges, and making them more discernible for subsequent imaging and analysis. Electroless deposition enhances contrast and visibility by selectively depositing metal onto the fingerprint ridges, thereby aiding forensic investigators in identifying and analyzing latent fingerprints left at crime scenes.

## **2.4 Inductively Coupled Plasma – Optical Emission Spectroscopy**

Inductively Coupled Plasma – Optical Emission Spectroscopy (ICP-OES), also known as Inductively Coupled Plasma Atomic Emission Spectroscopy (ICP-AES), is a powerful analytical technique used for the detection and quantification of trace elements in diverse types of samples. It is widely used in environmental, pharmaceutical, industrial, and geological fields, among others, for its precision, rapid analysis, and ability to handle various elements [76]. ICP-OES can detect and measure the concentrations of multiple elements simultaneously, making it highly efficient for comprehensive analysis [77]. The high sensitivity of ICP-OES allows it to detect trace amounts of elements, down to parts per billion (ppb) levels, with high accuracy. It also offers a relatively broad dynamic range of concentration detection, effectively allowing for the analysis of very low and higher concentrations [78].

The sample, typically in liquid form, is introduced into the instrument through a nebulizer which converts it into an aerosol. This aerosol is then carried into the plasma torch. The ICP-OES technique's core is plasma generation, typically done using argon gas. This gas is ionized



using a radio frequency (RF) coil, creating a high-temperature plasma (approximately 10,000 K). The high energy within the plasma efficiently excites the atoms within the aerosolized sample. When the atoms from the sample are excited in the high-temperature environment of the plasma, they emit light as they return to their ground state. The wavelength of this light is specific to the elements present in the sample. The emitted light is passed through a spectrometer, which separates the light into its component wavelengths. Each element emits light at characteristic wavelengths, and by measuring the intensity of these emissions, the concentration of each component of the sample can be determined.

Atomic emission depends on the Boltzmann Distribution, shown below, which describes the ratio of excited atoms ( $N_j$ ) to ground state atoms ( $N_0$ ). In this equation,  $g_j$  and  $g_0$  represent the degeneracy of the excited and ground state, respectively,  $\Delta E$  represents the difference in energy between the excited and ground state and  $k$  is Boltzmann's constant equivalent to  $1.38 \times 10^{-23} \text{ J/K}$ . The equation shows that the ratio is dependent on temperature, and the higher temperature of ICP allows for more atoms in the excited state and, thus, more atomic emission to be measured.

$$\frac{N_j}{N_0} = \frac{g_j}{g_0} \exp\left(-\frac{\Delta E}{kT}\right)$$

Equation 27: Boltzmann distribution equation describing the ratio of the number of atoms in an excited state ( $N_j$ ) to the number of atoms in the ground state ( $N_0$ )

In this dissertation, the application of Inductively Coupled Plasma – Optical Emission Spectroscopy (ICP-OES) is pivotal in enhancing the forensic analysis of four distinct metal substrates. ICP-OES allows for a comprehensive quantification of how metal concentrations evolve due to corrosive processes over time by systematically sampling these substrates at

predetermined intervals throughout the corrosion experiments. This approach provides robust empirical data that elucidate the rate and pattern of corrosion across each substrate, identifying which metals are most susceptible under various experimental conditions, including different environmental factors and treatments. Moreover, this technique greatly assists in determining how these conditions influence the stability and longevity of forensic evidence on metallic substrates. Ultimately, the strategic use of ICP-OES validates the experimental findings with hard data and deepens our understanding of the mechanisms driving metal degradation in forensic contexts. This insight is crucial for forensic science, offering a clearer perspective on preserving evidence and interpreting crime scene data, thereby enhancing the reliability of forensic investigations involving metallic evidence.

## **2.5 Grading Fingerprint Development**

Images of the samples are taken before and after measurements using a Leica Wild M10 optical microscope with a Meiji Techno Fiber Optic Light Source FL-150 with an Omax Back-Illuminated Digital Imaging camera or an Amscope ZM-4T stereomicroscope with an attached digital camera. The targeted corrosion enhancement of each fingerprint is assessed using the before and after image sets of each metal substrate and given a numerical grade using the grading system developed by Bandey et al. [79], reproduced in Table 3:

Table 3: Bandey grading system for fingerprint development

| Grade | Comments  |
|-------|---|
| 0     | No development  |
| 1     | Less than one third of fingerprint displays continuous ridges     |
| 2     | One third to two thirds of fingerprint displays continuous ridges |
| 3     | Greater than two thirds of fingerprint display continuous ridges  |
| 4     | Entire fingerprint displays clear, continuous ridges              |

## Chapter 3: Targeted Corrosion Enhancement of Latent Fingerprints

### 3.1 Introduction

The recovery of latent fingerprints from challenging substrates, such as fired cartridge casings and other metal surfaces exposed to extreme conditions, remains a significant challenge in forensic science. Traditional fingerprint development techniques often fail to yield satisfactory results, leading to a low recovery rate of latent prints. In response to this challenge, novel approaches are needed to enhance latent fingerprint visualization on difficult substrates and improve the overall success rate of fingerprint recovery.

This chapter focuses on applying targeted corrosion enhancement as a novel method for developing latent fingerprints on challenging metal substrates. By exploiting electrochemical corrosion reactions between eccrine secretion components and metal surfaces, this approach aims to enhance the visibility of latent prints where traditional residue-based methods may falter. The primary objective is to develop a method that effectively targets and enhances corroded fingerprint ridges, enabling imaging, mapping, and positive suspect identification.

To achieve this objective, experiments were conducted to investigate various aspects of targeted corrosion enhancement. These experiments include electrolyte soak tests to identify suitable electrolyte solutions, open circuit potential tests to evaluate the corrosion behavior of different metal alloys, and potentiodynamic, potentiostatic, and galvanostatic corrosion experiments to perform targeted corrosion enhancement of latent fingerprints.

Electrolyte soak tests were conducted to assess the suitability of different electrolyte solutions for inducing corrosion on metal substrates. This involved immersing metal samples in various electrolytes for 24 hours and evaluating their corrosion behavior. The goal was to identify electrolytes that would facilitate corrosion while minimizing unwanted side effects such as hydrogen evolution.

Open circuit potential tests were performed to measure the corrosion potential of different metal alloys in selected electrolyte solutions. This provided valuable insights into the metal substrates' electrochemical behavior and helped select appropriate conditions for targeted corrosion enhancement experiments.

Potentiodynamic corrosion experiments were conducted to investigate the corrosion kinetics of metal substrates in electrolyte solutions. By applying a linear voltage sweep across the metal surface, the corrosion current and potential were measured, allowing corrosion rates and mechanisms to be determined.

Potentiostatic and galvanostatic corrosion experiments were conducted to study the effects of applying constant voltage or current to the metal substrates. These experiments aimed to explore the feasibility of controlling the corrosion process and optimizing the development of latent fingerprints through targeted corrosion enhancement.

Overall, the data and results obtained from these experiments provide valuable insights into the feasibility and effectiveness of targeted corrosion enhancement for developing latent fingerprints on challenging metal substrates. By systematically investigating the electrochemical behavior of metal alloys in different electrolyte solutions and under various experimental

conditions, this research contributes to the development of innovative forensic techniques for latent fingerprint analysis.

### **3.2 Materials and Methods**

In this section, the materials and methods employed for conducting targeted corrosion enhancement of latent fingerprints are outlined. The methodology encompasses a series of experiments designed to investigate various aspects of corrosion behavior on metal substrates and evaluate the efficacy of targeted corrosion enhancement techniques. The following summary provides an overview of the materials and methods used in this study, referencing relevant sections and subsections from Chapter 2 where applicable.

Metal substrates (described in section 2.1 of Chapter 2) used in this study were carefully chosen based on their relevance to forensic investigations and their susceptibility to corrosion. The selection process is informed by the literature review presented in Section 1.1, which discusses the significance of metal substrates in latent fingerprint analysis and their behavior under different environmental conditions.

Electrolyte solutions for conducting corrosion experiments were prepared according to the protocols outlined in Section 2.3.1 of Chapter 2. These solutions were chosen based on their ability to induce corrosion on metal substrates while minimizing unwanted side effects. The electrolyte soak tests were conducted to assess the suitability of these solutions for targeted corrosion enhancement. The electrochemical behavior of different metal alloys was characterized using open circuit potential tests, as described in Section 2.3.2 of Chapter 2. This involved

measuring the corrosion potential of each alloy in selected electrolyte solutions to evaluate their susceptibility to corrosion.

Potentiodynamic corrosion experiments were conducted to elucidate the corrosion kinetics of metal substrates in various electrolyte solutions. The methodology for these experiments closely follows the procedures outlined in Section 2.3.3 of Chapter 2, which details applying a linear voltage sweep to the metal surface while monitoring the resulting corrosion current and potential. During the potentiodynamic corrosion experiments, voltammograms were recorded to capture the electrochemical response of the metal substrates to the applied potential sweep. These voltammograms were subsequently analyzed using Tafel analysis, as described in Section 2.3.3. Performing Tafel analysis on the resulting voltammograms provides a deeper understanding of the corrosion behavior of metal substrates in different electrolyte solutions. This analysis allows us to quantify key corrosion parameters and assess the effectiveness of targeted corrosion enhancement techniques in promoting the development of latent fingerprints. The insights gained from Tafel analysis will be instrumental in optimizing the corrosion process and refining our approach to latent fingerprint analysis on challenging substrates.

Potentiostatic and galvanostatic corrosion experiments were conducted to study the effects of applying constant voltage or current to the metal substrates. The experimental setup and procedures for these experiments are described in Section 2.3, which discusses the methodology for controlling the corrosion process and optimizing the development of latent fingerprints.

Overall, the materials and methods employed in this study are designed to systematically investigate the electrochemical behavior of metal substrates and evaluate the feasibility of targeted corrosion enhancement for latent fingerprint analysis. By following established

protocols and referencing relevant sections and subsections from Chapter 2, this research aims to contribute to the development of innovative forensic techniques for enhancing latent fingerprints on challenging substrates.

### **3.3 Results and Discussion**

This section presents the results of targeted corrosion enhancement experiments aimed at developing latent fingerprints on challenging metal substrates. The investigation involved a comprehensive analysis of the corrosion behavior of metal alloys submerged in various electrolyte solutions, followed by potentiodynamic, potentiostatic, and galvanostatic corrosion techniques. These experiments were conducted in accordance with the outlined methodologies to systematically evaluate the efficacy of different corrosion-based approaches in enhancing the visibility of latent fingerprints.

Through meticulous experimentation and analysis, optimal conditions for promoting the development of discernible fingerprint ridges on metal substrates subjected to harsh environmental conditions were sought. The results presented in this section provide valuable insights into the electrochemical processes underlying targeted corrosion enhancement and offer a basis for further refinement and optimization of latent fingerprint development techniques. By elucidating the relationships between electrolyte composition, corrosion kinetics, and fingerprint visibility, contributions to advancing forensic science methodologies are made, enhancing the understanding of corrosion-based approaches in forensic fingerprint analysis.



### 3.3.1 Electrolyte Solution Soak Tests

All electrochemical methods and corrosion characterization experiments within this dissertation necessitate an electrolyte solution. To identify the most suitable electrolyte solution for each of the four substrates—6061-Aluminum alloy, C260 brass, low-carbon steel, and 400-Nickel alloy—comprehensive soak tests were conducted. These tests were structured to cover three separate conditions for each metal: non-fingerprinted, with eccrine fingerprints, and with sebaceous fingerprints. For each condition, each substrate underwent three trials in each of the four different electrolyte solutions: 0.1M H<sub>2</sub>SO<sub>4</sub>, 0.1M KCl, 0.1M Na<sub>2</sub>SO<sub>4</sub>, and ultrapure water as a control. This resulted in a total of twelve trials per metal per condition, with each trial lasting 24 hours.

The extended duration of the soak tests was crucial to allow for the initiation and progression of corrosion reactions without any applied potential or current, providing a clear picture of how each substrate interacts with different solutions. These foundational experiments served as a pivotal exploration of substrate-solution interactions, crucial for achieving the objectives of targeted corrosion enhancement aimed at promoting pitting corrosion and etching any existing fingerprints into the substrate surface. Consequently, electrolyte solutions that induced severe corrosion without external stimuli were deemed unsuitable.

The results of these soak tests provided crucial insights into the corrosion behavior of the substrates under different conditions, which informed subsequent decisions regarding the selection of electrolyte solutions for further experimentation. The insights gleaned from the experiments under each condition were instrumental in understanding how different substrates

react to the same corrosive environments, which is vital for targeted corrosion enhancement in forensic applications.

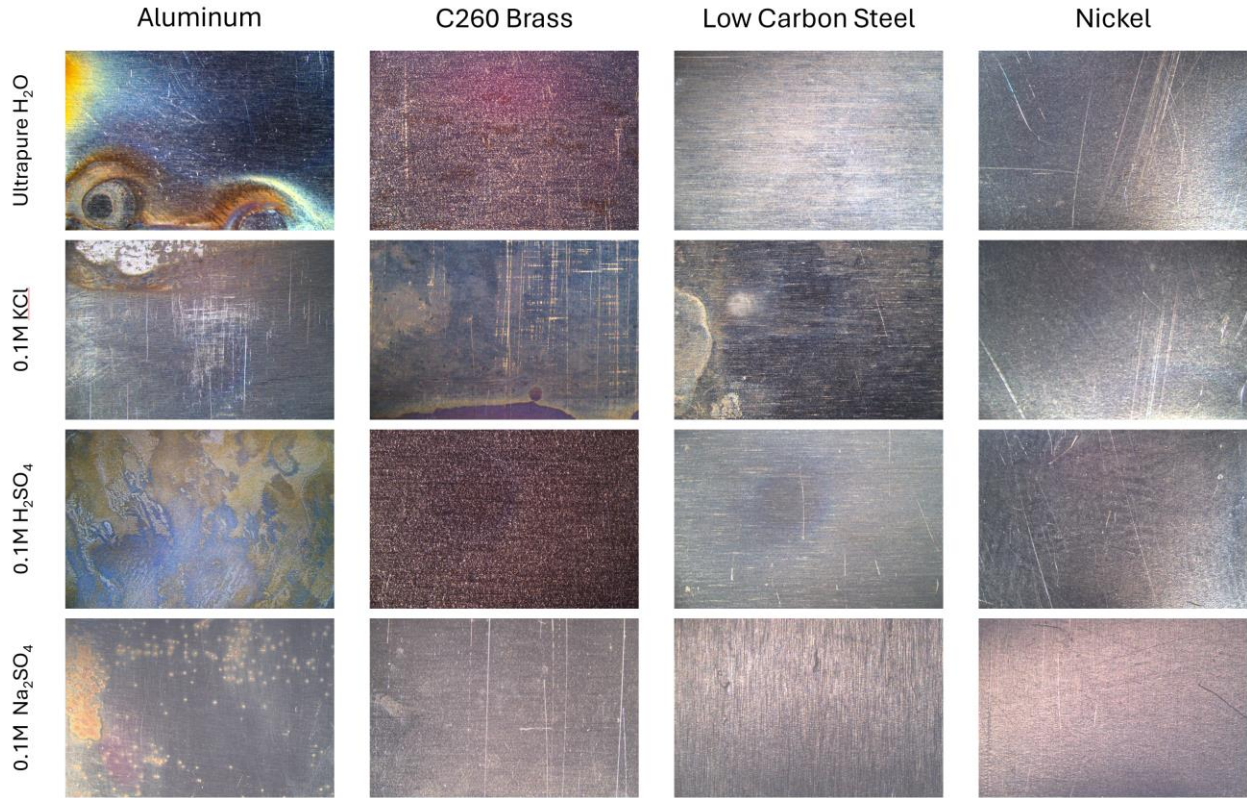


Figure 9: Images of each of the four substrates, without fingerprints applied, after soaking for 24 hours in each of the four listed electrolyte solutions. Note that Ultrapure H<sub>2</sub>O is the control for this experiment

Soak tests on each of the four substrates, without fingerprints, are shown above in Figure 9. Soaking the substrates in ultrapure water caused severe, uneven corrosion on the 6061-Aluminum alloy samples and did not appear to cause visible corrosion on the surfaces of the C260 brass, low-carbon steel and 400-Nickel alloy samples. Some cloudiness, however, did appear on the C260 brass, low-carbon steel and 400-Nickel alloy samples after being dried with

KimWipes. This may be due to the formation of a thin passive oxide layer on the C260 brass and low-carbon steel samples. The images clearly show that 0.1M KCl causes severe, uneven corrosion on all four substrates. 0.1M H<sub>2</sub>SO<sub>4</sub> caused severe, uneven corrosion on the 6061-Aluminum alloy samples but left the C260 brass with only a slight cloudiness on the surface after drying with KimWipes. Low-carbon steel samples were left with some darker, uneven spots and some lines or streak patterns appeared on two of the three 400-Nickel alloy samples after they were dried with KimWipes. 0.1M Na<sub>2</sub>SO<sub>4</sub> caused severe, uneven corrosion on the 6061-Aluminum alloy samples and moderate, uneven corrosion on the C260 brass samples. It did not appear to have any visible effect on the low-carbon steel or 400-Nickel alloy samples.

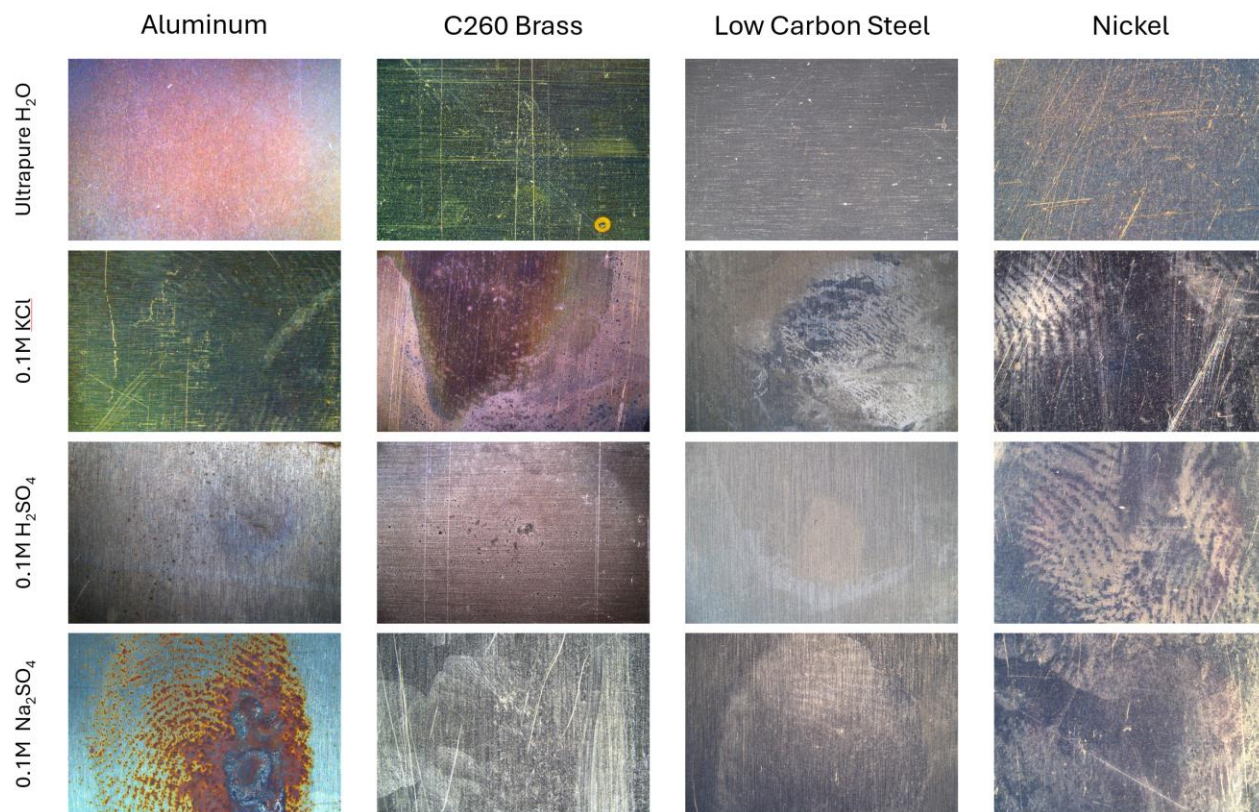


Figure 10: Images of each of the four substrates, with eccrine fingerprints applied, after soaking for 24 hours in each of the four listed electrolyte solutions. Note that Ultrapure H<sub>2</sub>O is the control for this experiment

The results of soak tests on eccrine fingerprinted substrates are shown above in Figure 10. Ultrapure water caused severe corrosion to the 6061-Aluminum alloy and C260 brass samples. It caused some slight cloudiness to appear on the low-carbon steel and 400-Nickel alloy samples which, again, may be due to the formation of a passive oxide layer on the substrate surfaces. Another similarity shared is the severe, uneven corrosion caused by 0.1M KCl on the C260 brass and low-carbon steel samples. In this case, 0.1M KCl did cause corrosion to occur on the 6061-Aluminum alloy and 400-Nickel alloy samples, but it revealed some visible portions of the applied eccrine fingerprint in one of each of the samples. 0.1M H<sub>2</sub>SO<sub>4</sub> allowed for part of the

applied eccrine fingerprints to be visible in all three 6061-Aluminum alloy, C260 brass, and 400-Nickel alloy samples. This electrolyte solution showed darker, uneven spots on all three low-carbon steel samples, though the general outline of the fingerprint was distinguishable. 0.1M  $\text{Na}_2\text{SO}_4$  caused severe, uneven corrosion on the 6061-Aluminum alloy, C260 brass and 400-Nickel alloy samples. It did, however, allow for some portions of the eccrine fingerprint to become visible in two of the low-carbon steel samples.

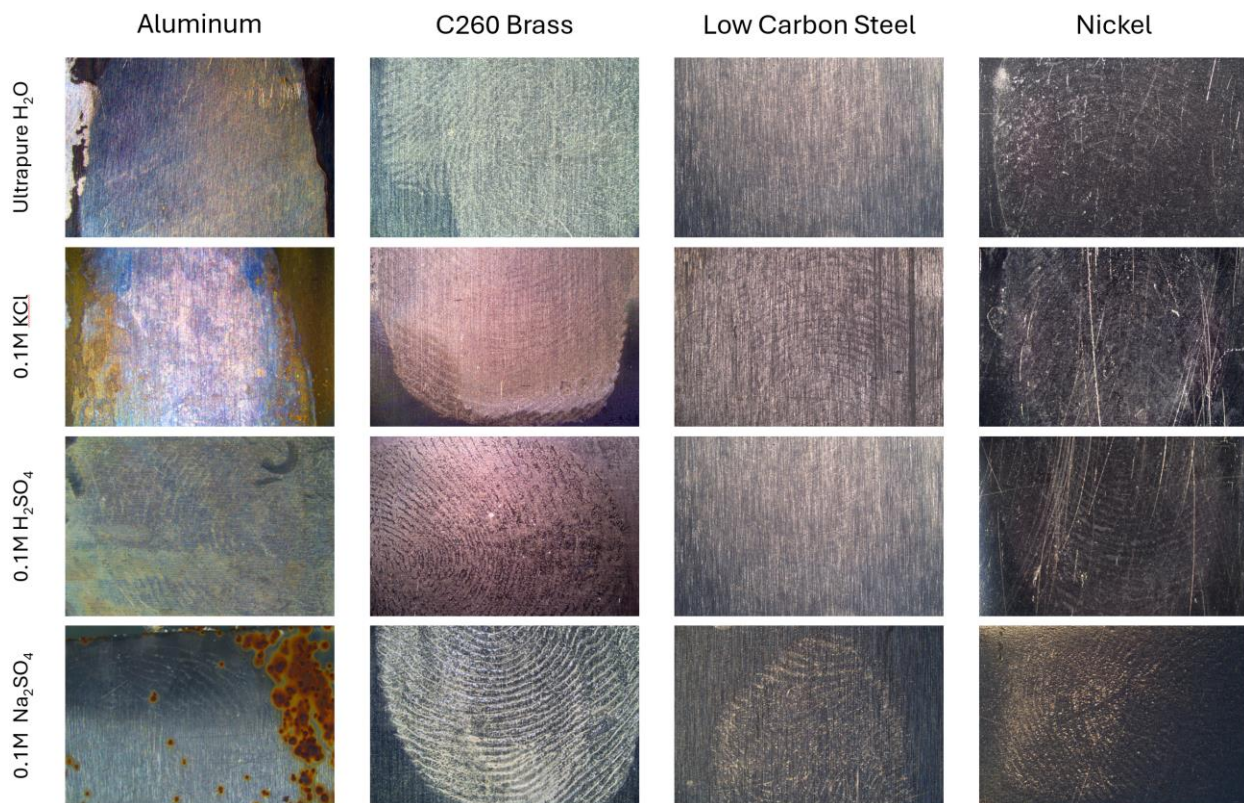


Figure 11: Images of each of the four substrates, with sebacic fingerprints applied, after soaking for 24 hours in each of the four listed electrolyte solutions. Note that Ultrapure  $\text{H}_2\text{O}$  is the control for this experiment

Results from soak tests performed on sebaceous fingerprinted substrates are shown above in Figure 11. Ultrapure water caused severe, uneven corrosion on the 6061-Aluminum alloy samples and caused a slight cloudiness over the background of C260 brass, low-carbon steel and 400-Nickel alloy samples where there was no fingerprint residue. This is likely because the sebaceous residue is acting as an insulator for the substrate surfaces. It is important to note that applied sebaceous fingerprints were visible prior to the soak tests and remained unchanged in all samples aside from 6061-Aluminum alloy. If similar fingerprints had been found during a forensic investigation, they would not have warranted any of the processing methods discussed in this dissertation. 0.1M KCl showed results similar to ultrapure water with all 6061-Aluminum alloy samples suffering severe, uneven corrosion and the remaining three substrate types showing visible sebaceous fingerprints both before and after soaking. The results from 0.1M H<sub>2</sub>SO<sub>4</sub> showed visible sebaceous fingerprints both before and after soaking on each sample for all four substrate types. 6061-Aluminum alloy samples all displayed uneven corrosion that interfered with visibility of approximately one third of each fingerprint. 0.1M Na<sub>2</sub>SO<sub>4</sub> caused severe, uneven corrosion on the 6061-Aluminum alloy samples and left clearly visible fingerprints on all remaining substrate types and samples.

The inherent visibility of sebaceous fingerprints shown in most samples across the four substrate types after having been submerged in water, acidic solutions, and other aqueous electrolyte solutions for 24 hours, coupled with the success of well-established fingerprint development techniques for organic fingerprint residue components, marked the end of sebaceous fingerprint research in this dissertation. Decisions regarding suitable electrolyte solutions for the experiments that follow were made based on results from non-fingerprinted and eccrine-fingerprinted samples. The results of the control samples, those submerged in ultrapure

water, also did not contribute to decisions regarding electrolyte solutions. The summary of all data obtained, shown below in Table 4, has the remaining results printed in bold and italicized text for clarity.

Table 4: Electrolyte solution soak test results

|                         | Fingerprints | Ultrapure H <sub>2</sub> O | 0.1M H <sub>2</sub> SO <sub>4</sub> | 0.1M KCl                       | 0.1M Na <sub>2</sub> SO <sub>4</sub> |
|-------------------------|--------------|----------------------------|-------------------------------------|--------------------------------|--------------------------------------|
| <b>6061-Aluminum</b>    | None         | Severe corrosion           | <i>Severe corrosion</i>             | <i>Severe corrosion</i>        | <i>Severe corrosion</i>              |
|                         | Eccrine      | Severe corrosion           | <i>Visible print shown 3:3</i>      | <i>Visible print shown 1:3</i> | <i>Severe corrosion</i>              |
|                         | Sebaceous    | Severe corrosion           | Uneven corrosion                    | Severe corrosion               | Severe corrosion                     |
| <b>C260 Brass</b>       | None         | Slight cloudiness          | <i>Slight cloudiness</i>            | <i>Severe corrosion</i>        | <i>Moderate corrosion</i>            |
|                         | Eccrine      | Severe corrosion           | <i>Visible print shown 3:3</i>      | <i>Severe corrosion</i>        | <i>Severe corrosion</i>              |
|                         | Sebaceous    | Visible print shown 3:3    | Visible print shown 3:3             | Visible print shown 3:3        | Visible print shown 3:3              |
| <b>Low-carbon Steel</b> | None         | Slight cloudiness          | <i>Darker spots</i>                 | <i>Severe corrosion</i>        | <i>No visible corrosion</i>          |
|                         | Eccrine      | Slight cloudiness          | <i>Darker spots</i>                 | <i>Severe corrosion</i>        | <i>Visible print shown 2:3</i>       |
|                         | Sebaceous    | Visible print shown 3:3    | Visible print shown 3:3             | Visible print shown 3:3        | Visible print shown 3:3              |
| <b>400-Nickel</b>       | None         | Slight cloudiness          | <i>Some streaking</i>               | <i>Severe corrosion</i>        | <i>No visible corrosion</i>          |
|                         | Eccrine      | Slight cloudiness          | <i>Visible print shown 3:3</i>      | <i>Visible print shown 1:3</i> | <i>Severe corrosion</i>              |



|           |                            |                            |                            |                            |
|-----------|----------------------------|----------------------------|----------------------------|----------------------------|
| Sebacious | Visible print<br>shown 3:3 | Visible print<br>shown 3:3 | Visible print<br>shown 3:3 | Visible print<br>shown 3:3 |
|-----------|----------------------------|----------------------------|----------------------------|----------------------------|

The results of the soak tests suggest that 0.1M KCl may not be suitable for use because it caused severe corrosion to all samples of all substrate types. Despite it revealing portions of an eccrine fingerprint in one 6061-Aluminum alloy and one 400-Nickel alloy sample, it does not provide enough evenness, in terms of corrosion, or reliability to be selected as the electrolyte solution for further research. The soak tests pointed to 0.1M H<sub>2</sub>SO<sub>4</sub> as the best electrolyte solution for 6061-Aluminum alloy, C260 brass and 400-Nickel alloy as all three samples across these substrate types showed corrosion that was largely even across the surface, while also revealing portions of the eccrine fingerprints in each sample. Unlike 0.1M KCl, the entire fingerprint was developed more evenly in each of these samples as well. Lastly, the results indicated that 0.1M Na<sub>2</sub>SO<sub>4</sub> is likely suitable for low-carbon steel measurements with the eccrine fingerprints on two out of three samples having been revealed. Due to the varying levels in surface corrosion observed in 6061-Aluminum alloy, C260 brass, low-carbon steel, and 400-Nickel alloy in 0.1M H<sub>2</sub>SO<sub>4</sub> during the qualitative assessment, a concentration comparison study including 0.5M H<sub>2</sub>SO<sub>4</sub> was added to the open circuit potential studies.

### 3.3.2 Open Circuit Potential Studies

These experiments aim to better explain the qualitative results from the electrolyte solution soak tests. Open circuit potential measurements were conducted to quantitatively characterize the substrate-solution interactions and potentially explain variations that can arise from these interactions as well as electrolyte solution concentration. These studies were done on samples without fingerprints to remove the additional variables stemming from fingerprint residue components. A comprehensive understanding of the open circuit potential is paramount because this value is required for the optimization of other corrosion measurements and, more importantly, it directly correlates to the unique corrosion potential for each of the four substrates.

Ten open circuit potential measurements for each substrate type in each electrolyte solution, including the two varying concentrations for sulfuric acid, were conducted. Each trial ran for exactly one hour to evaluate the stability of open circuit potential values over time. Figures 12 and 13 are graphical representations of the open circuit potential values over the course of one hour. Figure 12 displays the concentration comparison study between 0.1M H<sub>2</sub>SO<sub>4</sub> and 0.5M H<sub>2</sub>SO<sub>4</sub> and Figure 13 displays the values for all substrates in the other two electrolyte solutions: 0.1M KCl and 0.1M Na<sub>2</sub>SO<sub>4</sub>. Each line represents the average of the ten trials conducted per substrate type.

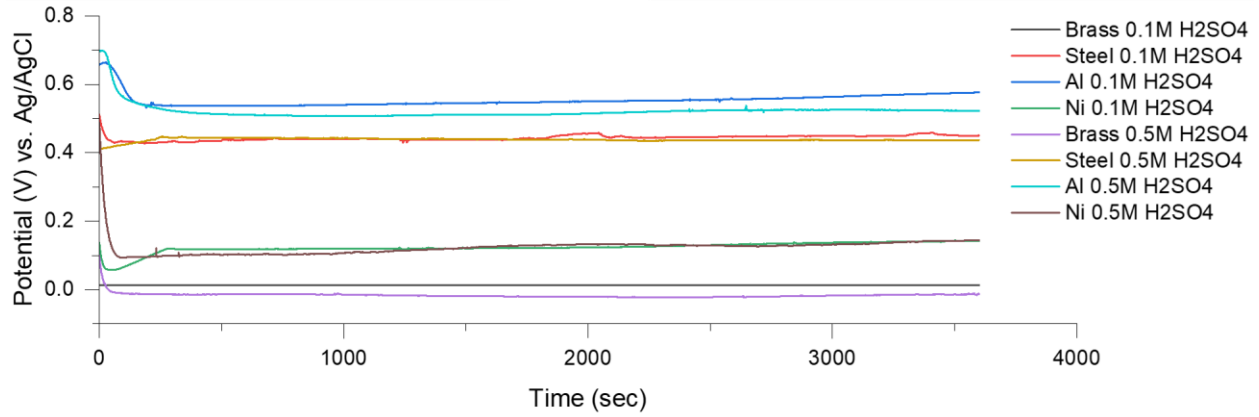


Figure 12: Open circuit potential graph with each line representing the average of 10 trials of each respective substrate in varying concentrations (0.1M H<sub>2</sub>SO<sub>4</sub> and 0.5M H<sub>2</sub>SO<sub>4</sub>) of sulfuric acid

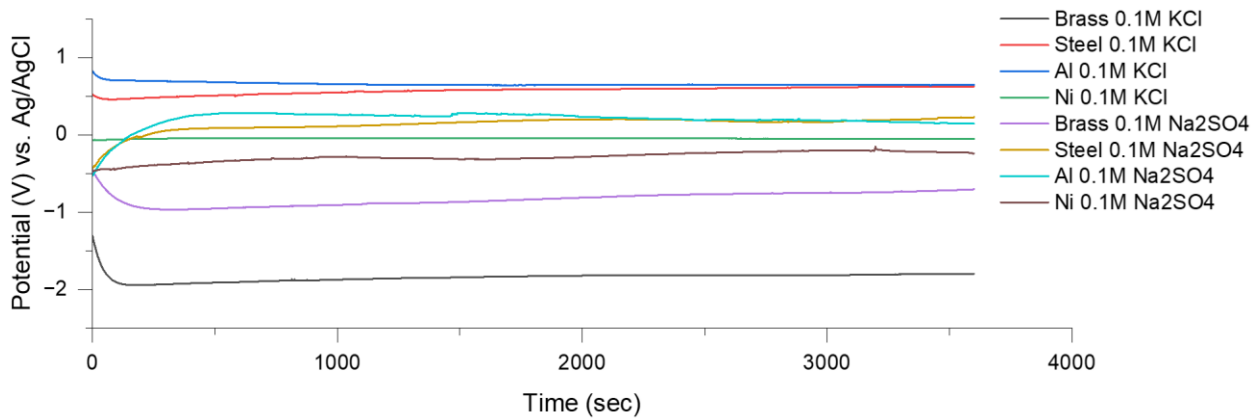


Figure 13: Open circuit potential graph with each line representing the average of 10 trials of each respective substrate in either 0.1M KCl or 0.1M Na<sub>2</sub>SO<sub>4</sub>

Comparing the effects of electrolyte solution concentration, 0.5M H<sub>2</sub>SO<sub>4</sub> produced consistently lower corrosion potential values across all four substrate types. A lower corrosion potential indicates that the substrates are corroding more readily, which was to be expected with

the higher concentration of sulfuric acid. The higher acid concentration also yielded less repeatable results. This, combined with the fact that increasing acid concentration increases cost per trial, ruled out 0.5M H<sub>2</sub>SO<sub>4</sub> as a suitable electrolyte solution.

Perhaps the most important discovery was the hydrogen gas evolution that occurred on all low-carbon steel samples placed in either 0.1M H<sub>2</sub>SO<sub>4</sub> or 0.5M H<sub>2</sub>SO<sub>4</sub> electrolyte solution. Again, this is without the addition of an applied potential or current. Considering the addition of potential or current would only increase this effect, the gas bubbles formed on the substrate surface would undoubtedly interfere with targeted corrosion enhancement of any present latent fingerprints. In line with the previous findings, these results reinforce ruling out 0.1M H<sub>2</sub>SO<sub>4</sub> or 0.5M H<sub>2</sub>SO<sub>4</sub> for low-carbon steel measurements. These results also reinforce ruling out 0.1M KCl as an electrolyte solution due to the inconsistency across trials per substrate and the current limit of the instrument having been reached for all but one of the C260 brass samples. This may be due to the aggressive chloride ions present in this solution. Table 5 depicts the mean corrosion potential over the last 3000 seconds of the hour-long measurements for ten trials of each substrate in each electrolyte solution and varying concentration.

Table 5: Electrolyte solution and electrolyte concentration effects on corrosion potential with potentials measured versus Ag/AgCl reference electrode

|                         | $E_{Corr}$ (mV)<br>0.1M H <sub>2</sub> SO <sub>4</sub> | $E_{Corr}$ (mV)<br>0.5M H <sub>2</sub> SO <sub>4</sub> | $E_{Corr}$ (mV)<br>0.1M KCl | $E_{Corr}$ (mV)<br>0.1M Na <sub>2</sub> SO <sub>4</sub> |
|-------------------------|--|--|-----------------------------|---|
| <b>6061-Aluminum</b>    | 554  | 521  | -657                        | -225  |
| <b>C260 Brass</b>       | -13.0  | -17.0  | -1843                       | -829  |
| <b>Low-carbon Steel</b> | 476  | 379  | -571                        | -438  |
| <b>400-Nickel</b>       | 134  | 123  | -47                         | -283  |

When interpreting the corrosion potential values obtained from the open circuit potential measurements, it is essential to understand the implications of these values on the corrosion behavior of the substrates. The corrosion potential indicates the tendency of a metal to corrode in a given environment. More positive values generally signify a lower tendency for corrosion, as the metal is more noble and less likely to lose electrons and undergo oxidation. Conversely, more negative values indicate a higher propensity for corrosion, as the metal is more active and more likely to oxidize.

For the purposes of this study, the preferred corrosion potential values depend on the specific objectives of the corrosion enhancement technique. If the goal is to achieve a controlled and uniform corrosion process that can enhance the visibility of latent fingerprints, slightly negative corrosion potential values may be preferred. These values suggest a moderate corrosion rate that can etch the fingerprint patterns into the substrate without causing excessive damage or uneven corrosion. For example, the 0.1M H<sub>2</sub>SO<sub>4</sub> solution showed more stable and moderate

corrosion potential values for 6061-Aluminum and 400-Nickel alloy, which can be beneficial for targeted corrosion enhancement. On the other hand, extremely negative corrosion potential values, such as those observed with 0.1M KCl for C260 brass (-1843 mV) and 6061-Aluminum (-657 mV), indicate aggressive corrosion. This level of corrosion may not be desirable as it can lead to rapid and uneven degradation of the metal surface, potentially obliterating the fine details of the fingerprint patterns. Therefore, the optimal corrosion potential values for corrosion enhancement are those that are negative enough to promote corrosion but not so negative that they cause excessive or uneven degradation. In this study, 0.1M H<sub>2</sub>SO<sub>4</sub> for most metals and 0.1M Na<sub>2</sub>SO<sub>4</sub> for low-carbon steel provided the best balance of corrosion activity and stability, making them suitable choices for further targeted corrosion enhancement experiments.

In summary, while both more positive and more negative corrosion potential values have their implications, a moderate negative corrosion potential value tends to provide the most controlled and effective corrosion for the purpose of enhancing latent fingerprints. This balance is crucial for achieving the desired forensic outcomes while preserving the integrity of the fingerprint details.

### **3.3.3 Dissolved Oxygen Study**

It is important to note that C260 brass and low-carbon steel samples yielded the most repeatable measurements overall in their respective optimized electrolyte solutions. Some variation among corrosion potential values is to be expected as corrosion systems are time-varying, and not mass-transport controlled, which ultimately complicates reproducibility of

results. To understand if the effects of this can be reduced, a dissolved oxygen study was conducted. Because C260 brass and low-carbon steel yielded the most repeatable results thus far, three trials of corrosion potential measurements for each substrate, in their respective optimized electrolyte solutions, were conducted in two different environments. Three trials of each substrate were conducted while exposed to ambient air, as with all other research thus far, and a second set of three trials of each substrate utilized electrolyte solutions de-gassed with Nitrogen for 20 minutes prior to experimentation. A nitrogen blanket was also maintained inside the electrochemical cell for the duration of each de-gassed experiment to ensure that the electrolyte solutions remained free of dissolved oxygen. The open circuit potential values were monitored for one hour and the standard deviation amongst the three trials for each substrate in either environment was compared. Table 6 displays the results from these measurements along with their standard deviations.

Table 6: Results of dissolved oxygen study where metal substrates exposed to ambient air, and those kept in an environment free of dissolved oxygen, were compared to elucidate the effects on standard deviation amongst trials. Potentials measured versus Ag/AgCl reference electrode

|                         | $E_{Corr}$ (mV) | $E_{Corr}$ (mV)          |
|-------------------------|-----------------|--------------------------|
|                         | Ambient Air     | N <sub>2</sub> De-gassed |
| <b>C260 Brass</b>       | -18.7 ± 0.030   | -46.8 ± 0.017            |
| <b>Low-carbon Steel</b> | -545 ± 0.034    | -676 ± 0.037             |

The standard deviation amongst the C260 brass trials decreased with de-gassed electrolyte solutions but the change is not significant enough to suggest that removing dissolved oxygen would decrease variation between samples in any meaningful way. Standard deviation amongst low-carbon steel samples was essentially unaffected which also does not support the additional step of removing dissolved oxygen. Naturally, de-gassing the solutions also significantly increases the cost of this technique which is not justified by the findings herein.

### **3.3.4 Potentiodynamic Corrosion Studies**

Proceeding with 0.1M H<sub>2</sub>SO<sub>4</sub> as the electrolyte solution for 6061-Aluminum alloy, C260 brass and 400-Nickel alloy, and 0.1M Na<sub>2</sub>SO<sub>4</sub> for low carbon steel, a preliminary corrosion characterization assessment was conducted in ambient air to begin baseline optimization of targeted corrosion enhancement as a latent fingerprint development technique. Five linear sweep voltammetry measurements were performed on each of the four substrates. These measurements consisted of a potential sweep from -250 mV to +250 mV with respect to the open circuit potential and lasted approximately 55 minutes per trial. The substrates each possessed one eccrine fingerprint.

Figures 14 through 17 represent before and after photos of three trials of each of the four substrates. These are meant to serve as a qualitative analysis of the overall success of targeted corrosion enhancement as a latent fingerprint technique. Table 7 is a summary of all development grades obtained for each of the four substrates, relying solely on the before and after images and the grading system put forth by Bandey et al. Tafel plots and the corresponding



values obtained using linear sweep voltammetry, constituting the quantitative half of the analysis, is discussed immediately after.

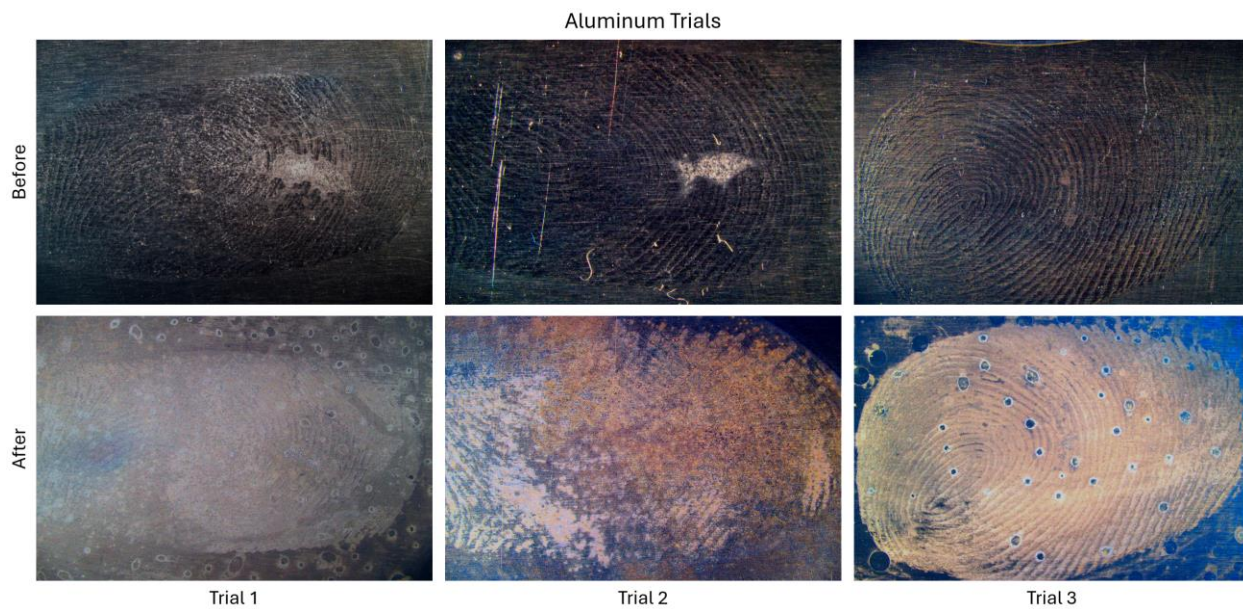


Figure 14: Before and after images of three out of five 6061-Aluminum alloy samples subject to potentiodynamic corrosion via linear sweep voltammetry ranging from + 250 mV to – 250 mV versus the open circuit potential of the substrate

Figure 14 displays before and after images for three of five 6061-Aluminum alloy samples subjected to targeted corrosion enhancement. It is important to note that four of these samples had visible fingerprint residue on the surface prior to enhancement. After enhancement, small dots of uneven corrosion or uneven corrosion across the surface were observed. Due to the visibility of fingerprint residue prior to enhancement, targeted corrosion enhancement would likely not be necessary. The unevenness of corrosion seen in both the soak tests and now the

potentiodynamic corrosion studies suggest that 6061-Aluminum alloy may not be a candidate for corrosion-based enhancement methods.

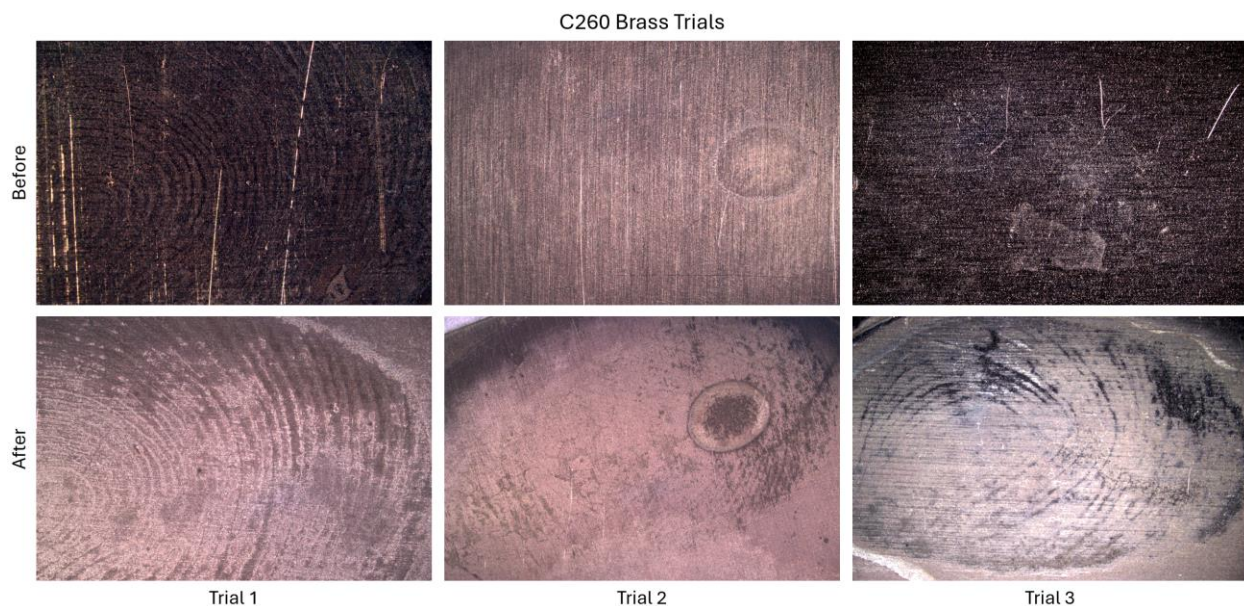


Figure 15: Before and after images of three out of five C260 brass samples subject to potentiodynamic corrosion via linear sweep voltammetry ranging from + 250 mV to – 250 mV versus the open circuit potential of the substrate

Figure 15 displays before and after images for three of five C260 brass samples subjected to targeted corrosion enhancement. Unlike the 6061-Aluminum alloy samples, fingerprint residue and discernible fingerprint ridges were completely absent prior to enhancement in three of five samples, and only one third of a fourth sample had discernible fingerprint ridges. Trial 1 in Figure 15 shows the only sample that had more than one third of a discernible fingerprint. The result after targeted corrosion enhancement, when compared with the other C260 brass samples, suggests that more fingerprint residue yields greater clarity and resolution in the developed

fingerprint after targeted corrosion enhancement. However, the remaining samples demonstrate that a large amount of fingerprint residue is not necessary for targeted corrosion enhancement to generate a fingerprint that is able to be visualized. These results suggest that this is a viable enhancement method for latent fingerprints on C260 brass substrates. This is encouraging as C260 brass is the specific type of brass used in ammunition manufacturing.

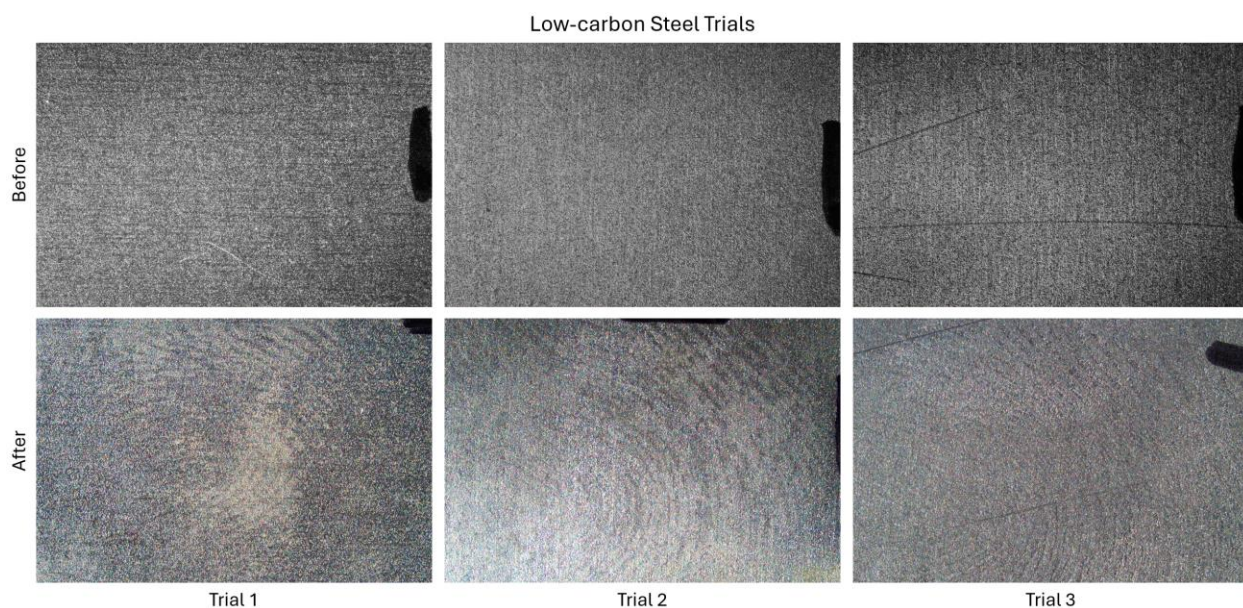


Figure 16: Before and after images of three out of five low-carbon steel samples subject to potentiodynamic corrosion via linear sweep voltammetry ranging from + 250 mV to – 250 mV versus the open circuit potential of the substrate

Figure 16 shows three sets of before and after photos of low-carbon steel samples subjected to targeted corrosion enhancement. There was no visible fingerprint residue or discernible fingerprint ridges in any of the five samples. Upon completion of linear sweep voltammetry, all samples displayed a development grade of 3 or higher. Though corrosion was

uneven across the surface of some samples, the fingerprint ridges were still very clearly resolved. Amongst the four metal substrates, the most consistent development in terms of both starting and ending grades was seen in the low-carbon steel samples. In Figure 16 above, it is interesting that Trial 3 shows the corrosion of the substrate was enough to etch the fingerprint into the surface and also reduce, but not completely get rid of, some of the linear scratches that were present on the substrate surface from the manufacturer. This provides some insight as to the amount of surface corrosion necessary to etch, yet not destroy, the fingerprint. To quantify this, further studies may aim to measure the average depth of the etched fingerprint ridges.

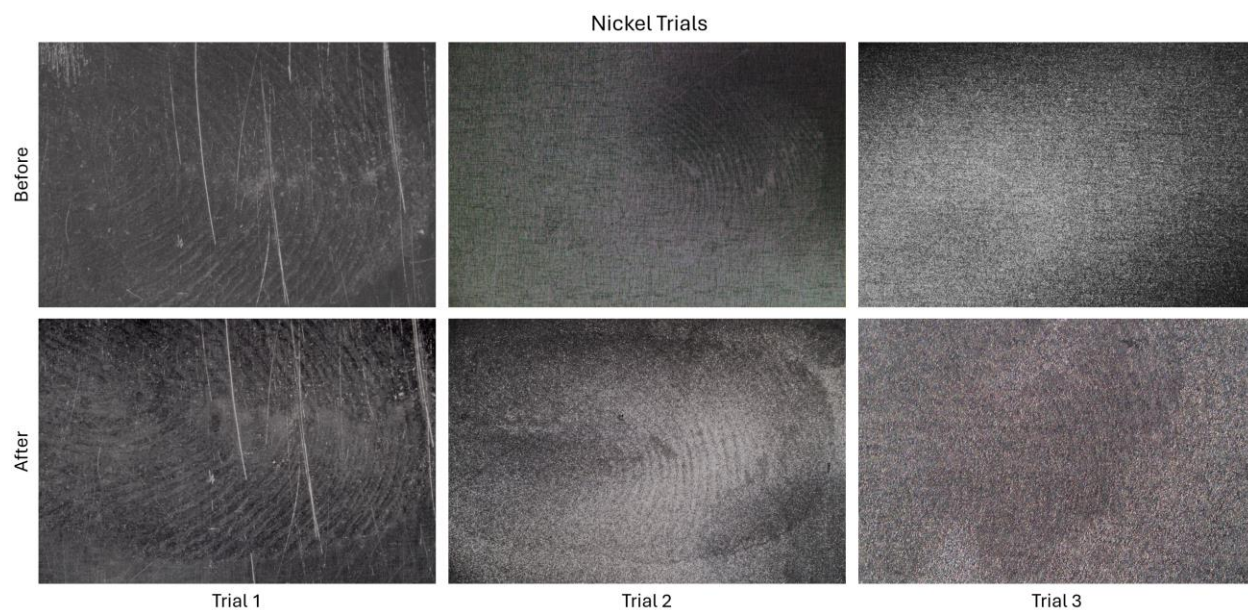


Figure 17: Before and after images of three out of five 400-Nickel alloy samples subject to potentiodynamic corrosion via linear sweep voltammetry ranging from + 250 mV to - 250 mV versus the open circuit potential of the substrate

Figure 17 displays three sets of before and after photos of 400-Nickel alloy samples subjected to the same targeted corrosion enhancement as the other substrates. At the start, two samples had no visible fingerprint residue or discernible fingerprint ridges, two samples displayed less than one third of a discernible fingerprint and one sample (Trial 1 in Figure 17 above) displayed two thirds of a discernible fingerprint. Similar to the results seen with the C260 brass samples, a larger amount of visible fingerprint residue at the start correlated to more resolution within the developed fingerprint after targeted corrosion enhancement. Also similar to the C260 brass results, the remaining samples show that the technique is still successful with little to no visible fingerprint residue at the start. Similar to the 400-Nickel alloy samples, uneven corrosion across the substrate surface was observed but the fingerprint ridges were still very clearly resolved after targeted corrosion enhancement. The unevenness caused darker and lighter areas within the developed fingerprint which may be due to variations in passive oxide layers formed on the 400-Nickel alloy surface. Of the four metal substrates, this is the most corrosion-resistant material which may have a more pronounced effect on fingerprint development than what was previously seen with the other substrates.

Table 7: Average fingerprint development grades on four substrates

|                         | <b>Average<br/>Starting Grade</b> | <b>Average<br/>End Grade</b> | <b>Average <math>\Delta</math><br/>Fingerprint Grade</b> |
|-------------------------|-----------------------------------|------------------------------|--|
| <b>6061-Aluminum</b>    | 3.2                               | 3.4                          | 0.2  |
| <b>C260 Brass</b>       | 0.4                               | 3.4                          | 3.0  |
| <b>Low-carbon Steel</b> | 0                                 | 3.4                          | 3.4  |
| <b>400-Nickel</b>       | 0.8                               | 3                            | 2.2  |

Table 7 is representative of the average starting grades, average end grades, and the average overall change in fingerprint development per each metal substrate type. Eccrine fingerprint residue remains very visible on 6061-Aluminum alloy substrates; this technique is likely unnecessary for that reason. However, an average change in fingerprint grade of 0.2 suggests that this technique is simply not viable for 6061-Aluminum alloy substrates, regardless of fingerprint residue visibility. C260 brass and low-carbon steel, with an average overall change in fingerprint development of 3.0 and 3.4, respectively, saw dramatic improvements in fingerprint visibility after targeted corrosion enhancement. The data demonstrates that this technique can successfully etch fingerprints into these metal substrates for improved visibility and subsequent use in the identification of suspects. 400-Nickel alloy samples displayed an average overall change in fingerprint development of 2.2 which may make it an attractive area for further research. Utilizing a score of 3.0 as the benchmark for success, the results of 400-Nickel alloy studies suggest that improved optimization of parameters may yield a higher development grade and increased visualization after targeted corrosion enhancement.

Figures 18 through 21 display the resulting voltammograms from linear sweep voltammetry performed on 6061-Aluminum alloy, C260 brass, low-carbon steel and 400-Nickel alloy, respectively. Three trials of each substrate, without applied fingerprints, are shown. Samples without fingerprints were utilized in this study to minimize variability caused by components of fingerprint residue and gain more accurate values for further studies.

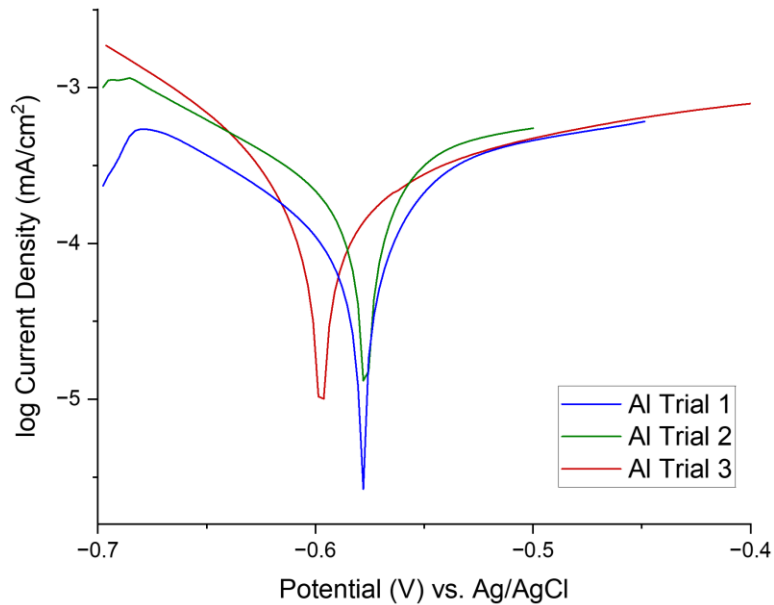


Figure 18: Linear sweep voltammogram and resulting Tafel plot overlay for three trials of 6061-Aluminum alloy in 0.1M H<sub>2</sub>SO<sub>4</sub> electrolyte solution for the commencement of potentiodynamic corrosion

Voltammogram results from 6061-Aluminum alloy trials were extremely inconsistent with some trials showing an  $E_{Corr}$  value of up to -0.18 V. This was the largest difference in  $E_{Corr}$  values seen across the four substrates. The resulting voltammograms were also often noisy with the pertinent end values difficult to distinguish at all. Nine trials, in total, were performed to

obtain three trials that were reasonably aligned in terms of the values obtained with Tafel analysis. The potential range also needed adjusting to reduce noise in the voltammograms. This inconsistency may be due to the formation of an aluminum oxide passivation layer on the surface, which varies in thickness and composition across different samples. It may also be due to the level of pitting corrosion that initiates on the substrate surface given the circumstances. To mitigate these discrepancies, future studies could involve pre-treating the aluminum samples to standardize the oxide layer or employing more controlled environmental conditions to reduce variability.

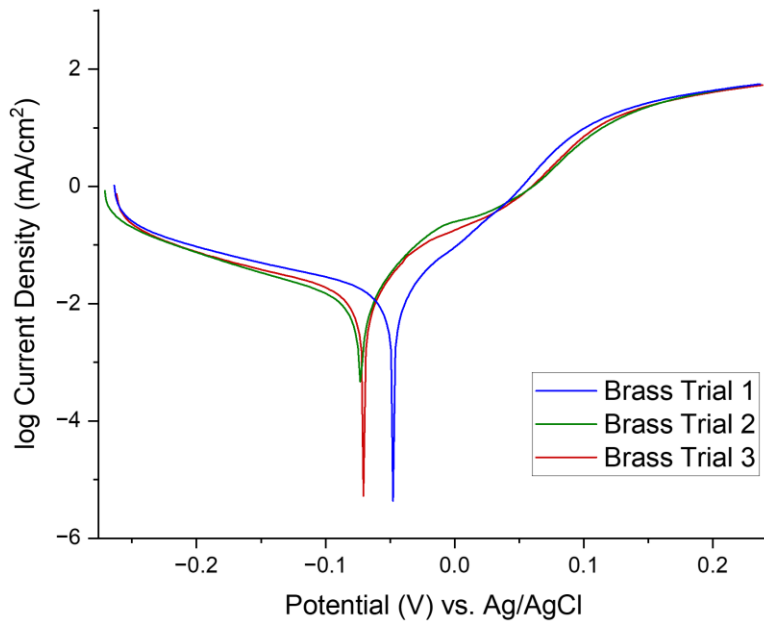


Figure 19: Linear sweep voltammograms and resulting Tafel plot overlay for three trials of C260 brass in 0.1M H<sub>2</sub>SO<sub>4</sub> electrolyte solution for the commencement of potentiodynamic corrosion



C260 brass voltammograms shown in Figure 19 were more repeatable and the increase in preciseness that is typically seen in the cathodic half of Tafel plots was present. None of the voltammograms exhibited the noise that was seen in some of the 6061-Aluminum alloy samples. Both the cathodic and anodic halves of the voltammograms exhibit similar shape and slope amongst the three trials which supports the accuracy of the values obtained for  $E_{Corr}$  and  $I_{Corr}$ . The voltammograms, repeatability and accuracy all support 0.1M H<sub>2</sub>SO<sub>4</sub> as the optimal electrolyte solution choice for C260 brass measurements.

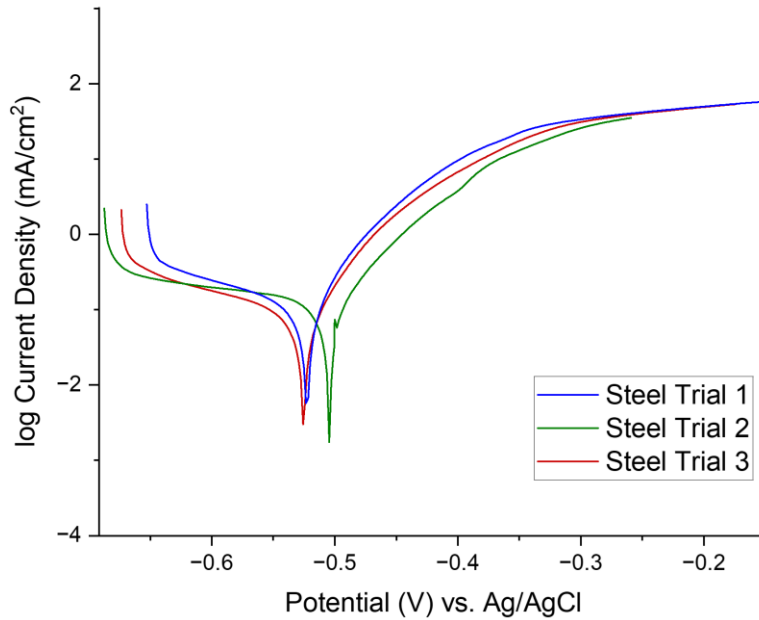


Figure 20: Linear sweep voltammograms and resulting Tafel plot overlay for three trials of low-carbon steel in 0.1M Na<sub>2</sub>SO<sub>4</sub> electrolyte solution for the commencement of potentiodynamic corrosion

Figure 20 represents three linear sweep voltammograms for low-carbon steel. Results like those obtained in the C260 brass voltammograms were also obtained with the low-carbon steel

samples. Repeatability was not a challenge faced and additional trials, aside from the three that were planned, were not required to obtain values for  $E_{Corr}$  and  $I_{Corr}$  that were reasonably close. The noise exhibited in the 6061-Aluminum alloy samples was absent aside from one small area in the anodic region of trial 2, as shown above. It is also important to note that hydrogen evolution was absent in all three trials, despite them spanning a range of 0.5 V and lasting for approximately 55 minutes each. No air bubbles or other unevenness in surface corrosion that would interfere with fingerprint visibility was noted in any of the three trials. This supports 0.1M  $\text{Na}_2\text{SO}_4$  as the optimal electrolyte solution choice for low-carbon steel measurements. The subtle differences in the Tafel plots may be caused by variations in the surface treatment of the substrates prior to the studies. Standardizing the pre-treatment processes, such as gentle polishing or alternate methods of cleaning prior to electrochemical corrosion, could help mitigate these differences and improve the reproducibility of the results.

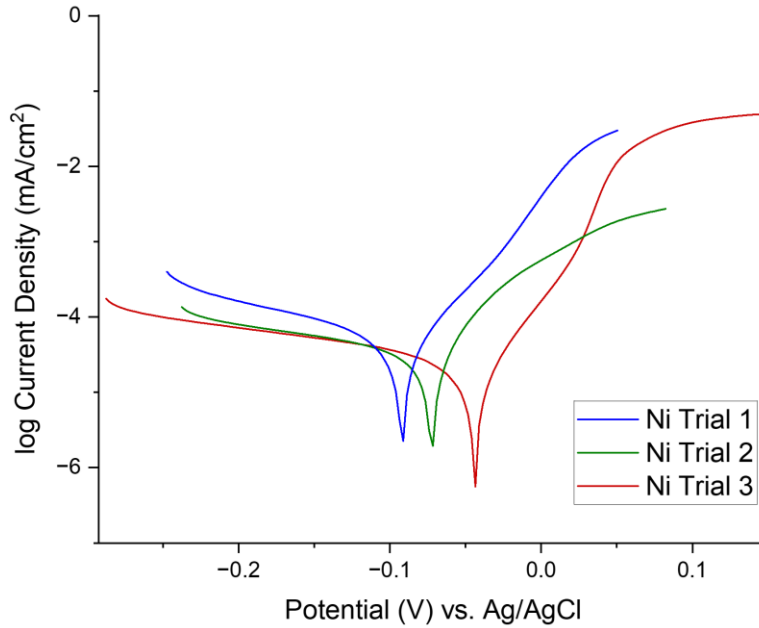


Figure 21: Linear sweep voltammogram and resulting Tafel plot overlay for three trials of 400-Nickel alloy in 0.1M  $H_2SO_4$  electrolyte solution for the commencement of potentiodynamic corrosion

400-Nickel alloy voltammograms experienced the same challenge with repeatability that was present with 6061-Aluminum alloy trials. Neither the anodic nor cathodic slopes are closely aligned in the three trials. Six trials, in total, were performed to obtain three trials that were reasonably aligned in terms of the values elucidated during Tafel analysis. None of the 400-Nickel alloy voltammograms exhibited any noise and there was no unevenness in surface corrosion noted on any of the sample substrate surfaces. Despite the absence of noise, the results indicate that further optimization may be required for 400-Nickel alloy substrates as the values obtained from Tafel analysis are not as consistent as the values for C260 brass and low-carbon steel. This may also be a product of the fact that 400-Nickel alloy is the most corrosion resistant substrate of the four tested and initiating corrosion reactions on this substrate surface requires a

more substantial energy input than the others. Pre-treatment processes, such as using different electrolyte compositions, could be explored to enhance the consistency of results.

Tafel analysis performed on the resulting voltammograms yielded values for the corrosion potential ( $E_{corr}$ ), corrosion current density ( $I_{corr}$ ), and cathodic ( $\beta_C$ ) and anodic ( $\beta_A$ ) Tafel coefficient values. The results of Tafel analysis using the Tafel Fit Tool within the BioLogic software, as described above using Equation 23, are displayed below in Table 8. Ultra-formable C260 brass substrates returned a more noble  $E_{corr}$  value of -66.7 mV and a  $I_{corr}$  value of 12.9  $\mu$ A. Low-carbon steel substrates returned a more active  $E_{corr}$  value of -525 mV and a  $I_{corr}$  value of 106  $\mu$ A. Though the data shows 6061-Aluminum alloy, low-carbon steel and 400-Nickel alloy substrates require less of an applied electrical potential to initiate corrosion, it also demonstrated that the C260 brass substrates require the least current to initiate corrosion which is an important consideration for any future galvanostatic corrosion studies. 6061-Aluminum alloy, low-carbon steel and 400-Nickel alloy substrates all require a larger applied current to initiate corrosion of the substrate with 400-Nickel alloy requiring the most current. This aligns with it being the most corrosion resistant substrate of the four tested.

Table 8: Tafel analysis yielding corrosion potential, corrosion current, cathodic tafel coefficient, and anodic tafel coefficient for both C260 brass and low-carbon steel substrates

| Substrate               | $E_{Corr}$ (mV) | $I_{Corr}$ ( $\mu A$ ) | $\beta_c$ (mV/Decade) | $\beta_A$ (mV/Decade) |
|-------------------------|-----------------|------------------------|-----------------------|-----------------------|
| <b>6061-Aluminum</b>    | -584            | 92.1                   | 337                   | 71.3                  |
| <b>C260 Brass</b>       | -66.7           | 12.9                   | 156                   | 62.6                  |
| <b>Low-carbon Steel</b> | -525            | 106                    | 299                   | 59.0                  |
| <b>400-Nickel</b>       | -71.3           | 144                    | 146                   | 64.0                  |

Comparing the values in Table 8 with those in Tables 5 and 6 above, some deviation amongst corrosion potential values is observed. Corrosion systems are time-varying which may account for some of this deviation. There is also variation amongst batches of metal samples that likely causes some deviation as well. The differences in the batches may arise from variations in the manufacturing process, including differences in alloy composition, surface finish, and previous exposure to environmental conditions. These factors can lead to inconsistencies in the surface properties and, consequently, the corrosion behavior. To mitigate these differences, ensuring uniform pre-treatment processes such as consistent polishing, cleaning, and storage conditions before experiments is essential.

Lastly, it is well documented that due to variations amongst potentiostat software, equations used and the human-controlled component of choosing linear regions to extrapolate for Tafel slopes yields a level of variation by default [80], [81]. Potentiostatic and galvanostatic studies should then serve to refine the values for  $E_{Corr}$  and  $I_{Corr}$  that were obtained, as well as elucidate optimal parameters for fingerprint visualization with these methods of corrosion.

Further research should also focus on addressing and controlling the underlying reasons for variability in the 6061-Aluminum alloy and 400-Nickel alloy experiments. Possible causes include the formation of uneven passive oxide layers, variations in sample preparation, and inherent differences in the microstructure of the alloy. Standardizing sample preparation, conducting more controlled environmental studies, and exploring different electrolyte compositions could help address these issues and improve repeatability.

### **3.3.5 Potentiostatic Corrosion Studies**

It is important to note that potentiodynamic corrosion of the substrate takes approximately 55 minutes per sample to complete. Potentiostatic and galvanostatic corrosion are considered in this research as potentially attractive alternatives because they take advantage of the unique properties of each metal substrate, thus exploiting exact parameters to initiate corrosion and enhance fingerprints in a much shorter time frame. The primary objective for potentiostatic and galvanostatic corrosion studies is to optimize the targeted corrosion enhancement technique for performance in under 5 minutes per sample. Naturally, this reduction in time would substantially improve evidence processing throughput, making targeted corrosion enhancement a more feasible option for fingerprint enhancement and visualization. Interestingly, the potential and/or current ranges responsible for hydrogen evolution on steel samples are not reached within the 5-minute time frame and 0.1M H<sub>2</sub>SO<sub>4</sub> could theoretically be utilized as the electrolyte solution for both brass and steel samples. While this would make it easier in terms of preparation and more cost effective with less required solutions, the unevenness in corrosion

witnessed in the soak tests suggest that 0.1M Na<sub>2</sub>SO<sub>4</sub> is still the best choice for low-carbon steel substrates.

Potentiostatic corrosion measurements were conducted on 6061-Aluminum alloy, C260 brass, low-carbon steel and 400-Nickel alloy substrate samples taking the  $E_{Corr}$  value as the starting point and moving 50 mV, 1 V, 1.5 V, and 2 V in the cathodic direction, holding the sample at this applied potential for 5 minutes. The substrates had starting potential points of -554 mV, -66.7 mV, -525 mV and -71.3 mV, respectively. Three trials at each cathodic applied potential were conducted. Because strict control of all potential variables is near impossible with evidence as metals can be from various manufacturers, various places, of various ages, with varying levels of passivation, the applied voltage was also moved by 50 mV, 1 V, 1.5 V, and 2 V, in the anodic direction, to assess fingerprint visibility in both directions. Similarly, three trials at each anodic applied potential were conducted. In each trial, before and after images are assessed for grading. A table with resulting average development grades from each applied potential is shown below in Table 9.

With the addition of +1.0 V with respect to  $E_{Corr}$ , 6061-Aluminum alloy substrates reached the highest average development grade of 1.3. C260 brass substrates reached the highest average development grade of 2.0 at +1.5 V with respect to  $E_{Corr}$ , low-carbon steel substrates reached a grade of 2.0 at an applied potential of +1 V with respect to  $E_{Corr}$  and, finally, 400-Nickel alloy substrates reached a grade of 1.8 at an applied potential of +2.0 V with respect to  $E_{Corr}$ . These findings align with the initial corrosion potential measurements that found low-carbon steel to be more active, or less corrosion resistant, than brass and they also align with the fact that 400-Nickel alloy is the most corrosion-resistant substrate evaluated.

Table 9: Average development grades of ultra-formable C260 brass and low-carbon steel after potentiostatic corrosion. Each sample was held at the listed potential for 5 minutes

|                    | <b>6061-Al</b><br><b>Average <math>\Delta</math></b><br><b>Fingerprint</b><br><b>Grade</b> | <b>C260 Brass</b><br><b>Average <math>\Delta</math></b><br><b>Fingerprint</b><br><b>Grade</b> | <b>Low-carbon Steel</b><br><b>Average <math>\Delta</math></b><br><b>Fingerprint</b><br><b>Grade</b> | <b>400-Nickel</b><br><b>Average <math>\Delta</math></b><br><b>Fingerprint</b><br><b>Grade</b> |
|--------------------|--|---|---|---|
| $E_{Corr} + 2 V$   | 0.3  | 1.3   | 1.3   | 1.8   |
| $E_{Corr} + 1.5 V$ | 0  | 2.0   | 2.0   | 1.3   |
| $E_{Corr} + 1 V$   | 1.3  | 1.3   | 2.3   | 1.3   |
| $E_{Corr} + 50 mV$ | 0  | 1.8   | 1.8   | 0.3   |
| $E_{Corr}$         | 0  | 0.3   | 0.3   | 0   |
| $E_{Corr} - 50 mV$ | 0  | 0   | 0.3   | 0   |
| $E_{Corr} - 1 V$   | 0  | 0   | 0   | 0   |
| $E_{Corr} - 1.5 V$ | 0  | 0   | 0   | 0   |
| $E_{Corr} - 2 V$   | 0  | 0   | 0   | 0   |

Comparing these results to the potentiodynamic corrosion results in Table 7 where C260 brass and low-carbon steel samples had a change in development of 3.0 and 3.4, respectively, the data supports potentiodynamic corrosion as the optimal method of latent fingerprint enhancement and visualization. Overall, fewer samples that were tested from each of the four substrates displayed any development whatsoever of the applied latent fingerprint. The variability and lack of repeatability seen across samples within their respective substrate type are also both indicative of potentiodynamic corrosion as the best choice for targeted corrosion enhancement. For 400-Nickel alloy, further investigations should include higher potentials, such as +2.5 V or even higher, to determine if a plateau in corrosion rates and fingerprint development



grades would be observed. Extending the potential range could provide additional data points to better understand the behavior of nickel alloys under more aggressive corrosion conditions and ensure that the applied potential is sufficient to overcome the inherent passivation and fully exploit the electrochemical processes necessary for effective corrosion and fingerprint development.

### 3.3.6 Galvanostatic Corrosion Studies

Galvanostatic corrosion measurements were conducted on 6061-Aluminum alloy, C260 brass, low-carbon steel and 400-Nickel alloy substrate samples as they were above.

Galvanostatic measurements utilized  $I_{Corr}$ , the corrosion current value, as the starting point. The substrates had starting corrosion points of 92.1  $\mu\text{A}$ , 12.9  $\mu\text{A}$ , 106  $\mu\text{A}$  and 144  $\mu\text{A}$ , respectively. From these starting points, 10  $\mu\text{A}$ , 20  $\mu\text{A}$ , 30  $\mu\text{A}$  and 40  $\mu\text{A}$  were added to this value to assess corrosion when held at these currents. For reasons mentioned previously in potentiostatic studies, 10  $\mu\text{A}$ , 20  $\mu\text{A}$ , 30  $\mu\text{A}$  and 40  $\mu\text{A}$  were also subtracted from this value to assess corrosion at these currents as well. Three samples were conducted at each of the 9 current values, including the individual  $I_{Corr}$  values, themselves. Each measurement lasted a total of five minutes. Before and after images were assessed as they were previously. Table 10 displays the results of these studies.

The highest overall change in development grade of 0.3 for 6061-Aluminum alloy samples was observed at 20 and 30  $\mu\text{A}$  above the  $I_{Corr}$  value. The highest grade of 1.3 was noted at 20  $\mu\text{A}$  above the  $I_{Corr}$  value for C260 brass samples and 30  $\mu\text{A}$  above the  $I_{Corr}$  value for low-

carbon steel samples. In 400-Nickel alloy samples, the highest overall change of 0.7 was observed at 40  $\mu\text{A}$  above the  $I_{\text{Corr}}$  value. The highest average changes in fingerprint grades of 1.3 for both C260 brass and low-carbon steel substrates indicates that galvanostatic corrosion is less effective than both potentiodynamic and potentiostatic corrosion in terms of development of latent fingerprints. The highest changes of 0.3 and 0.7 for 6061-Aluminum alloy and 400-Nickel alloy, respectively, indicate the same. With galvanostatic corrosion producing even less developed samples than potentiostatic corrosion, this points to potentiodynamic as the superior means of targeted corrosion enhancement for the development and visualization of latent fingerprints. Despite the time saved per trial, the data and results do not support the use of galvanostatic corrosion for fingerprint visualization.

Table 10: Average development grades of ultra-formable C260 brass and low-carbon steel after galvanostatic corrosion. Each sample was held at the listed potential for 5 minutes

|   | <b>6061-Al</b><br><b>Average <math>\Delta</math></b><br><b>Fingerprint</b><br><b>Grade</b> | <b>C260 Brass</b><br><b>Average <math>\Delta</math></b><br><b>Fingerprint</b><br><b>Grade</b> | <b>Low-carbon Steel</b><br><b>Average <math>\Delta</math></b><br><b>Fingerprint</b><br><b>Grade</b> | <b>400-Nickel</b><br><b>Average <math>\Delta</math></b><br><b>Fingerprint</b><br><b>Grade</b> |
|---|--|---|---|---|
| <b><math>I_{Corr} + 40 \mu A</math></b> | 0  | 0.7   | 0.7   | 0.7   |
| <b><math>I_{Corr} + 30 \mu A</math></b> | 0.3  | 1.0   | 1.3   | 0.3   |
| <b><math>I_{Corr} + 20 \mu A</math></b> | 0.3  | 1.3   | 0.3   | 0   |
| <b><math>I_{Corr} + 10 \mu A</math></b> | 0  | 0.7   | 1.3   | 0   |
| <b><math>I_{Corr}</math></b>            | 0  | 0.3   | 0.3   | 0   |
| <b><math>I_{Corr} - 10 \mu A</math></b> | 0  | 0   | 0.3   | 0   |
| <b><math>I_{Corr} - 20 \mu A</math></b> | 0  | 0   | 0   | 0   |
| <b><math>I_{Corr} - 30 \mu A</math></b> | 0  | 0   | 0   | 0   |
| <b><math>I_{Corr} - 40 \mu A</math></b> | 0  | 0   | 0   | 0   |

Comparing the results to the potentiodynamic corrosion measurements, the data clearly supports potentiodynamic corrosion as the optimal method for latent fingerprint enhancement. Despite potentiostatic and galvanostatic measurements taking less time, the substantial improvements in fingerprint development seen with potentiodynamic corrosion justify the additional time required. Similar to the potentiostatic studies, further galvanostatic studies should consider extending the current range beyond  $40 \mu A$  above the corrosion current value, particularly for 400-Nickel alloy. Testing higher currents such as  $50 \mu A$  or more above  $I_{Corr}$  could determine if a plateau in fingerprint development is achieved and provide a more

comprehensive understanding of the electrochemical behavior of the nickel alloy under varying current densities.

### **3.4 Conclusion and Future Work**

With the goal of optimizing parameters around the electrochemical corrosion reactions taking place on the substrate surfaces, the electrolyte solution soak tests centered around elucidating proper electrolyte solutions for each substrate type. Across almost all samples from the non-fingerprinted, eccrine fingerprinted and sebaceous fingerprinted groups, 0.1M KCl caused severe, uneven corrosion and was effectively ruled out as an electrolyte solution for any of the four substrate types. Within the samples that were not fingerprinted, 6061-Aluminum alloy did not appear to react well with any electrolyte solution options, C260 brass appeared to interact most favorably with 0.1M H<sub>2</sub>SO<sub>4</sub>, low-carbon steel with 0.1M Na<sub>2</sub>SO<sub>4</sub> and 400-Nickel alloy samples appeared to favor 0.1M H<sub>2</sub>SO<sub>4</sub> but did exhibit some streak marks upon drying.

Amongst samples containing eccrine fingerprints, which comprised the bulk of the data affecting decision-making in this regard, 0.1M H<sub>2</sub>SO<sub>4</sub> yielded the most visibility of the applied eccrine fingerprints in all three 6061-Aluminum alloy, C260 brass, and 400-Nickel alloy samples. Low-carbon steel samples also demonstrated partial visibility of fingerprints despite darker spots and unevenness in corrosion appearing on the substrate surfaces as well. The electrolyte solution yielding the most visibility in the eccrine fingerprint samples on low-carbon steel, however, was 0.1M Na<sub>2</sub>SO<sub>4</sub>. These samples were the driving factor behind the decision to

move forward with 0.1M on 0.1M H<sub>2</sub>SO<sub>4</sub> for 6061-Aluminum alloy, C260 brass and 400-Nickel alloy, and 0.1M Na<sub>2</sub>SO<sub>4</sub> for low-carbon steel.

The sebaceous printed metal samples provided the least in terms of insight. 6061-Aluminum alloy samples displayed severe, uneven corrosion and moderate loss of fingerprint residue regardless of electrolyte solution. However, the majority of samples across all four substrate types displayed visible fingerprint residue and discernible fingerprint ridges both before and after the soak tests. The ambiguity of the majority, coupled with the fact that this technique would not be necessary on a sample that already had a visible fingerprint, was not conducive to elucidating superior electrolyte solutions which is why sebaceous fingerprint results were disregarded in electrolyte solution selection.

Open circuit potential measurements conducted over 60 minutes quantitatively characterize the interactions taking place between substrates and their respective electrolyte solutions. Ten trials for each substrate were conducted in 0.1 and 0.5M H<sub>2</sub>SO<sub>4</sub>, 0.1M KCl and 0.1M Na<sub>2</sub>SO<sub>4</sub>. Amongst the two concentrations of sulfuric acid, the higher concentration produced more negative open circuit potentials and more noise across trials. These results confirmed 0.1M H<sub>2</sub>SO<sub>4</sub> as the optimal electrolyte solution for 6061-Aluminum alloy, C260 brass and 400-Nickel alloy. Hydrogen evolution noted on low-carbon steel samples in both sulfuric acid concentrations confirmed that neither is suitable for low-carbon steel measurements. Lastly, 0.1M KCl provided inconsistent results across trials, across substrate types. This underscores the previous findings of 0.1M KCl being unfit for these measurements and optimization of this latent fingerprint development technique.

Throughout all experiments conducted thus far, C-260 brass and low-carbon steel samples delivered the highest level of consistency across trials and samples. To see if this

consistency could be increased further, dissolved oxygen studies were conducted to assess whether the removal of oxygen in the electrochemical cell yielded a significant decrease in standard deviation amongst trials. Ultimately, de-gassing the electrolyte solutions for C-260 brass and low-carbon steel for 20 minutes prior to experimentation, as well as maintaining a nitrogen blanket within the electrochemical cell, did not provide a meaningful decrease in standard deviation amongst trials. The standard deviation amongst C-260 brass samples was 0.030 for trials conducted in ambient air and 0.017 for those with dissolved oxygen removed. Low-carbon steel samples experienced a nominal increase in standard deviation from 0.034 to 0.037 with the removal of dissolved oxygen from the electrochemical cell. Neither the C-260 brass results nor the low-carbon steel support the removal of dissolved oxygen causing any meaningful improvement in consistency amongst trials. In fact, the data suggests it may worsen results for low-carbon steel. In terms of cost for targeted corrosion enhancement as a latent fingerprint development technique, this is good news. The removal of dissolved oxygen from solution poses a significant addition to the overall cost of the technique and the best-case scenario, here, was for it to be found unnecessary as it was.

With initial characterization complete, three types of corrosion were investigated and compared to determine which yielded the highest grade of fingerprint development and thus, would become the cornerstone of targeted corrosion enhancement as a forensic investigative technique. Pitting corrosion is exploited using potentiodynamic, potentiostatic, and galvanostatic corrosion methods to identify which of the three is best able to target any present eccrine fingerprint residue corrosion and enhance it such that it can be used to positively identify suspects of crime.

Potentiodynamic corrosion, or corrosion over a range of applied electrical potentials, was accomplished via LSV and these measurements yield three important results. Each sample is imaged and assessed, before and after potentiodynamic corrosion, to quantify the change in fingerprint development grade. These grade numbers are then averaged per substrate. Secondly, Tafel analysis is performed on the resulting voltammogram generated through LSV for each sample to generate an  $E_{Corr}$  and  $I_{Corr}$  value, along with anodic ( $\beta_A$ ) and cathodic ( $\beta_C$ ) Tafel coefficients.

To accomplish the first goal, an average fingerprint development grade, the system developed by Bandey et al., was used. Five samples of each of the four metal substrates were imaged, subjected to potentiodynamic corrosion, and then imaged again. Four of five 6061-Aluminum alloy samples displayed discernible fingerprint ridges and the associated residue which equated to an average starting grade of 3.2. After potentiodynamic corrosion, the average end grade was 3.4 which resulted in an average change of 0.2 for 6061-Aluminum alloy samples. This was the lowest average change amongst the four samples. However, the data suggests that 6061-Aluminum alloy surfaces may intrinsically allow for better visualization of latent fingerprints and discernment of ridges than the other metal substrates would without some application of one or more development methods. The results of soak tests and potentiodynamic corrosion of 6061-Aluminum alloy samples suggest that, overall, 6061-Aluminum alloy may not be a prime candidate for corrosion-based enhancement methods.

In contrast to the 6061-Aluminum alloy samples, C260 brass samples had an average starting grade of 0.4 with fingerprint residue and discernible ridges absent completely in three of five samples. After potentiodynamic corrosion, the average end grade achieved was 3.4, yielding an average change of 3.0. One C-260 brass sample displayed approximately two thirds of a

visible fingerprint prior to corrosion and this sample achieved the highest resolution after corrosion. These results imply that more fingerprint residue increases overall resolution of the latent fingerprint after corrosion. However, the remaining four samples and the average change of 3.0 for C-260 brass indicate that this method is still successful in cases where fingerprint residue is almost or completely absent. Lastly, these results align with insight gained from the soak tests which pointed to 0.1M H<sub>2</sub>SO<sub>4</sub> as the optimal electrolyte solution for targeted corrosion enhancement of latent fingerprints on C-260 brass substrates.

Low-carbon steel samples showed no initial fingerprint residue or discernible ridges for an average starting grade of 0. However, potentiodynamic corrosion yielded a development grade of 3 or higher in each of the five samples for an average change in fingerprint grade of 3.4. Despite corrosion having happened somewhat unevenly across the substrate surfaces, fingerprint ridges were still very clearly resolved with this method. Interestingly, Trial 3 displays that potentiodynamic corrosion was sufficient to remove some of the linear scratches that were present on the surface, while also making the latent fingerprint visible. Further research could be aimed at quantifying the depth of corrosion within the fingerprint ridges to better understand the amount of surface corrosion needed to etch, and not destroy, any present latent fingerprints.

400-Nickel alloy substrate samples began with a relatively low average starting grade of 0.8. As previously observed with C-260 brass samples, more fingerprint residue present correlated to higher resolution amongst fingerprint ridges after potentiodynamic corrosion. However, the average end grade and average change in fingerprint grade of 3.0 and 2.2 respectively, indicate that the technique is successful regardless of whether fingerprint residue is initially present on the substrate surface. 400-Nickel alloy is the most corrosion-resistant substrate of the four and this may be the reason for the decreased average change in fingerprint



grade when compared to the 3.0 average for C-260 brass and 3.4 for low-carbon steel. The inherent corrosion resistance opens an area of possible further research. Despite the higher concentration of sulfuric acid decreasing stability in 60-minute open circuit potential measurements, stronger acid electrolyte solutions could potentially yield increased fingerprint development. This was not tested in this dissertation as simplicity and reduced cost were goals outlined in the research fellowship and low-carbon steel already required a different electrolyte solution than the other substrates.

Fingerprint residue adds inherent variability amongst metal substrate samples in LSV measurements. To increase accuracy and precision of values obtained for both  $E_{Corr}$  and  $I_{Corr}$ , three non-fingerprinted samples of each metal substrate type were subjected to the same LSV measurements as the previously imaged and graded fingerprinted samples. This additional step was taken due to the importance of  $E_{Corr}$  and  $I_{Corr}$  values in the potentiostatic and galvanostatic measurements that follow.

Nine total trials of 6061-Aluminum alloy substrate samples were run to obtain three Tafel plots that were reasonably aligned with one another. 6061-Aluminum alloy trials exhibited the highest level of inconsistency and noise across trials with the potential range having been adjusted to reduce both. The aluminum oxide passivation layer and the amount of pitting corrosion initiating on the surface may be the source of discrepancy. Overall, 6061-Aluminum alloy substrate samples yielded an  $E_{Corr}$  value of -584 mV, an  $I_{Corr}$  value of 92.1  $\mu$ A, a cathodic Tafel coefficient of 337 mV/decade and anodic Tafel coefficient of 71.3 mV/decade. C260 brass samples exhibited repeatability, accuracy, and preciseness. Values for  $E_{Corr}$  and  $I_{Corr}$  were -66.7 mV and 12.9  $\mu$ A, respectively, with  $\beta_C$  and  $\beta_A$  values of 156 mV/decade and 62.6 mV/decade. Similarly, low-carbon steel voltammograms were repeatable and provided an  $E_{Corr}$  value of -525

mV,  $I_{Corr}$  of 106  $\mu$ A, and  $\beta_C$  and  $\beta_A$  values of 299 mV/decade and 59 mV/decade. Both C260 brass and low-carbon steel had Tafel plots well within reasonable alignment after three trials and required no further measurements to be done. This, too, supports the choices for optimal electrolyte solutions regarding these two substrates. 400-Nickel alloy samples experienced the same issues with repeatability as 6061-Aluminum alloy, requiring six trials to find three within reasonable alignment. Overall, the values for  $E_{Corr}$  and  $I_{Corr}$  were -71.3 mV and 144  $\mu$ A with  $\beta_C$  and  $\beta_A$  values of 146 and 64.

Potentiostatic measurements with the potential held at various increments above the  $E_{Corr}$  value yielded less reliable results and lower average change in fingerprint grade values across all four substrates. 6061-Aluminum alloy samples experienced the highest average change in fingerprint grade of 1.3 at +1 V above the  $E_{Corr}$  value. C260 brass samples achieved the highest average change in fingerprint grade of 2.0 at +1.5 V above  $E_{Corr}$ . Low-carbon steel, with the best results in terms of potentiostatic corrosion, reached the highest average change in fingerprint grade of 2.3 at +1 V above  $E_{Corr}$ . Lastly, 400-Nickel alloy samples reached an average change in fingerprint grade of 1.8 at +2 V above  $E_{Corr}$ . This, again, aligns with the fact that 400-Nickel alloy is the most corrosion resistant substrate being tested. These numbers are significantly lower than those achieved through potentiodynamic corrosion which indicates that potentiodynamic corrosion performs better than potentiostatic in terms of targeted corrosion enhancement of latent fingerprints. Similarly, galvanostatic corrosion measurements did not exceed those achieved through potentiodynamic corrosion. 6061-Aluminum alloy samples reached a high of 0.3 at both +20 and +30  $\mu$ A above  $I_{Corr}$ . C260 brass samples saw their best average change in fingerprint grade of 1.3 at +20  $\mu$ A above  $I_{Corr}$ . Low-carbon steel achieved the same high of 1.3 at +30  $\mu$ A above  $I_{Corr}$ . And, lastly, 400-Nickel alloy reached a high of 0.7 at

+40  $\mu\text{A}$  above  $I_{\text{Corr}}$ , likely due to its corrosion resistance. The average change in fingerprint grades achieved here are also substantially lower than those gained through potentiodynamic corrosion and provide further evidence that the latter is superior for targeted corrosion enhancement. Despite potentiodynamic corrosion measurements taking approximately 55 minutes to complete, the substantially higher changes in fingerprint grades support the additional time required versus the shorter potentiostatic and galvanostatic measurements.

While potentiodynamic corrosion has shown superior results, it is important to explore alternative conditions that could provide more favorable corrosion for substrates like Ni and Al, which form inherent oxide layers that passivate the surface. For aluminum, studies have shown that corrosion can be enhanced in alkaline solutions such as sodium hydroxide (NaOH) or potassium hydroxide (KOH) [82], [83]. These solutions can dissolve the protective oxide layer, promoting more uniform corrosion and potentially improving fingerprint development. For example, the corrosion-dissolution characteristics of pure aluminum in concentrated NaOH solutions demonstrate that aluminum exhibits passive behavior in the potential range from  $-1\text{V}$  to  $-0.5\text{V}$ , but the presence of impurities like iron in the NaOH can increase the corrosion current, thereby facilitating more aggressive corrosion [84]. Future studies should investigate the use of these alkaline solutions for aluminum substrates to see if they yield better results. Additionally, increasing the temperature during the corrosion process might improve the effectiveness of these methods [85].

For nickel alloys, incorporating chloride-containing solutions like hydrochloric acid (HCl) or using mixed electrolyte systems (e.g.,  $\text{H}_2\text{SO}_4$  with NaCl) could help achieve more consistent and reproducible corrosion. For instance, a study on the corrosion behavior of nickel-based alloys in environments containing HCl and  $\text{H}_2\text{S}$  demonstrated that such environments

significantly affect the corrosion susceptibility of these alloys depending on the pH and presence of H<sub>2</sub>S [86]. The results indicated that nickel alloys exhibited lower corrosion rates in near-neutral pH environments, suggesting that adjusting the pH of the electrolyte solution could optimize corrosion conditions. The addition of heat could also be explored to improve effectiveness. A study found that higher temperatures tend to increase the corrosion rates due to enhanced ion mobility and increased chemical reaction rates [87]. These alternative approaches could be explored to optimize the corrosion process for nickel substrates and enhance fingerprint development.

In summary, the comprehensive investigation into electrolyte solutions and electrochemical corrosion reactions on various substrate surfaces has yielded valuable insights for the development of targeted corrosion enhancement techniques in forensic investigations. Through meticulous experimentation and analysis, it was determined that 0.1M KCl is unsuitable for all substrate types due to its propensity to induce severe and uneven corrosion. Conversely, 0.1M H<sub>2</sub>SO<sub>4</sub> emerged as the optimal electrolyte solution for 6061-Aluminum alloy, C260 brass, and 400-Nickel alloy substrates, exhibiting relatively uniform corrosion patterns and facilitating the visibility of eccrine fingerprints. Furthermore, 0.1M Na<sub>2</sub>SO<sub>4</sub> showed promise for low-carbon steel, offering partial visibility of fingerprints despite some unevenness in corrosion.

Moreover, the subsequent exploration of potentiodynamic, potentiostatic, and galvanostatic corrosion methods provided deeper insights into the efficacy of targeted corrosion enhancement for latent fingerprint development. While potentiodynamic corrosion proved to be the most effective method, yielding significant improvements in fingerprint visibility across all substrate types, potentiostatic and galvanostatic corrosion methods fell short in comparison. The findings underscore the importance of methodological optimization and electrolyte selection in

achieving superior results in fingerprint enhancement. Moving forward, these insights pave the way for further refinement and application of targeted corrosion enhancement techniques in forensic science, ultimately enhancing the capabilities of law enforcement agencies in solving crimes through advanced fingerprint analysis.

## **Chapter 4: A Qualitative Analysis of Corrosion Processes in Alloys Commonly Encountered in Forensic Investigations Using Inductively Coupled Plasma–Optical Emission Spectroscopy**

### **4.1 Introduction**

With the inherent repeatability challenges and unevenness in substrate surface corrosion faced by 6061-Aluminum alloy and 400-Nickel alloy, it became apparent that any improvement of the electrochemical and electroanalytical methods outlined in Chapter 3 would require a more comprehensive understanding of how much and in what way the metal substrates are corroding over time. Addressing ambiguous results and defining processes associated with the corrosion are both critical steps in reducing the barriers to implementation faced by all novel forensic methods.

It is also important to note that there are areas of ambiguity and variability that are not fully explained and understood based on the investigations in this dissertation. For instance, variations in fingerprint residue composition, environmental exposure of pieces of evidence, age of the fingerprint, and variations in metal alloy manufacturing will always cause some level of variability in the overall success of the suggested electrochemical and electroanalytical methods utilized in latent fingerprint visualization and enhancement. However, trace metal analysis (TEA), specifically ICP-OES, can assist in understanding which specific metal elements in each alloy are corroding at various points during a potential sweep in LSV measurements which can help explain the data obtained and challenges faced in Chapter 3.

Multipurpose 6061-Aluminum alloy, ultra-formable C260 brass, low-carbon steel, and multipurpose 400-Nickel alloy are all alloyed to some extent. Formal reduction potentials and Pourbaix diagrams are two helpful points of reference regarding corrosion properties for each metal alloy and provide valuable information as to what will be revealed in future TEA experiments. Referring to the percent compositions listed in Table 1, 6061-Aluminum alloy is over 95% aluminum which means the chemical properties of aluminum are likely dictating corrosion of this substrate. Low-carbon steel is over 99% iron; thus, iron will dictate the corrosion of this substrate. Ultra-formable C260 brass is 68.5-71.5% copper and 28.38-31.38% zinc, which means that more than one element can affect corrosion characteristics. More specifically, brass undergoes a process called dezincification whereby the zinc characteristically corrodes away before the copper [88], [89], [90]. This is because zinc is higher than copper on the reactivity series of metals. Lastly, multipurpose 400-Nickel alloy is 60.7-72% 400-Nickel alloy and 28-34% copper suggesting that its corrosion properties will be dictated by both 400-Nickel alloy and copper. Table 11 lists the reduction potentials of the most abundant elements found in each alloy.

Table 11: List of reduction potentials relevant to the most abundant elements in each alloy

| Half Cell                             | Reduction Reaction                             | $E^0$ (V) |
|---------------------------------------|--|-----------|
| <b>Cu Cu<sup>+</sup></b>              | $\text{Cu}^+ + e^- \rightarrow \text{Cu}$      | 0.52      |
| <b>Cu Cu<sup>2+</sup></b>             | $\text{Cu}^{2+} + 2e^- \rightarrow \text{Cu}$  | 0.34      |
| <b>Cu<sup>+</sup> Cu<sup>2+</sup></b> | $\text{Cu}^{2+} + e^- \rightarrow \text{Cu}^+$ | 0.16      |
| <b>Ni Ni<sup>2+</sup></b>             | $\text{Ni}^{2+} + 2e^- \rightarrow \text{Ni}$  | -0.26     |
| <b>Fe Fe<sup>2+</sup></b>             | $\text{Fe}^{2+} + 2e^- \rightarrow \text{Fe}$  | -0.44     |
| <b>Zn Zn<sup>2+</sup></b>             | $\text{Zn}^{2+} + 2e^- \rightarrow \text{Zn}$  | -0.76     |
| <b>Al Al<sup>2+</sup></b>             | $\text{Al}^{3+} + 3e^- \rightarrow \text{Al}$  | -1.66     |

In examining the reduction potentials listed in Table 11, it is possible to infer the sequence of oxidation of the elements during corrosion studies of the substrates. The reduction potential ( $E^0$ ) of an element is a key indicator of its tendency to lose electrons, and consequently, its susceptibility to oxidation. A lower (more negative) value indicates a higher likelihood of the element being oxidized first.

Among the elements analyzed, aluminum, with a reduction potential of -1.66 V, exhibits the most negative potential, indicating it is the most prone to oxidation among the assessed metals. This suggests that in environments conducive to corrosion, aluminum in the 6061-Aluminum alloy substrate would be expected to oxidize before other metals.

Following aluminum, zinc with a reduction potential of -0.76 V, is the next element likely to oxidize. This is particularly relevant for the C260 brass substrate, which consists



significantly of zinc. The dezincification process observed in C260 brass, where zinc corrodes preferentially relative to copper, can be explained by zinc's higher oxidation tendency compared to copper as well as its higher position in the reactivity series of metals.

Iron, with a reduction potential of  $-0.44$  V, would oxidize following zinc. This is critical for substrates like low-carbon steel, which is predominantly composed of iron. This sequential oxidation can significantly impact the corrosion behavior and the resultant electrochemical stability of the steel substrate.

Copper, with more positive reduction potentials of  $0.34$  V and  $0.52$  V for its  $+2$  and  $+1$  oxidation states respectively, is less prone to oxidation compared to zinc, iron, and aluminum. This influences the corrosion resistance observed in copper-rich substrates such as C260 brass and multipurpose 400-Nickel alloy, which also contains significant amounts of copper.

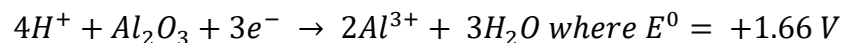
Lastly, nickel, with a reduction potential of  $-0.26$  V, while more resistant to oxidation than aluminum, zinc, and iron, is still more likely to oxidize before copper. This characteristic impacts the corrosion behavior of 400-Nickel alloy, where both nickel and copper contribute to the overall corrosion dynamics.

Understanding these oxidation sequences helps in predicting the durability and corrosion behavior of different metal substrates under various environmental conditions. Aluminum, comprising the majority of 6061-Aluminum alloy, possesses the most negative reduction potential of  $-1.66$  V, indicating that this material is most susceptible to corrosion out of the four substrate types. Iron, comprising the majority of low-carbon steel, has a less negative reduction potential of  $-0.44$  V making it slightly more noble than the 6061-Aluminum alloy. C260 brass would have a reduction potential based on those of copper and zinc and multipurpose 400-Nickel

alloy would have a reduction potential based on those of 400-Nickel alloy and copper. Using standard reduction potentials, alone, places these two substrates above low-carbon steel and 6061-Aluminum alloy in terms of nobility.

While the reduction potentials of pure metals are crucial for understanding their basic electrochemical properties, in practical environments, corrosion behavior is often significantly influenced by the formation of metal oxides. These oxides can alter the corrosion dynamics by providing either protective barriers or additional pathways for corrosion, depending on their stability and environmental conditions.

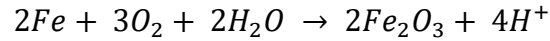
Aluminum, for instance, is known for its rapid natural passivation in atmospheric conditions due to the formation of a thin, protective aluminum oxide ( $\text{Al}_2\text{O}_3$ ) layer. This oxide layer effectively shields the underlying metal from further oxidation. The formation of this layer is crucial in understanding aluminum's corrosion behavior because it alters the effective reduction potential that must be overcome for further oxidation to occur. The reaction involving the reduction of aluminum oxide in acidic conditions can be represented as follows:



Equation 28: Reduction of aluminum oxide in the formation of a protective passive oxide layer

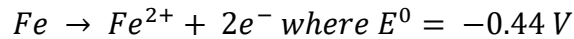
This reaction indicates that the presence of the oxide layer changes the dynamics of aluminum corrosion, potentially increasing the resistance of aluminum to corrosion under certain conditions. The electrochemical stability of aluminum oxide and its impact on the corrosion process highlights the importance of considering the electrochemical properties of oxides, not just the pure metals.

Iron commonly forms iron (III) oxide ( $\text{Fe}_2\text{O}_3$ ), especially under oxygen-rich, aqueous conditions. This oxide, often referred to as rust, can form protective barriers but can also flake off, exposing fresh metal to the environment:



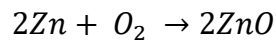
Equation 29: The formation of iron (III) oxide in aqueous conditions

However, in the acidic conditions used in these experiments, the stability of this oxide layer is compromised. The acidic environment, combined with the applied potential, can lead to the breakdown of this passive layer, allowing the underlying iron to corrode. The dissolution reaction of iron in acidic conditions can be represented as follows:



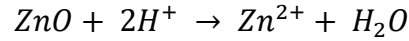
Equation 30: The dissolution reaction of iron in acidic conditions

Zinc oxide ( $\text{ZnO}$ ) is another example, forming a stable, protective layer that inhibits further oxidation under certain conditions:



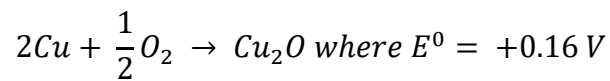
Equation 31: The formation of zinc oxide

However, in acidic environments, zinc oxide can dissolve, leading back to increased corrosion rates:

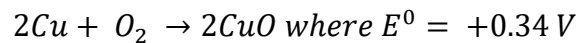


Equation 32: The dissolution of zinc oxide

Copper forms copper (I) oxide ( $\text{Cu}_2\text{O}$ ) and copper (II) oxide ( $\text{CuO}$ ). These oxides are capable of providing a notable level of protection against corrosion, stabilizing copper's surface from further attack:

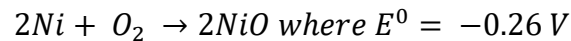


Equation 33: The formation of copper (I) oxide or cuprous oxide



Equation 34: The formation of copper (II) oxide or cupric oxide

Nickel predominantly forms nickel (II) oxide ( $\text{NiO}$ ), which is relatively stable and can enhance the corrosion resistance of nickel in a variety of environments:



Equation 35: The formation of nickel (II) oxide

The potentials associated with the formation of metal oxides are generally more positive than the pure metal oxidation potentials. This indicates that the oxides provide a protective barrier that needs a higher potential to break down compared to the oxidation of the pure metal itself. For example, aluminum's oxide formation potential is significantly more positive than its pure metal oxidation potential (-1.66 V), highlighting the protective nature of the oxide layer.

Understanding the reduction potentials and stability of these oxides is crucial for a comprehensive analysis of corrosion processes. The protective nature of these oxides, as well as their potential to deteriorate or dissolve under specific environmental conditions, plays a significant role in the corrosion resistance of the metals. Thus, both the electrochemical properties of the metals and their oxides must be considered to predict corrosion behavior accurately. Finally, the solution conditions and composition play a role as pH can influence oxide formation and degradation.

To clarify the complex interactions between potential, pH, and the corrosion stability of metals and their oxides, Pourbaix diagrams are an essential tool. These diagrams, plotted with potential on the vertical axis and pH on the horizontal axis, offer a visual representation of the thermodynamic stability of various species across a range of pH levels and potentials. They enable the prediction of which forms (e.g., metal, oxide, ion) are most stable under specific environmental conditions. By integrating both the electrochemical potential and pH factors, Pourbaix diagrams assist in understanding the conditions under which metals are likely to corrode or passivate, which is critical for forensic science where precise detection and analysis of trace elements are required.



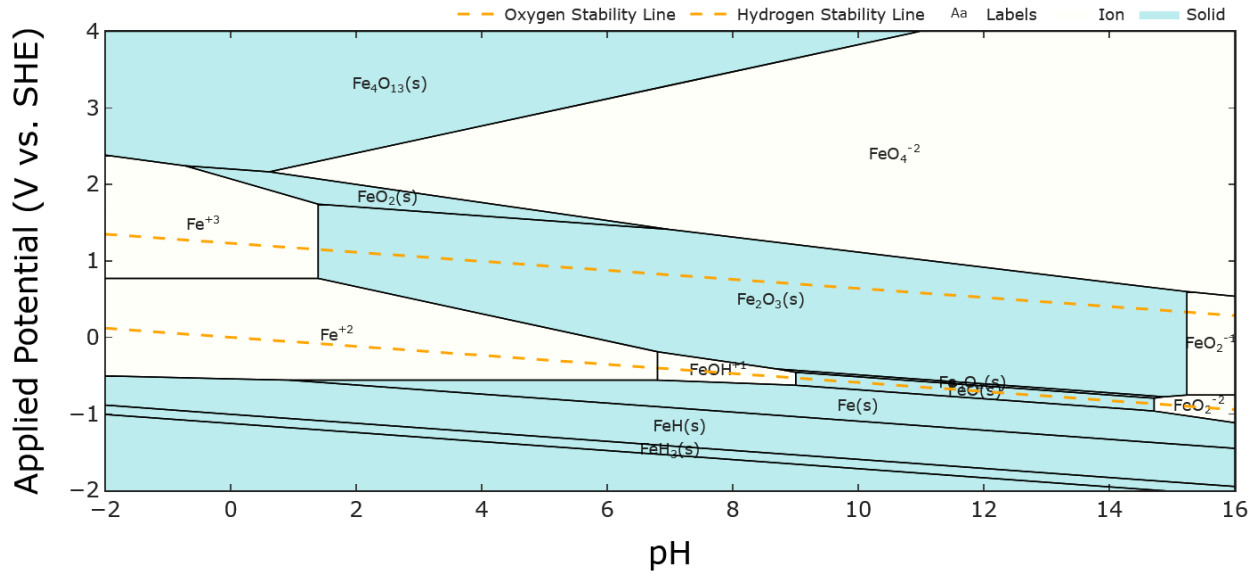


Figure 24: Pourbaix diagram for iron corresponding to low-carbon steel

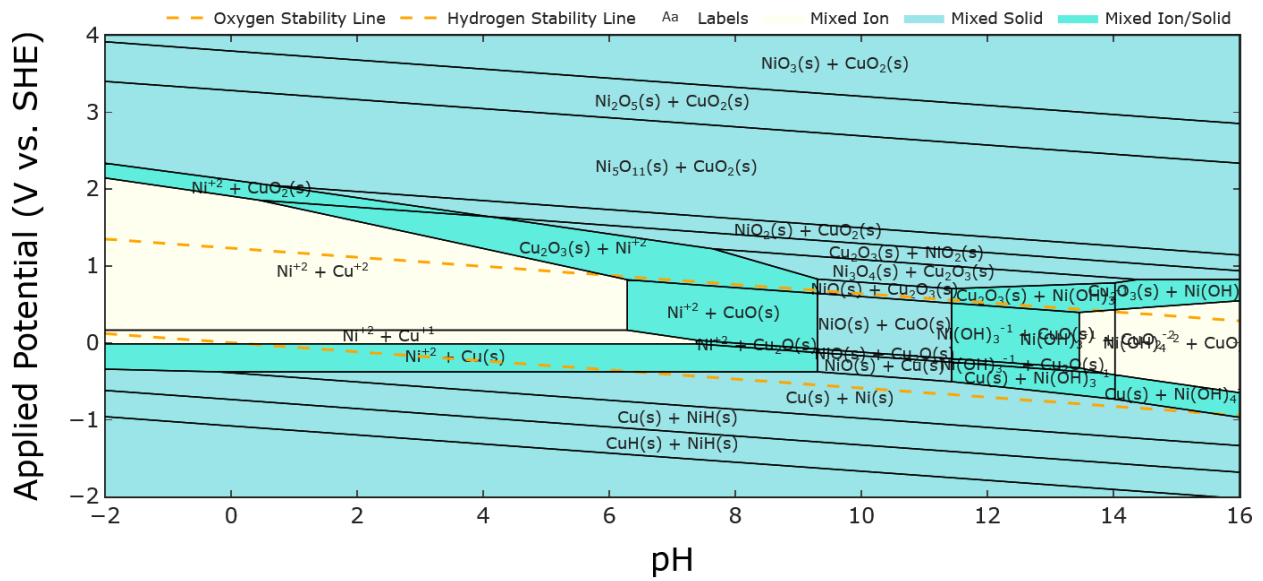


Figure 25: Pourbaix diagram for nickel and copper corresponding to 400-Nickel alloy

Figures 22 through 25, which represent Pourbaix diagrams for the metals discussed, visually demonstrate these interactions and serve as a practical guide for predicting the conditions under which forensic evidence involving metal substrates might be compromised or preserved. This insight is invaluable in forensic investigations, where understanding the chemical and physical changes to metal surfaces can reveal crucial details about the conditions and timelines of criminal events.

Open source software from The Materials Lab built by Berkeley University was used to generate these Pourbaix diagrams [91], [92], [93], [94]. Potentiodynamic, potentiostatic and galvanostatic measurements conducted in chapter one utilized 0.1M H<sub>2</sub>SO<sub>4</sub> and 0.1M Na<sub>2</sub>SO<sub>4</sub>, with pH values of 0.699 and 7.5, respectively. These specific pH conditions are critical as they influence which metal species are more prone to corrosion and the type of corrosion processes that occur.

For example, at a pH of 0.699 (acidic conditions), it is expected that aluminum be found in its Al<sup>3+</sup> ionic form, leading to active corrosion as indicated by the Pourbaix diagram. This prediction aligns with the observed high corrosion rate of 6061-Aluminum alloy under acidic conditions, making it crucial to monitor aluminum ion concentration during forensic analysis. Similarly, for C260 brass at the same pH, the presence of Zn<sup>2+</sup> and Cu<sup>+</sup> ions suggests active dezincification, where zinc corrodes preferentially, compromising the structural integrity of the brass.

In contrast, at a pH of 7.5 (neutral conditions), low-carbon steel predominantly forms Fe<sup>2+</sup> ions, indicating a more stable environment where the formation of protective iron oxides is likely. The Pourbaix diagrams show iron in a passivation region, suggesting the formation of protective oxide layers that inhibit further corrosion. Understanding when passivation is expected



can aid in developing mitigation techniques that remove this layer and enhance latent fingerprint development.

These pH conditions and the corresponding electrochemical environments are directly tied to the expected ions in Trace Element Analysis (TEA) experiments, which are detailed in Table 12. This table summarizes the expected predominant ionic species for each substrate under the tested conditions, providing a clear link between the electrochemical theory and the practical outcomes.

Table 12: Expected ions in TEA experiments based on standard reduction potentials and Pourbaix diagrams

| <b>Substrate</b>        | <b>pH</b> | <b>Potential Sweep</b> | <b>Expected In TEA</b>                                |
|-------------------------|-----------|------------------------|---|
| <b>6061-Aluminum</b>    | 0.699     | -0.7 to -0.4 V         | Al <sup>3+</sup>                                      |
| <b>C260 Brass</b>       | 0.699     | -0.3 to +0.3 V         | Zn <sup>2+</sup> , Cu <sup>+</sup> , Cu <sup>2+</sup> |
| <b>Low-carbon Steel</b> | 7.5       | -0.7 to -0.1 V         | Fe <sup>2+</sup>                                      |
| <b>400-Nickel</b>       | 0.699     | -0.3 to +0.2 V         | Ni <sup>2+</sup> , Cu <sup>+</sup> , Cu <sup>2+</sup> |

Subjecting 6061-Aluminum alloy to a pH of 0.699 and a potential sweep from -0.7 to -0.4 V, Al<sup>3+</sup> ions are expected, consistent with the aluminum Pourbaix diagram indications of oxide dissolution into ionic forms under acidic conditions. Similarly, at pH 0.699 with a potential sweep from -0.3 to +0.3 V, Zn<sup>2+</sup>, Cu<sup>+</sup>, and Cu<sup>2+</sup> ions are expected from C260 brass, highlighting the susceptibility of zinc to corrosion (dezincification) and the relatively stable nature of copper. Subjecting low-carbon steel to a pH of 7.5 and a potential sweep from -0.7 to -0.1 V, Fe<sup>2+</sup> ions

are expected, indicating stability and less aggressive corrosion, aligning with the iron Pourbaix diagram's passivation regions. Lastly, subjecting 400-Nickel alloy to a pH of 0.699 and a potential sweep from -0.3 to +0.2 V,  $\text{Ni}^{2+}$ ,  $\text{Cu}^+$ , and  $\text{Cu}^{2+}$  ions are predominant, reflecting the complex interactions between nickel and copper under acidic conditions.

TEA using ICP-OES (described in section 2.4 of Chapter 2) allows for the identification of corrosion products, quantification of metal ion release rates, and elucidation of the underlying corrosion mechanisms. This comprehensive approach provides insights into why C260 brass and low-carbon steel exhibited more repeatable results throughout Chapter 3 and guides further optimization efforts. Additionally, the passive oxide formation on metal substrates, a process which can occur spontaneously even in humidified air environments, highlights the critical role of environmental conditions in forensic analyses. This spontaneous formation of oxides is a common but critical aspect that influences the stability and corrosion resistance of metals, thus impacting the preservation or deterioration of forensic evidence. Ultimately, this detailed understanding of the chemical reactions and species stability under specific pH and potential conditions offers valuable insights into passive oxide formation and corrosion behaviors on each metal substrate, crucial for forensic and other practical applications.

## **4.2 Materials and Methods**

This section delineates the materials and methods utilized for conducting TEA through ICP-OES. The methodology encompasses a comprehensive series of experiments aimed at elucidating the corrosion behavior of metal substrates and addressing knowledge gaps in latent

fingerprint enhancement techniques. The following summary outlines of the materials and methods employed in this research, referencing relevant sections and subsections from Chapter 2 where applicable.

The materials for this study were selected meticulously to ensure accuracy and reliability in the experimental procedures. Common metal substrates, including 6061-Aluminum alloy, C260 brass, low-carbon steel, and 400-Nickel alloy, were chosen based on their prevalence in forensic investigations, as discussed in Section 2.1 of Chapter 2. Samples were prepared as outlined in section 2.2 of Chapter 2.

Chemicals and solutions utilized for sample preparation and TEA experiments were selected based on their compatibility with the chosen substrates and ability to provide accurate trace metal analysis. The preparation of dilution standards for each metal substrate was conducted meticulously to ensure accurate calibration of the ICP-OES instrument and precise quantification of trace metal concentrations, as detailed in section 2.1 of Chapter 2.

Three fingerprinted samples and three non-fingerprinted samples were subjected to LSV identical to the measurements conducted in Chapter 3 for each of the four metal substrates. Throughout the procedure, to ensure that each 5mL aliquot reflected a homogeneous distribution of the bulk solution, the solution was agitated directly before the removal of each aliquot. This meticulous approach was crucial to maintain consistency and accuracy in sampling. As the linear sweep proceeded, 5mL aliquots of the electrolyte solution were removed at five pre-determined points on the Tafel plot. The first aliquot was taken directly before the start of the linear sweep and the second aliquot was removed halfway between the beginning of the linear sweep and the corrosion potential value of the metal alloy. The third aliquot was taken at the corrosion potential value of the metal alloy. The fourth aliquot was taken at the halfway point between the corrosion

potential value and the end of the linear sweep, and the fifth and final aliquot was taken at the end of the measurement. A Tafel plot schematic with the corresponding numbered aliquot removal positions is shown below for clarity:

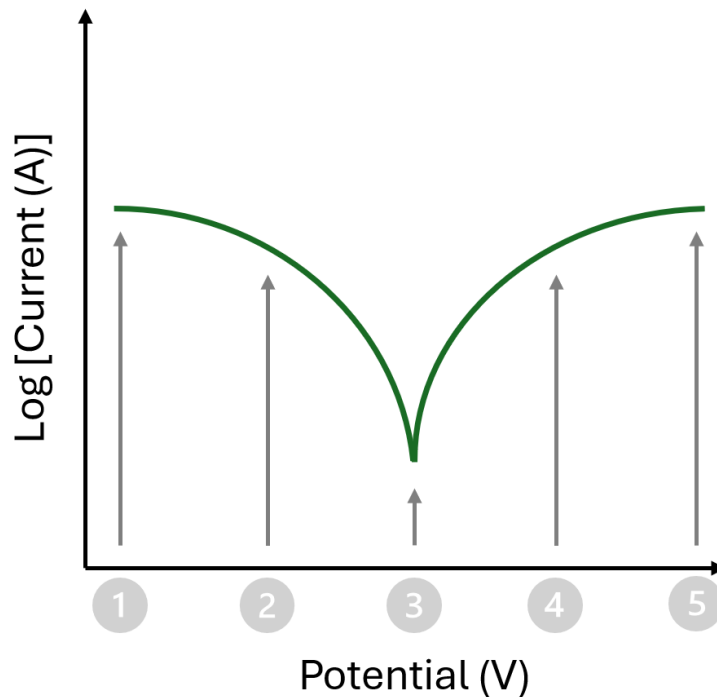


Figure 26: Tafel plot schematic with labeled aliquot removal points. The first 5mL aliquot is removed at point one, the second at point two, the third at point three, the fourth at point four, and the fifth at point five on the diagram

Utilizing the experimental design above, elemental corrosion over time for each metal alloy is established. The experimental methods employed in this research were designed to investigate the trace metal composition of metal substrates and their correlation with corrosion behavior. Subsequently, TEA experiments were conducted using ICP-OES to analyze the trace metal content of each substrate, as detailed in Section 2.4 of Chapter 2. These analyses provided

valuable insights into the corrosion mechanisms and passive oxide formation on the surface of the metal substrates.

## **4.3 Results and Analysis**

### **4.3.1 6061-Aluminum Alloy ICP-OES Results**

All 6061-Aluminum alloy samples were assessed for copper, iron, aluminum, and chromium as these elements establish the majority composition of the alloy. Three trials of fingerprinted and three trials of non-fingerprinted 6061-Aluminum alloy samples were conducted to understand the potential variations that may be caused by the presence of fingerprints on these measurements.

Table 13 displays the results of the ICP-OES measurements on three fingerprinted 6061-Aluminum alloy samples. The potentials corresponding to when each aliquot was removed from the bulk solution are also shown.

Table 13: ICP-OES measurement results of three trials of fingerprinted 6061-Aluminum alloy samples

| <b>E (V)</b> | <b>Avg Cu (ppm)</b> | <b>Avg Fe (ppm)</b> | <b>Avg Al (ppm)</b> | <b>Avg Cr (ppm)</b> |
|--------------|---------------------|---------------------|---------------------|---------------------|
| <b>-0.89</b> | 0.32 ± 0.2          | 0.037 ± 0.004       | 0.15 ± 0.03         | 0.035 ± 0.001       |
| <b>-0.77</b> | 0.59 ± 0.6          | 0.047 ± 0.006       | 0.15 ± 0.1          | 0.035 ± 0.001       |
| <b>-0.60</b> | 0.47 ± 0.4          | 0.076 ± 0.01        | 0.53 ± 0.2          | 0.041 ± 0.001       |
| <b>-0.46</b> | 0.44 ± 0.4          | 0.087 ± 0.01        | 1.83 ± 0.5          | 0.043 ± 0.001       |
| <b>-0.26</b> | 0.42 ± 0.4          | 0.10 ± 0.02         | 3.5 ± 1             | 0.046 ± 0.002       |

It is important to note that the E (V) values listed in the table are all versus an Ag/AgCl reference electrode, which has a standard reference electrode potential of 210 mV ± 5 mV with respect to the Standard Hydrogen Electrode (SHE). Iron and chromium concentrations remained low but consistent throughout the trials, indicating their presence in measurable amounts. This suggests that their relative percentages present within the alloy resulted in a minimal contribution to the corrosion process under the given conditions.

To determine if any of the concentrations align with the corrosion potential for the highest concentration, it is essential to compare the measured concentrations at various potentials with the known  $E_{Corr}$  value for 6061-Aluminum alloy. The standard  $E_{Corr}$  value for 6061-Aluminum alloy typically falls around -0.75 V vs. SHE. When converted to the Ag/AgCl reference scale, this corresponds to approximately -0.96 V after the following calculation:

$$-0.75 V - 0.210 V = -0.96 V \text{ vs. } Ag/AgCl$$

Equation 36: Conversion of aluminum corrosion potential vs. SHE to reflect the value vs. Ag/AgCl

At -0.77 V vs. Ag/AgCl, which is 0.19 V more positive than the converted  $E_{Corr}$  value, the concentration of aluminum is  $0.15 \pm 0.1$  PPM. This value is relatively low compared to the concentrations at higher potentials, such as -0.26 V vs. Ag/AgCl, where aluminum concentration peaks at  $3.5 \pm 1$  PPM. The concentrations of copper, iron, and chromium do not show a significant peak at -0.77 V vs. Ag/AgCl but instead vary across the range of potentials tested.

Several factors could explain why the highest concentrations do not align with the calculated  $E_{Corr}$  value. At potentials closer to the corrosion potential, the formation of a passive oxide layer might inhibit the dissolution of aluminum. As the potential moves more positive, this oxide layer could break down, resulting in higher concentrations of dissolved aluminum in the solution. The protective nature of aluminum oxide, which forms at and near  $E_{Corr}$ , suggests that substantial dissolution may not occur until the potential is sufficiently positive to disrupt this layer. Additionally, the dynamic nature of the potential sweep during LSV measurements means that the system might not be at equilibrium at each potential. This can result in delayed dissolution peaks as the corrosion process lags behind the applied potential. Moreover, different elements might corrode preferentially at different potentials, meaning aluminum might show increased dissolution at higher potentials due to specific electrochemical reactions that are more favorable under those conditions.

By understanding these factors, we can better interpret the ICP-OES results and their implications for the corrosion behavior of 6061-Aluminum alloy. Future studies could involve more detailed, stepwise potential holds to better capture the dissolution behavior near  $E_{Corr}$  and provide a clearer picture of the corrosion dynamics.

Figure 27 depicts how the concentration of each component within the fingerprinted 6061-Aluminum alloy samples changes throughout the linear potential sweep.

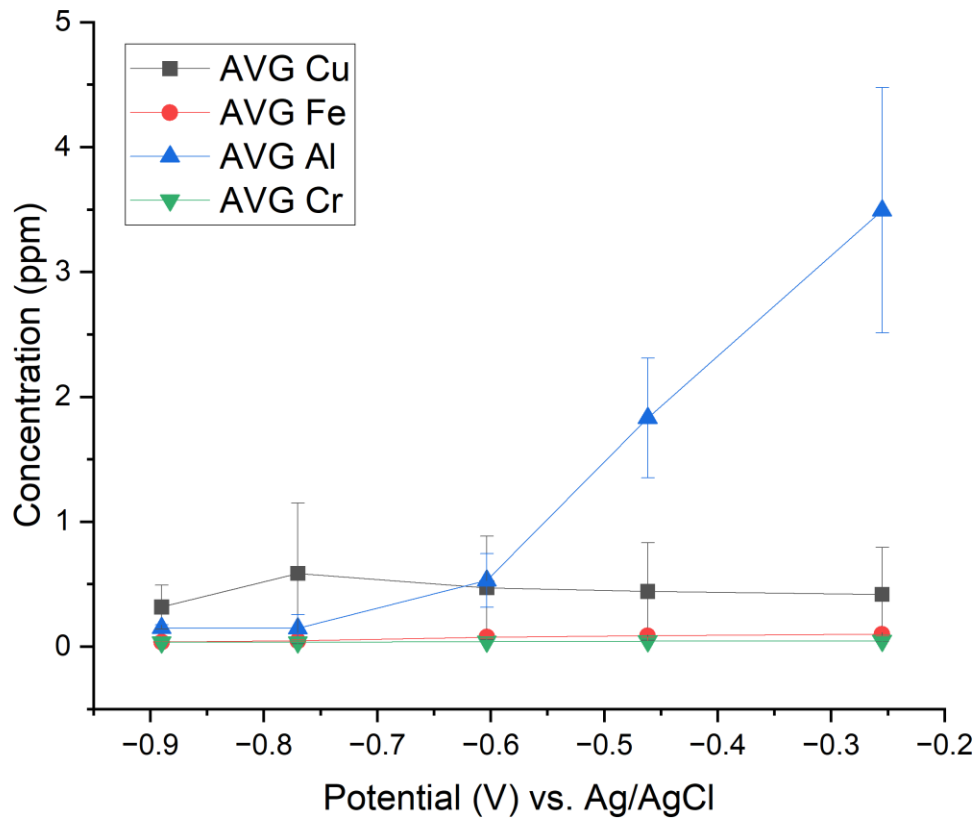


Figure 27: A graph displaying the ICP-OES results of fingerprinted 6061-Aluminum alloy samples. The concentrations of Cu, Fe, Al, and Cr are displayed for each corresponding aliquot taken from the bulk solution over the course of the applied linear potential sweep

Most notably, the concentration of copper appears to be slightly higher at the second aliquot than for the remaining aliquots. Error bars display relative error amongst the three trials and a relatively high error is noted in the copper concentrations for fingerprinted 6061-Aluminum alloy samples. The concentration of aluminum increases over time which is to be



expected as corrosion reactions proceed. However, the error amongst the three trials for aluminum concentration also increases over time. The data collected for iron and chromium concentrations remained negative which suggests that they were not present in any of the aliquots removed from the bulk solution or their concentrations were too low to be detected by the instrument. The repeatability and accuracy challenges seen above in the fingerprinted 6061-Aluminum alloy samples mirror the challenges encountered with targeted corrosion enhancement and provide further evidence that aluminum alloyed substrates may not be suitable for corrosion-based methods of latent fingerprint enhancement and development.

Table 14 displays the ICP-OES measurement data from the non-fingerprinted 6061-Aluminum alloy samples.

Table 14: ICP-OES measurement results of three trials of non-fingerprinted 6061-Aluminum alloy samples

| <b>E (V)</b> | <b>Avg Cu (ppm)</b> | <b>Avg Fe (ppm)</b> | <b>Avg Al (ppm)</b> | <b>Avg Cr (ppm)</b> |
|--------------|---------------------|---------------------|---------------------|---------------------|
| <b>-0.89</b> | 0.070 ± 0.01        | 0.052 ± 0.006       | 0 ± 0.005           | 0.0343 ± 0.0001     |
| <b>-0.77</b> | 0.068 ± 0.01        | 0.065 ± 0.02        | 0.20 ± 0.2          | 0.0344 ± 0.0002     |
| <b>-0.60</b> | 0.067 ± 0.01        | 0.095 ± 0.02        | 0.52 ± 0.2          | 0.040 ± 0.002       |
| <b>-0.46</b> | 0.066 ± 0.01        | 0.12 ± 0.04         | 0.85 ± 0.2          | 0.041 ± 0.001       |
| <b>-0.26</b> | 0.065 ± 0.01        | 0.17 ± 0.03         | 4.7 ± 0.2           | 0.049 ± 0.001       |

Iron and chromium concentrations continued to remain low and consistent, which matched what was seen in the fingerprinted samples. The final concentration of copper was

higher in the fingerprinted samples compared to the non-fingerprinted samples, implying that the presence of a fingerprint enhances corrosion of copper. In contrast, the final concentration of aluminum in fingerprinted samples was slightly lower than in non-fingerprinted samples, indicating that the presence of fingerprints may have a complex effect on aluminum corrosion.

Figure 28 represents the individual component changes throughout the linear potential sweep for three non-fingerprinted 6061-Aluminum alloy trials.

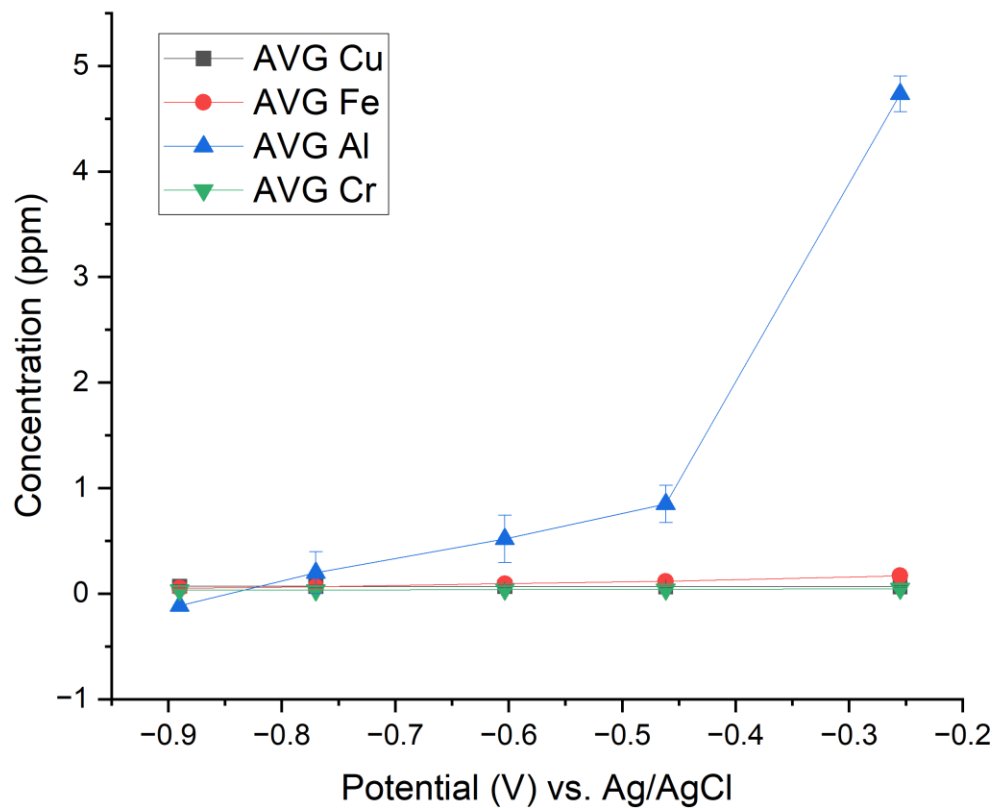


Figure 28: A graph displaying the ICP-OES results of non-fingerprinted 6061-Aluminum alloy samples. The concentrations of Cu, Fe, Al, and Cr are displayed for each corresponding aliquot taken from the bulk solution over the course of the applied linear potential

Unlike what was seen above in the fingerprinted trials, the non-fingerprinted 6061-Aluminum alloy samples have very low error across the four components. Error bars are not visible at all for copper, iron, and chromium. The error in aluminum concentration measurements is substantially smaller in the non-fingerprinted samples indicating that the absence of fingerprints results in less variability amongst trials. This, too, is evidence that 6061-Aluminum alloy substrates may not be compatible with corrosion-based latent fingerprint enhancement methods as the presence of fingerprints inhibits repeatability.

To improve the corrosion-based methods for latent fingerprint enhancement on 6061-Aluminum alloy, a review of literature on corrosion of this alloy in different chemical environments is necessary. Studies have shown that certain chemicals like sodium borohydride and nitric acid can significantly impact the corrosion behavior of aluminum alloys. Sodium borohydride ( $\text{NaBH}_4$ ), when prepared in an alkaline medium (such as  $\text{NaOH}$ ), acts as a strong reducing agent that can facilitate the removal of the protective oxide layer on aluminum, thereby increasing its susceptibility to corrosion. For instance, studies have indicated that sodium borohydride in alkaline conditions can lead to significant hydrogen evolution, which assists in breaking down the oxide layer and exposing fresh aluminum surface to further corrosion. Conducting LSV measurements in a 0.1M  $\text{NaBH}_4$  solution can provide valuable data on the impact of this chemical on aluminum corrosion.

Similarly, nitric acid ( $\text{HNO}_3$ ), an oxidizing agent, can disrupt the oxide layer and accelerate corrosion processes. Nitric acid is known for its ability to penetrate and uniformly corrode the oxide layer due to its strong oxidizing properties. Dilute nitric acid solutions (e.g., 0.1M  $\text{HNO}_3$ ) can be used in LSV measurements to evaluate the extent of corrosion and the

presence of aluminum ions in the solution. A sequential treatment combining  $\text{NaBH}_4$  followed by  $\text{HNO}_3$  might yield even better results by leveraging the strengths of both chemicals to achieve more pronounced and consistent corrosion.

By incorporating these specific chemical agents known for their effectiveness in corroding aluminum, it is anticipated that the visibility of latent fingerprints on 6061-Aluminum alloy surfaces can be significantly improved. These redesigned experiments aim to achieve a more consistent and pronounced corrosion process, thus enhancing the overall effectiveness of forensic methods.

A key factor in the corrosion resistance of 6061-Aluminum alloy is the presence of a naturally occurring protective oxide layer which acts as a barrier, inhibiting further oxidation of the underlying metal. In an article by Peng et al., the presence of chloride ions, which are common in eccrine sweat, are shown to penetrate and compromise this oxide layer, leading to localized corrosion [95]. This mechanism is crucial for forensic applications since the chloride ions from fingerprints can create weak points in the oxide layer, allowing for more effective corrosion-based enhancement methods. The article also notes that environmental exposure significantly impacts the corrosion behavior of 6061-Aluminum alloy. For instance, evidence such as shell casings, knives, or weapon components exposed to various environmental conditions will undergo different rates and types of corrosion. Factors like humidity, temperature, and the presence of pollutants can accelerate the corrosion process, leading to more pronounced and distinguishable fingerprint residues. Understanding these environmental influences allows for better control and optimization of corrosion conditions in forensic experiments.

Additionally, a paper by Liu et al. explains that the presence of intermetallic particles such as magnesium silicide ( $Mg_2Si$ ) and aluminum-iron-silicon ( $AlFeSi$ ) in 6061-Aluminum alloy significantly impacts its corrosion behavior [96]. These particles create defective oxide films and induce localized corrosion. Specifically, the preferential dissolution of magnesium from the  $Mg_2Si$  phase leaves behind a Si-rich residue, further promoting corrosion of the aluminum matrix. This understanding can be crucial in redesigning experiments to enhance corrosion at these weak points. For instance, magnesium in the alloy can be targeted to accelerate corrosion and improve the visibility of latent fingerprints. Furthermore, environmental exposure, such as in coastal atmospheres, can exacerbate the corrosion of aluminum alloys due to factors like humidity, temperature, and the presence of pollutants. This has implications for forensic evidence exposed to various environmental conditions, such as shell casings or weapon components left outdoors.

The formation of corrosion products like aluminum chloride ( $AlCl_3$ ), aluminum hydroxide ( $Al(OH)_3$ ), and aluminum oxide ( $Al_2O_3$ ) can initially protect the aluminum surface, but their protective effect diminishes over time due to the development of cracks and pores. By understanding the interactions between these factors and the inherent properties of 6061-Aluminum alloy, forensic scientists can better tailor their corrosion-based methods to enhance the visualization of latent fingerprints.

These insights from the literature underscore the importance of accounting for the specific chemical and environmental factors that influence the corrosion behavior of 6061-Aluminum alloy. Implementing these considerations in the experimental design can lead to more effective and reliable forensic techniques for latent fingerprint visualization.

### 4.3.2 C260 Brass ICP-OES Results

All C260 brass samples were assessed for copper, zinc, and iron as these elements establish the majority composition of the alloy. Following the procedure outlined above, three trials of fingerprinted and three trials of non-fingerprinted C260 brass samples were conducted.

Table 15 displays the results of the ICP-OES measurements on three fingerprinted C260 brass alloy samples along with the potentials corresponding to when each aliquot was removed from the bulk solution.

Table 15: ICP-OES measurement results of three trials of fingerprinted C260 brass samples

| <b>E (V)</b> | <b>Avg Cu (ppm)</b> | <b>Avg Zn (ppm)</b> | <b>Avg Fe (ppm)</b> |
|--------------|---------------------|---------------------|---------------------|
| <b>-0.26</b> | 0.52 ± 0.2          | 0.46 ± 0.1          | 0.074 ± 0.1         |
| <b>-0.14</b> | 0.84 ± 0.2          | 0.46 ± 0.1          | 0.088 ± 0.1         |
| <b>-0.04</b> | 0.87 ± 0.2          | 0.48 ± 0.1          | 0.093 ± 0.1         |
| <b>0.11</b>  | 6.3 ± 3             | 3.04 ± 1            | 0.11 ± 0.1          |
| <b>0.24</b>  | 120 ± 6             | 53.3 ± 2            | 0.20 ± 0.1          |

Iron remains relatively low but constant, likely because the applied potentials did not reach its corrosion potential of -0.44 V. This indicates that the experimental conditions were not sufficient to induce significant corrosion of iron in C260 brass, and its contribution to the overall

corrosion process is minimal under the given conditions. Figure 29 displays the change in concentration of copper, zinc, and iron in the fingerprinted C260 brass samples changes throughout the course of the applied linear potential sweep.

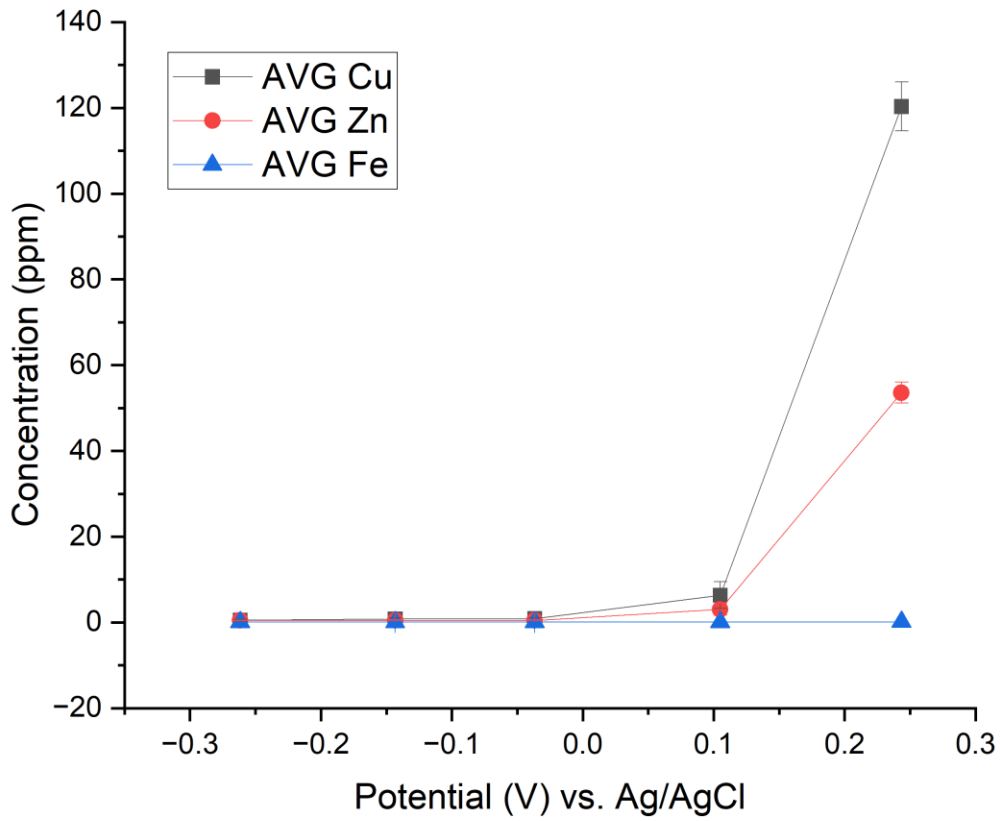


Figure 29: A graph displaying the ICP-OES results of fingerprinted C260 Brass samples. The concentrations of Cu, Zn, and Fe are displayed for each corresponding aliquot taken from the bulk solution over the course of the applied linear potential sweep

Error is smaller amongst the three trials of fingerprinted C260 brass samples when compared to the fingerprinted 6061-Aluminum alloy samples. This suggests that applied fingerprints result in less variability and may not hinder repeatability to the same extent on C260 brass substrate surfaces. The process of dezincification in brass, where zinc corrodes preferentially to copper, is evident from the increasing levels of zinc and copper over time, aligning with expectations. The concentrations of zinc and copper begin to significantly increase at potentials around 0.11 V and 0.24 V, respectively, which corresponds to the corrosion potentials of these elements. Zinc, with a corrosion potential of -0.76 V, starts to corrode earlier, leading to its gradual increase. Copper, with more positive corrosion potentials of 0.34 V and 0.52 V, shows a more substantial rise at higher potentials.

The data collected from three trials of non-fingerprinted C260 brass samples is shown in Table 16.

Table 16: ICP-OES measurement results of three trials of non-fingerprinted C260 brass samples

| <b>E (V)</b> | <b>Avg Cu (ppm)</b> | <b>Avg Zn (ppm)</b> | <b>Avg Fe (ppm)</b> |
|--------------|---------------------|---------------------|---------------------|
| <b>-0.26</b> | 0.33 ± 0.02         | 0.45 ± 0.05         | 0.079 ± 0.01        |
| <b>-0.14</b> | 0.95 ± 0.2          | 0.49 ± 0.06         | 0.102 ± 0.006       |
| <b>-0.04</b> | 0.97 ± 0.2          | 0.51 ± 0.07         | 0.12 ± 0.03         |
| <b>0.11</b>  | 6.6 ± 5             | 3.11 ± 2            | 0.10 ± 0.01         |
| <b>0.24</b>  | 74 ± 37             | 34 ± 16             | 0.128 ± 0.002       |



Iron concentrations remained relatively low and constant which mirrors what was seen in the fingerprinted trials. At the fifth and final aliquots removed from the fingerprinted samples, copper and zinc reached concentrations of 120 ppm and 53.3 ppm, respectively. In the non-fingerprinted samples, copper reaches a concentration of 74 ppm and zinc reaches 34 ppm. The presence of fingerprints increased corrosion of both copper and zinc in C260 brass substrates. This increase is likely due to the chloride ions present in eccrine sweat, which are known to penetrate the oxide layer and enhance corrosion. The observed increases in concentrations at specific potentials align well with the known corrosion potentials of the relevant elements, providing a clear link between the electrochemical properties of C260 brass and the experimental data. This alignment further supports the notion that the fingerprinted samples exhibit consistent corrosion behavior, making them more suitable for corrosion-based latent fingerprint enhancement methods compared to 6061-Aluminum alloy.

Figure 30 displays the change in concentration of copper, zinc, and iron in the non-fingerprinted C260 brass samples changes throughout the applied linear potential sweep.

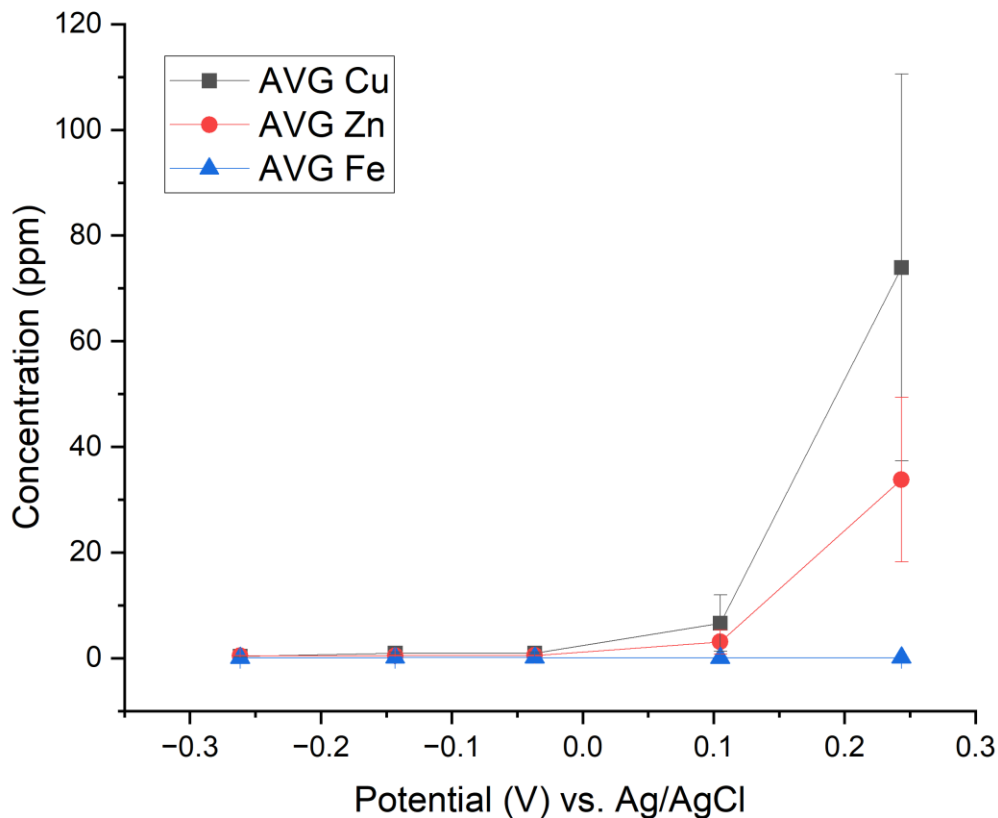


Figure 30: A graph displaying the ICP-OES results of non-fingerprinted C260 Brass samples. The concentrations of Cu, Zn, and Fe are displayed for each corresponding aliquot taken from the bulk solution over the course of the applied linear potential sweep

The data shows significant deviations in error between the non-fingerprinted and fingerprinted C260 brass samples, indicating that the presence of fingerprints has a pronounced effect on the corrosion process. The new data reveals larger error margins in the non-fingerprinted samples, especially for copper and zinc, with the error increasing over time as the potential becomes more positive. This suggests that the corrosion process in non-fingerprinted samples is less consistent and more variable, possibly due to the absence of chloride ions from

eccrine sweat, which are present in fingerprinted samples and contribute to a more uniform corrosion process.

The increasing error in copper and zinc concentrations over time in non-fingerprinted samples could be attributed to the heterogeneous nature of the corrosion process in the absence of fingerprints. Without the chloride ions to uniformly penetrate and compromise the oxide layer, the corrosion may occur more sporadically, leading to greater variability in the data. This variability contrasts with the more predictable corrosion observed in fingerprinted samples, where chloride ions facilitate a more consistent degradation of the protective oxide layer, resulting in steadier corrosion rates for both zinc and copper.

Moreover, the presence of fingerprints appears to create localized areas of higher corrosion activity, possibly due to the concentration of salts and other corrosive agents in sweat, which could lead to a more focused and uniform attack on the metal surface. This localized corrosion likely reduces the overall variability in the fingerprinted samples, resulting in smaller error bars.

The findings suggest that the corrosion behavior of C260 brass is significantly influenced by the presence of fingerprints, which act as a catalyst for a more uniform corrosion process. This is a crucial insight for forensic applications, as it highlights the importance of understanding the chemical interactions between fingerprint residues and metal substrates. The larger error margins in non-fingerprinted samples indicate that corrosion-based enhancement methods may be less reliable when fingerprints are not present, emphasizing the need for tailored approaches based on the specific conditions of the forensic evidence.

### 4.3.3 Low-carbon Steel ICP-OES Results

All low-carbon steel samples were assessed for iron and manganese, representing the majority composition of the alloy. Three trials of fingerprinted and three trials of non-fingerprinted low-carbon steel samples were conducted. Table 17 displays the results of the ICP-OES measurements on three fingerprinted low-carbon steel samples along with the potentials corresponding to when each aliquot was removed from the bulk solution.

Table 17: ICP-OES measurement results of three trials of fingerprinted low-carbon steel samples

| <b>E (V)</b> | <b>Avg Fe (ppm)</b> | <b>Avg Mn (ppm)</b> |
|--------------|---------------------|---------------------|
| <b>-0.70</b> | 4.01 ± 4            | 0.080 ± 0.02        |
| <b>-0.57</b> | 5.2 ± 4             | 0.095 ± 0.007       |
| <b>-0.43</b> | 6.0 ± 4             | 0.097 ± 0.01        |
| <b>-0.30</b> | 56 ± 11             | 0.18 ± 0.02         |
| <b>-0.20</b> | 253 ± 14            | 0.55 ± 0.03         |

Figure 31 displays the change in concentration of iron and manganese in the fingerprinted low-carbon steel samples changes throughout the course of the applied linear potential sweep.

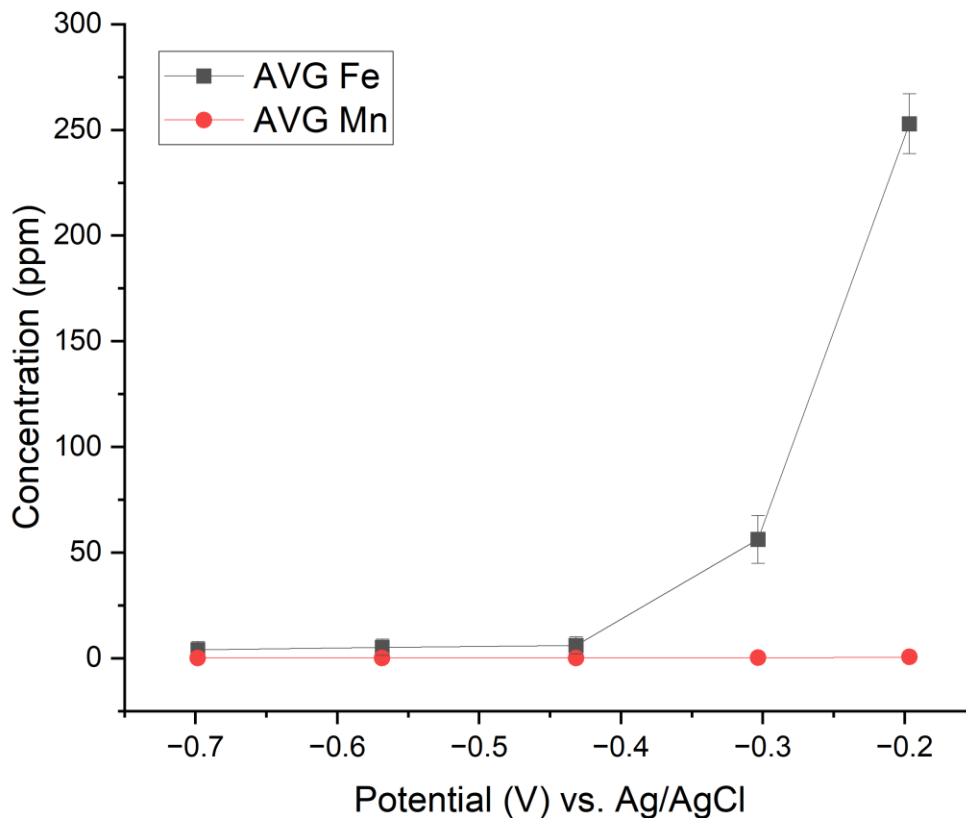
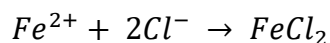


Figure 31: A graph displaying the ICP-OES results of fingerprinted low-carbon samples. The concentrations of Fe and Mn are displayed for each corresponding aliquot taken from the bulk solution over the course of the applied linear potential sweep

Iron concentrations increase significantly over time, which aligns with expectations based on the alloy composition and its corrosion potential. The potential at which these increases occur, particularly around -0.30 V and -0.20 V, suggests that the applied potentials are sufficient to induce corrosion of iron, whose corrosion potential is -0.44 V. This indicates that the electrochemical environment during the linear sweep voltammetry (LSV) measurements reaches the necessary conditions to overcome the natural passivation of iron.

Iron typically forms a passive oxide layer, primarily composed of iron (III) oxide ( $\text{Fe}_2\text{O}_3$ ), as noted in Equation 29, which acts as a protective barrier against further corrosion. This oxide layer is stable under neutral and slightly alkaline conditions, contributing to the material's overall resistance to corrosion. However, in the acidic conditions used in these experiments, the stability of this oxide layer is compromised. The acidic environment, combined with the applied potential, can lead to the breakdown of this passive layer, allowing the underlying iron to corrode. The dissolution reaction of iron in acidic conditions is represented in Equation 30. As the applied potential becomes more positive, the passive  $\text{Fe}_2\text{O}_3$  layer breaks down, exposing the iron to the corrosive environment and resulting in the observed increase in iron concentrations. The initial potentials of -0.70 V to -0.43 V are likely not high enough to fully disrupt the passive layer, leading to lower concentrations of iron in the initial aliquots. However, at potentials around -0.30 V and -0.20 V, the applied potential is sufficient to induce significant corrosion, resulting in a substantial increase in iron concentrations.

The error observed in the iron measurements is comparable to that seen in C260 brass samples, indicating that low-carbon steel samples also produce relatively consistent results during targeted corrosion enhancement. This consistency is likely due to the homogeneous nature of the steel alloy and the predictable behavior of its corrosion process once the passive layer is disrupted. The presence of chloride ions from eccrine sweat in fingerprinted samples accelerates the dissolution of the oxide layer and iron itself, forming soluble iron chloride complexes:



Equation 37: The formation of soluble iron chloride complexes

This process not only increases the rate of iron corrosion but also ensures a more uniform corrosion front, leading to the relatively consistent and predictable increase in iron concentrations observed in the fingerprinted samples. The homogeneous distribution of chloride ions in the sweat residues contributes to the lower variability and smaller error margins in these samples compared to the non-fingerprinted ones.

In summary, the significant increase in iron concentrations at potentials around -0.30 V and -0.20 V is a direct result of the electrochemical environment overcoming the natural passivation of iron, facilitated by the acidic conditions and the presence of chloride ions from fingerprints. This behavior is consistent with the known corrosion potentials and reactions of iron, providing a clear explanation for the observed data.

The data collected from three trials of non-fingerprinted low-carbon steel samples is shown in Table 18. Iron and manganese concentrations were measured, and both elements were present and detectable. The results for iron and manganese concentrations are shown below.

Table 18: ICP-OES measurement results of three trials of non-fingerprinted low-carbon steel samples

| <b>E (V)</b> | <b>Avg Fe (ppm)</b> | <b>Avg Mn (ppm)</b> |
|--------------|---------------------|---------------------|
| <b>-0.70</b> | 0.80 ± 0.2          | 0.071 ± 0.01        |
| <b>-0.57</b> | 1.68 ± 0.5          | 0.090 ± 0.004       |
| <b>-0.43</b> | 2.29 ± 0.5          | 0.092 ± 0.004       |
| <b>-0.30</b> | 35 ± 12             | 0.15 ± 0.02         |
| <b>-0.20</b> | 174 ± 45            | 0.40 ± 0.08         |

Figure 32 below displays the change in concentration of each component of the non-fingerprinted low-carbon steel samples changes throughout the course of the applied linear potential sweep.

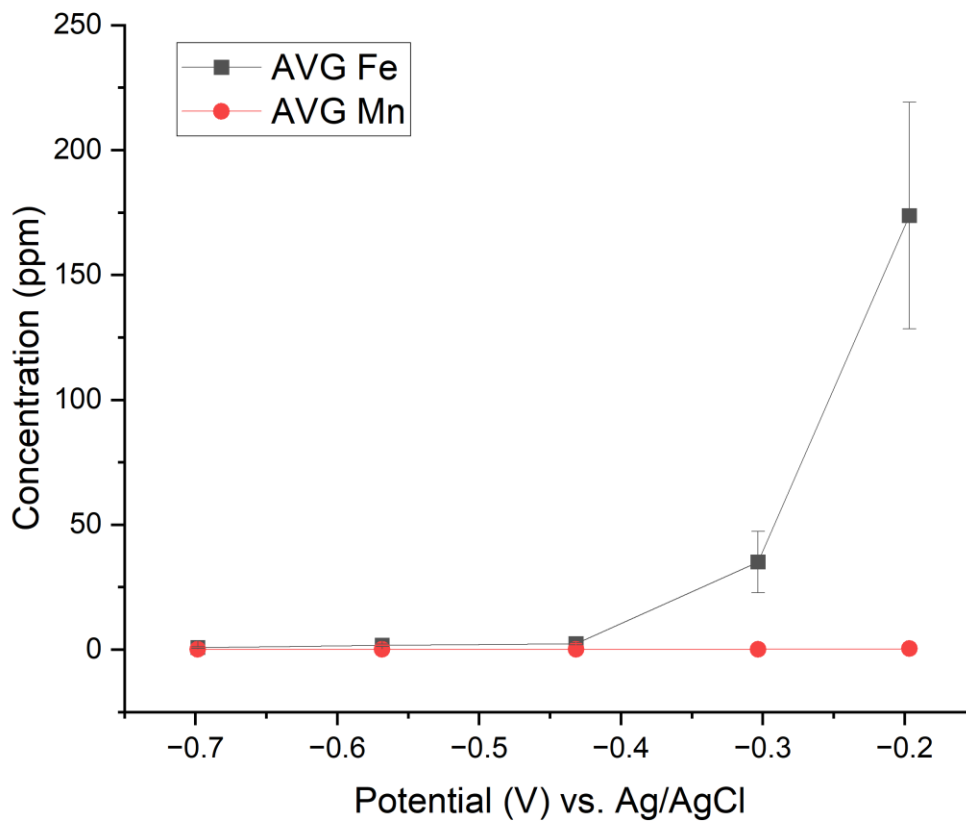


Figure 32: A graph displaying the ICP-OES results of non-fingerprinted low-carbon samples. The concentrations of Fe and Mn are displayed for each corresponding aliquot taken from the bulk solution over the course of the applied linear potential sweep



Iron concentrations increase significantly over time, particularly at potentials near -0.30 V and -0.20 V, which aligns with expectations based on the alloy composition and its corrosion potential of -0.44 V. This suggests that the applied potentials are sufficient to induce corrosion of iron. The dissolution reaction of iron in acidic conditions is represented in Equation 30, where the breakdown of the passive iron (III) oxide ( $\text{Fe}_2\text{O}_3$ ) layer occurs.

Manganese concentrations remain relatively low and stable throughout the experiments. This stability suggests that the applied potentials and experimental conditions were not sufficient to significantly induce the corrosion of manganese, whose standard reduction potential is -1.18 V. Consequently, manganese did not contribute significantly to the overall corrosion process under the tested conditions.

The error observed in the non-fingerprinted low-carbon steel samples is relatively high, indicating variability in the corrosion process. This variability could be due to the absence of chloride ions from eccrine sweat, which in fingerprinted samples facilitates a more uniform and predictable corrosion process. The formation of soluble iron chloride complexes, as shown in Equation 37, is accelerated by the presence of chloride ions, leading to a more consistent corrosion front in fingerprinted samples.

In summary, the significant increase in iron concentrations at potentials around -0.30 V and -0.20 V is a direct result of the electrochemical environment overcoming the natural passivation of iron, facilitated by the acidic conditions. The presence of manganese, though at lower concentrations, indicates its participation in the corrosion process, but the primary focus remains on the behavior of iron due to its higher concentration and significant increase under the applied potentials.

The findings suggest that the low-carbon steel samples produce relatively consistent results during targeted corrosion enhancement, with iron concentrations increasing predictably at specific potentials. The error in the non-fingerprinted samples indicates a less consistent corrosion process, likely due to the lack of chloride ions facilitating the breakdown of the passive Fe<sub>2</sub>O<sub>3</sub> layer. This emphasizes the importance of understanding the chemical interactions between fingerprint residues and metal substrates in forensic applications.

#### **4.3.4 400-Nickel alloy ICP-OES Results**

All 400-Nickel alloy samples were assessed for copper, iron, manganese, and nickel, representing the majority composition of the alloy. Three trials of fingerprinted and three trials of non-fingerprinted 400-Nickel alloy were conducted. Table 19 displays the results of the ICP-OES measurements on three fingerprinted 400-Nickel alloy samples with the corresponding potentials of each aliquot removed.

Table 19: ICP-OES measurement results of three trials of fingerprinted 400-Nickel alloy samples

| <b>E (V)</b> | <b>Avg Cu (ppm)</b> | <b>Avg Fe (ppm)</b> | <b>Avg Mn (ppm)</b> | <b>Avg Ni (ppm)</b> |
|--------------|---------------------|---------------------|---------------------|---------------------|
| <b>-0.22</b> | 0.42 ± 0.07         | 0.326 ± 0.001       | 0.3235 ± 0.0005     | 0.43 ± 0.6          |
| <b>-0.09</b> | 0.46 ± 0.01         | 0.3290 ± 0.0004     | 0.3251 ± 0.0004     | 16.3 ± 2            |
| <b>0.01</b>  | 0.49 ± 0.01         | 0.334 ± 0.005       | 0.3259 ± 0.0006     | 27.1 ± 4            |
| <b>0.13</b>  | 2.39 ± 0.2          | 0.45 ± 0.01         | 0.383 ± 0.005       | 829 ± 81            |
| <b>0.26</b>  | 26 ± 15             | 1.42 ± 0.3          | 0.88 ± 0.1          | 7654 ± 2069         |

Nickel and copper concentrations increase over time, which aligns with expectation, as well as the observations of the fingerprinted 400-Nickel alloy samples. The significant increase in nickel concentrations, particularly at potentials around 0.13 V and 0.26 V, suggests that the applied potentials are sufficient to induce corrosion of nickel, whose corrosion potential is -0.26 V. This aligns with the nickel reduction potential listed in Table 11 and indicates that the electrochemical environment during the linear sweep voltammetry (LSV) measurements reaches the necessary conditions to induce nickel corrosion. Copper concentrations also increase significantly at these potentials, aligning with its corrosion potentials of 0.34 V and 0.52 V.

The high error observed in the fingerprinted samples is likely due to the complex nature of the corrosion process involving multiple elements. The presence of chloride ions from eccrine sweat can disrupt the protective oxide layers on the alloy surface, accelerating the corrosion process and increasing variability. The breakdown of the passive nickel oxide layer (NiO), as discussed in Equation 35, further facilitates the corrosion of nickel.

Figure 33 depicts how the concentration of nickel within the fingerprinted 400-Nickel alloy samples changes throughout the linear potential sweep. To allow for better visualization, Figure 34 displays the changing concentrations of copper, iron, and manganese.

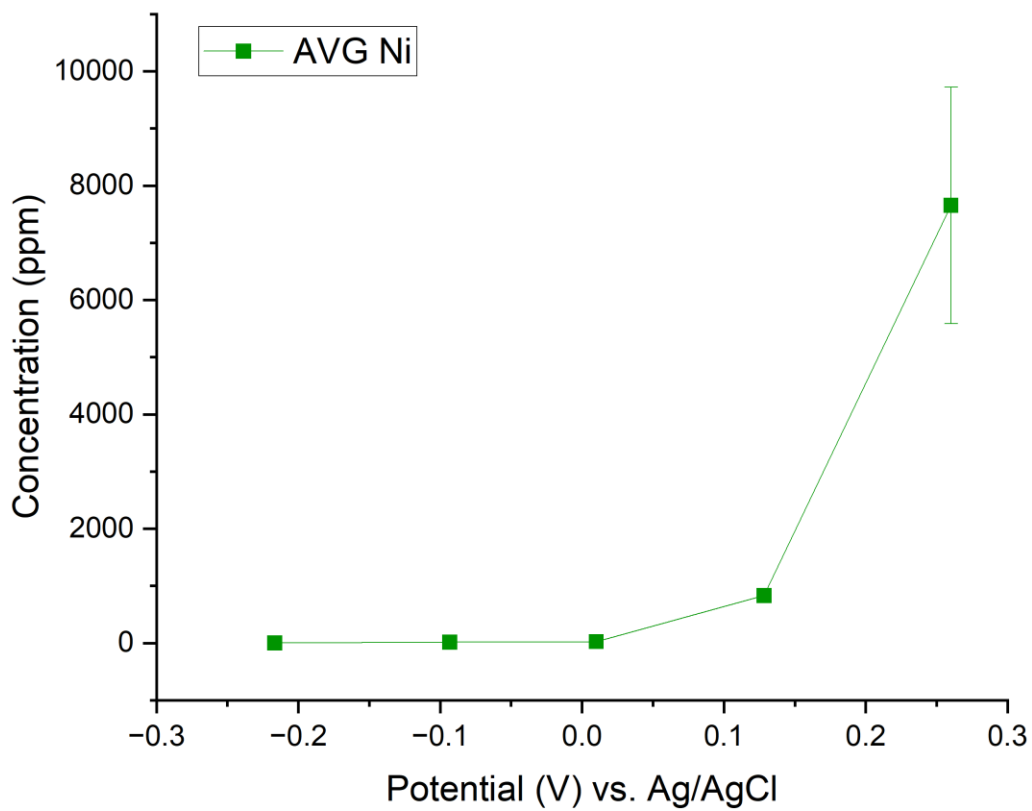


Figure 33: A graph displaying the ICP-OES results of fingerprinted 400-Nickel alloy samples. The concentration of Ni is displayed for each corresponding aliquot taken from the bulk solution over the course of the applied linear potential sweep

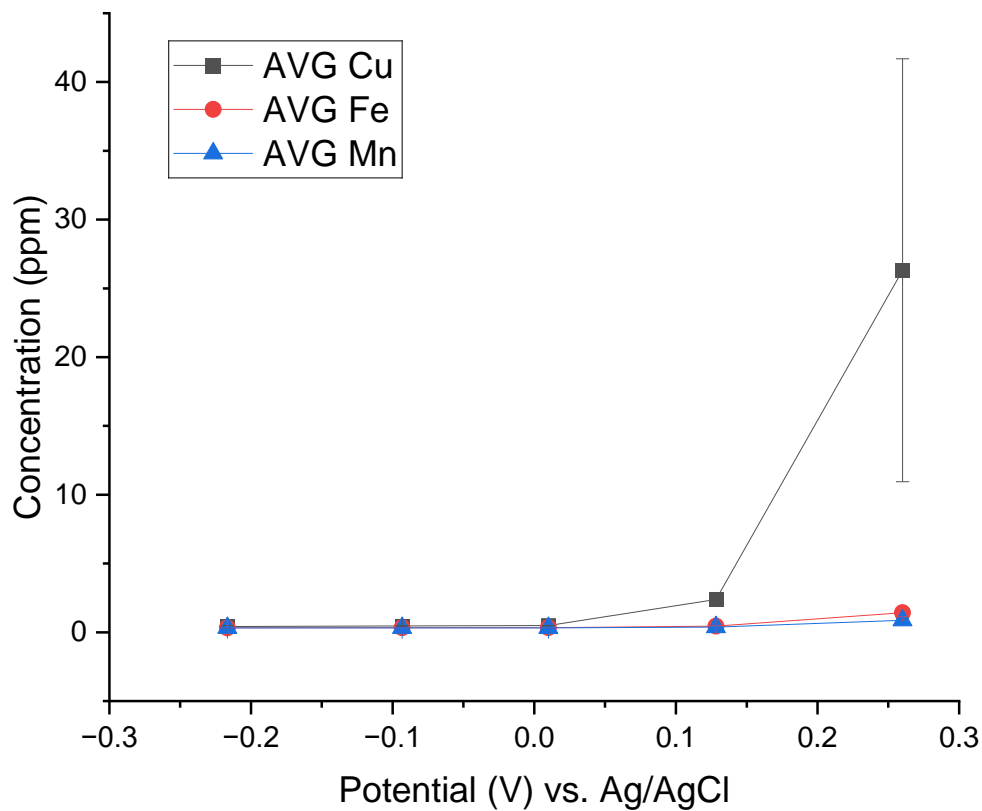


Figure 34: A graph displaying the ICP-OES results of fingerprinted 400-Nickel alloy samples. The concentrations of Cu, Fe, and Mn are displayed for each corresponding aliquot taken from the bulk solution over the course of the applied linear potential sweep

Fingerprinted 400-Nickel alloy samples displayed a high level of error similar to what was observed in the 6061-Aluminum alloy samples. Nickel and copper concentrations increase over time, which is aligned with expectations, but the error grows with each aliquot indicating that corrosion increases variability over time. Targeted corrosion enhancement results for 400-Nickel alloy were not repeatable which may be a result of this increased variability in corrosion over time.

Table 20 displays the ICP-OES measurement data from the non-fingerprinted 400-Nickel alloy samples.

Table 20: ICP-OES measurement results of three trials of non-fingerprinted 400-Nickel alloy samples

| <b>E (V)</b> | <b>Avg Cu (ppm)</b> | <b>Avg Fe (ppm)</b> | <b>Avg Mn (ppm)</b> | <b>Avg Ni (ppm)</b> |
|--------------|---------------------|---------------------|---------------------|---------------------|
| <b>-0.22</b> | 0.348 ± 0.006       | 0.3263 ± 0.0004     | 0.3232 ± 0.0005     | 3.3 ± 3             |
| <b>-0.09</b> | 0.47 ± 0.07         | 0.340 ± 0.008       | 0.328 ± 0.004       | 62 ± 60             |
| <b>0.01</b>  | 0.56 ± 0.07         | 0.35 ± 0.01         | 0.330 ± 0.006       | 97 ± 80             |
| <b>0.13</b>  | 1.69 ± 1.0          | 0.41 ± 0.06         | 0.36 ± 0.03         | 515 ± 440           |
| <b>0.26</b>  | 51 ± 5.0            | 1.92 ± 0.1          | 1.14 ± 0.07         | 11076 ± 1000        |

The data from non-fingerprinted 400-Nickel alloy samples show similar trends as the fingerprinted samples, with increasing concentrations of copper and nickel over time, and relatively low concentrations of iron and manganese. The potential at which these increases occur, particularly around 0.13 V and 0.26 V, aligns with the corrosion potentials of these elements. This confirms that the applied potentials were sufficient to induce significant corrosion of copper and nickel.

Figure 35 displays the changing concentration of nickel throughout the linear potential sweep for three non-fingerprinted 400-Nickel alloy trials. Figure 36 represents the changes in concentration of copper, iron, and manganese throughout the linear potential sweep for the same trials.

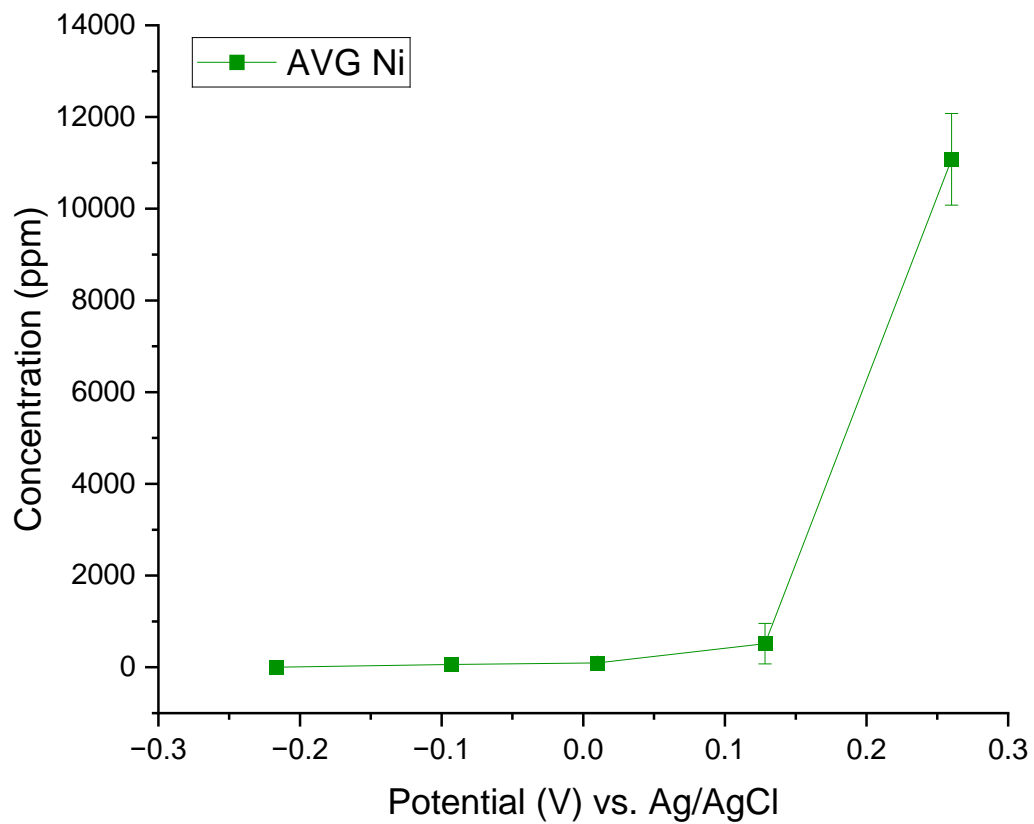


Figure 35: A graph displaying the ICP-OES results of non-fingerprinted 400-Nickel alloy samples. The concentration of Ni is displayed for each corresponding aliquot taken from the bulk solution over the course of the applied linear potential sweep

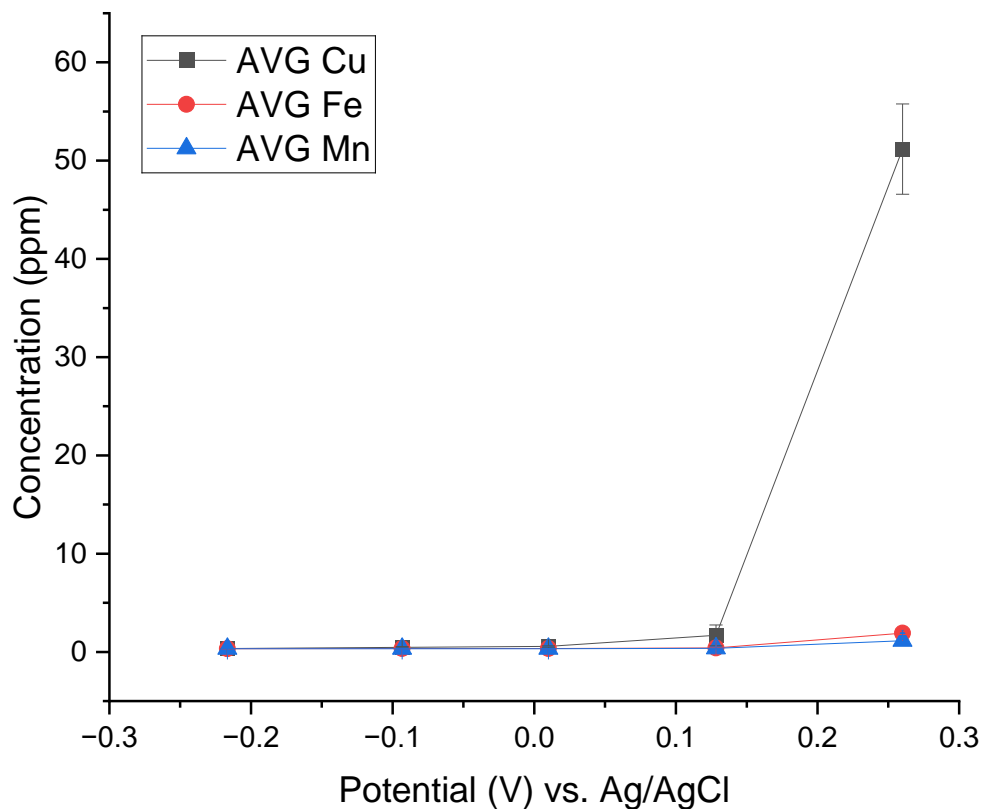


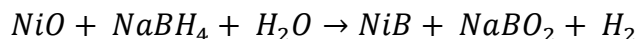
Figure 36: A graph displaying the ICP-OES results of non-fingerprinted 400-Nickel alloy samples. The concentrations of Cu, Fe, and Mn are displayed for each corresponding aliquot taken from the bulk solution over the course of the applied linear potential sweep

Nickel and copper concentrations increase over time, which aligns with expectations, as well as the observations of the fingerprinted 400-Nickel alloy samples. The non-fingerprinted samples display a smaller error than those with applied fingerprints, indicating that the presence of fingerprints increases variability and may inhibit repeatability. The high error observed in the fingerprinted samples may be due to the heterogeneous nature of the corrosion process in the presence of fingerprints.



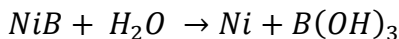
The 400-Nickel alloy samples exhibit significant increases in nickel and copper concentrations at higher potentials, which align with their respective corrosion potentials. The high error in fingerprinted samples suggests a complex and variable corrosion process, likely influenced by the presence of chloride ions from fingerprints. This variability makes 400-Nickel alloy less suitable for corrosion-based latent fingerprint development and enhancement methods compared to other tested substrates. To improve the corrosion-based methods for latent fingerprint enhancement on 400-Nickel alloy, a review of literature on corrosion of this alloy in different chemical environments is essential. Studies have shown that sodium borohydride and nitric acid can significantly impact the corrosion behavior of nickel alloys [97].

Sodium borohydride, when used in an alkaline medium, acts as a strong reducing agent. It can facilitate the removal of the protective oxide layer on nickel alloys, thereby increasing their susceptibility to corrosion. The interaction of NaBH<sub>4</sub> with the 400-Nickel alloy can lead to the formation of nickel borides on the surface, which could potentially alter the corrosion resistance of the alloy. The nickel (II) oxide layer, as described in Equation 35, is disrupted by the exposure to sodium borohydride:



Equation 38: Disruption of nickel (II) oxide layer by exposure to sodium borohydride forming nickel borides on the surface of the metal alloy substrate

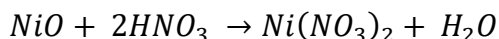
Then, after the protective oxide layer has been destroyed, the corrosion of nickel proceeds:



Equation 39: Corrosion of nickel through the removal of nickel borides formed on the surface

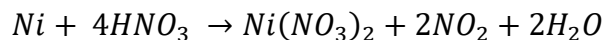
This process is beneficial for exposing latent fingerprints as it helps in breaking down the protective layers and exposing the underlying metal surface to further corrosion. Sodium borohydride in alkaline conditions can lead to significant hydrogen evolution, which assists in breaking down the oxide layer and exposing fresh nickel surface to further corrosion. Conducting LSV measurements in a 0.1M NaBH<sub>4</sub> solution can provide valuable data on the impact of this chemical on nickel alloy corrosion.

Similarly, nitric acid, a strong oxidizing agent, can disrupt the oxide layer and accelerate corrosion processes. Nitric acid is known for its ability to penetrate and uniformly corrode the oxide layer due to its strong oxidizing properties. Dilute nitric acid solutions (e.g., 0.1M HNO<sub>3</sub>) can be used in LSV measurements to evaluate the extent of corrosion and the presence of nickel ions in the solution. The interaction of nitric acid with nickel alloys involves the rapid attack of the alloy, especially in the presence of chlorides, leading to increased corrosion rates and the formation of nickel nitrates. The nickel (II) oxide layer, as described in Equation 35, is disrupted by the exposure to nitric acid:



Equation 40: Disruption of nickel (II) oxide layer by exposure to nitric acid

Without the protection of the oxide layer, corrosion of nickel proceeds:



Equation 41: Corrosion of nickel after destruction of nickel (II) oxide layer

Exposure to sodium borohydride or nitric acid could enhance the visibility of latent fingerprints by uniformly corroding the surface and exposing the underlying nickel metal. A sequential treatment combining  $\text{NaBH}_4$  followed by  $\text{HNO}_3$  might yield even better results by leveraging the strengths of both chemicals to achieve more pronounced and consistent corrosion. The reducing environment created by  $\text{NaBH}_4$  can break down the initial oxide layer, and the subsequent oxidizing environment provided by  $\text{HNO}_3$  can further corrode the exposed nickel surface. Their combined use could provide a robust method for revealing latent fingerprints by ensuring thorough and uniform corrosion, making 400-Nickel alloy a more viable substrate for corrosion-based forensic techniques.

#### **4.4 Conclusions and Future Work**

Chapter 4 provided a detailed examination of the corrosion behaviors of 6061-Aluminum alloy, C260 brass, low-carbon steel, and 400-Nickel alloy, employing linear sweep voltammetry techniques and Inductively Coupled Plasma–Optical Emission Spectroscopy (ICP-OES). The results highlighted significant differences in the repeatability and uniformity of corrosion across these substrates, which are crucial for their forensic applicability.

C260 brass and low-carbon steel demonstrated the highest levels of consistency and lowest levels of error with the employed linear sweep voltammetry and ICP-OES methods, showing consistent and predictable patterns of corrosion. The repeatability and uniformity observed in these substrates mirror the findings from targeted corrosion enhancement, further confirming their suitability for forensic applications. The presence of fingerprints in C260 brass

facilitated a more uniform corrosion process, likely due to chloride ions in eccrine sweat disrupting the oxide layer and enhancing corrosion. The dezincification process observed in C260 brass, where zinc corrodes preferentially to copper, created a controlled corrosion environment beneficial for forensic analysis. Similarly, low-carbon steel exhibited significant increases in iron concentrations at specific potentials, aligning with its corrosion potential of -0.44 V. The presence of chloride ions in fingerprinted samples facilitated a more uniform corrosion front, leading to lower variability and smaller error margins. The corrosion process in low-carbon steel was predictable once the passive iron (III) oxide layer was disrupted, making it a suitable candidate for forensic enhancements.

On the other hand, 6061-Aluminum and 400-Nickel alloys displayed significant challenges. The analysis revealed substantially larger errors in both fingerprinted and non-fingerprinted samples, creating challenges with repeatability. These substrates experienced inherent variability in their respective corrosion behaviors, which could undermine the reliability of forensic analyses conducted on them. The high error observed in fingerprinted samples of 400-Nickel alloy suggested a complex and variable corrosion process, likely influenced by the presence of chloride ions from fingerprints. The breakdown of the passive nickel oxide layer further facilitated the corrosion of nickel, but the overall variability made 400-Nickel alloy less suitable for corrosion-based latent fingerprint development and enhancement methods. Similarly, the variability and repeatability issues observed with 6061-Aluminum alloy indicate that current corrosion-based methods may not be optimal for this substrate.

The ICP-OES findings provided valuable insights into the specific metal elements influencing corrosion in each alloy and underscored the importance of substrate selection in forensic applications. The data from 6061-Aluminum alloy and 400-Nickel alloy suggested that

these materials might not be suitable for current corrosion-based enhancement methods due to their inherent variability and the technical challenges in controlling their corrosion responses. The analysis highlighted the critical role of understanding the electrochemical properties of the substrates, as evidenced by the differing corrosion susceptibilities and behaviors observed among the metals tested. These differences are pivotal in determining the effectiveness of forensic enhancement techniques, emphasizing the need for a tailored approach based on the specific properties of each substrate.

The findings from Chapter 4 underscore the complexity of applying corrosion-based methods across different metal substrates for forensic purposes. While C260 brass and low-carbon steel emerge as more suitable candidates for such applications, the challenges observed with 6061-Aluminum alloy and 400-Nickel alloys reflect the limitations of a one-size-fits-all approach. This chapter has successfully filled some of the knowledge gaps and resolved ambiguities regarding the corrosion behaviors of the investigated substrates, providing a clearer picture of their potential and limitations in forensic science. Future work should focus on optimizing the corrosion conditions for each substrate, exploring the use of different chemical agents such as sodium borohydride and nitric acid to enhance corrosion-based forensic techniques, and investigating the long-term stability of corrosion products in various environmental conditions. The proposed new methods for 6061-Aluminum and 400-Nickel alloys, involving treatments with sodium borohydride and nitric acid, should be pursued to address the identified challenges and improve the reliability of corrosion-based latent fingerprint development on these substrates.

## **Chapter 5: Electrodeposition and Other Electroanalytical Methods as Forensic Investigative Techniques**

### **5.1 Introduction**

In forensic science, effectively visualizing latent fingerprints on metal substrates exposed to harsh conditions is essential for criminal investigations. This chapter investigates the innovative application of electrodeposition and electroless deposition techniques, specifically tailored to enhance latent fingerprints on challenging substrates. These electroanalytical methods, expanded upon from the experimental foundations in Chapter 2, are explored as solutions where traditional fingerprint recovery techniques fall short, particularly with fired cartridge casings and submerged weapons.

This chapter begins with a review of how these methods have been adapted from their industrial applications to forensic science, focusing on their theoretical basis and the detailed procedures for implementing them as described in Chapter 2. Electrodeposition uses an electric current to deposit a metal layer onto a conductive substrate. In forensic applications, this method can selectively enhance the ridge details of latent fingerprints by depositing metals on the ridge areas, providing a contrast necessary for high-resolution imaging. This section will delve into the specific parameters optimized through experimental methods, which are crucial for achieving the best results without damaging the underlying fingerprint.

Unlike electrodeposition, electroless deposition does not require an external electrical source, making it suitable for treating non-conductive surfaces and offering broader application

potential in forensic investigations. This process utilizes a chemical reduction reaction in which a metal ion in a solution is reduced and deposited onto a catalytic surface, facilitated by a reducing agent. The metal ions gain electrons from the reducing agent, turning into a solid metal that forms a layer over the substrate, adhering closely to the contours of any fingerprint residues present. By providing a continuous supply of metal ions and reducing agent, the deposition process proceeds autonomously, enhancing the latent fingerprints by depositing a fine metallic film that increases the contrast and visibility of the ridge details under forensic examination. This method may also be effective for enhancing latent fingerprints on non-conductive surfaces, thereby expanding the types of evidence that can be processed in forensic labs.

Adopting new technologies in forensic labs involves careful consideration of their practicality and integration into existing workflows. This chapter assesses the operational implications of introducing electrodeposition and electroless deposition, including the required equipment, effectiveness, and toxicity concerns. Additionally, it evaluates the reproducibility and reliability of these methods in a forensic context to discuss whether they meet the rigorous standards required for courtroom evidence.

## **5.2 Materials and Methods**

This section outlines the materials and methods utilized in the experiments concerning electrodeposition and electroless deposition techniques for forensic applications, as detailed in Chapter 2: Experimental Methods. These foundational elements are critical for the successful adaptation of these techniques in the forensic analysis of latent fingerprints on metal substrates.

As described in Section 2.1 of Chapter 2, the materials used in this study included various metals commonly encountered in forensic evidence, such as 6061-Aluminum alloy, C260 brass, low-carbon steel, and 400-Nickel alloy, all sourced from McMaster-Carr. The reagents and solutions used for both electrodeposition and electroless deposition, including the electrolyte solutions and metal salts, were also specified in this section.

The electrodeposition experiments were conducted using the setups and parameters outlined in Section 2.3.4 of Chapter 2. This involved applying an electric current across an electrochemical cell to induce the deposition of metal ions onto the conductive substrate. The precise control of current and voltage was essential for ensuring that the metal deposition enhanced the fingerprint details without damaging the substrate. The operational details of the electrodeposition process, including the use of specific electroplating solutions and equipment settings, are integral to replicating the results in forensic contexts.

Section 2.3.5 of Chapter 2 detailed the methods used for electroless deposition, which does not require an external electrical source. This process relies on the chemical reduction of metal ions from a solution onto a catalytic surface of the substrate, facilitated by a reducing agent. The autocatalytic nature of this process allows for continuous metal deposition, enhancing the visibility of latent fingerprints.

The characterization of the deposited materials and the analysis of the enhanced fingerprints were primarily assessed using optical microscopy techniques as outlined in Section 2.5 of Chapter 2. This provided a systematic approach to evaluating the clarity and continuity of the fingerprint ridges after treatment.



The integration of these methods into forensic workflows involves not only the adaptation of the experimental setups described in Chapter 2 but also the careful consideration of the practical and logistical aspects of conducting these techniques in a forensic setting. This includes ensuring the reproducibility of the results, adherence to forensic standards, and the feasibility of implementing these methods in typical forensic laboratories.

## **5.3 Results and Analysis**

### **5.3.1 Electrodeposition of Gold**

Gold is deposited first in any vacuum metal deposition technique for its superior adherence onto metallic surfaces, and thus, this research began with the electrodeposition of Krohn 24K gold electroplating solution onto C260 brass and low-carbon steel samples.

Three trials were conducted at each of the various applied potentials and corresponding amounts of time to find both the potential and time that yielded optimal latent fingerprint enhancement and visualization. Before and after images were utilized to grade the development of each fingerprint.

The table below shows the average change in fingerprint development grades after electrodeposition of gold onto C260 brass substrates after various applied potentials for various lengths of time. Ultimately, these measurements found the optimal parameters for C260 brass samples to be the application of 4V for a total of 20 seconds.

Table 21: Electrodeposition of gold onto C260 brass substrates and the average change in fingerprint grade for various applied potentials and time frames

|                      | <b>C260 Brass</b>                                    |
|----------------------|--|
|                      | <b>Average <math>\Delta</math> Fingerprint Grade</b> |
| <b>2V for 15 sec</b> | 0  |
| <b>2V for 60 sec</b> | 0.3  |
| <b>3V for 30 sec</b> | 0.3  |
| <b>3V for 60 sec</b> | 0.7  |
| <b>4V for 15 sec</b> | 2.3  |
| <b>4V for 20 sec</b> | 3  |
| <b>4V for 30 sec</b> | 2.3  |

Electrodeposition of gold onto C260 brass substrates achieved the highest average change of 3 at the optimal parameters listed. Although this is the same as the change of 3 achieved with targeted corrosion enhancement, electrodeposition yielded uneven surface coverage with holes appearing in some of the coated fingerprints. Figure 37 below shows one of three trials conducted and the results obtained. Because these results clearly display that electrodeposition can develop latent fingerprints, future research may be aimed at optimizing electrodeposition on its own, or in tandem with other development methods. The hole toward the top of the fingerprint interferes with resolution of fingerprint ridges in that area and the formation of these uneven areas was common amongst the trials. The short time frame of the measurements combined with

the thick, green precipitate that forms almost immediately make it very difficult to monitor, address, and prevent the formation of these holes in the fingerprints. Figure 38, then, is meant to serve as a stepwise guide of what was observed at each step throughout this electrodeposition measurement to aid these efforts.



Figure 37: One of three trials of gold electrodeposited onto C260 brass using an applied potential of 4V for a total of 20 seconds

### C260 Brass



Figure 38: One of three trials of Au electrodeposited onto C260 brass using an applied potential of 4V for a total of 20 seconds. Images are taken before electrodeposition, after electrodeposition whilst still in solution, after electrodeposition solution has been poured off and the sample rinsed with ultrapure water, and lastly, after the sample has been removed from the flat platform cell and dried with a KimWipe

Low-carbon steel samples did not demonstrate the same repeatability and the optimal parameters were more difficult to elucidate from the data and results obtained. The electrodeposition of gold was uneven and incomplete across the substrate surface of each sample. Often, an agglomeration of gold atoms would form in one area of the substrate surface. This may be a result of lower levels of conductivity in low-carbon steel, as opposed to C260 brass, causing lower adhesion of gold atoms to the substrate surface. Table 22 displays the results of the average change in fingerprint grade over three trials at each applied potential and given time frame.

Table 22: Electrodeposition of gold onto low-carbon steel substrates and the average change in fingerprint grade for various applied potentials and time frames

|                      | <b>Low-carbon Steel</b>                              |
|----------------------|--|
|                      | <b>Average <math>\Delta</math> Fingerprint Grade</b> |
| <b>2V for 15 sec</b> | 0  |
| <b>2V for 60 sec</b> | 0.3  |
| <b>3V for 15 sec</b> | 0.3  |
| <b>3V for 30 sec</b> | 1.3  |
| <b>3V for 60 sec</b> | 1.7  |
| <b>3V for 90 sec</b> | 1.7  |
| <b>4V for 15 sec</b> | 1  |

The highest average change in fingerprint grade achieved with electrodeposition of gold onto low-carbon steel is 1.7 corresponding to an applied potential of 3V for both 60 and 90 seconds. This is substantially lower than the average change in fingerprint grade of 3.4 for targeted corrosion enhancement via potentiodynamic corrosion and these results indicate that the former is better suited to develop latent fingerprints. Figure 39 shows the results of three trials of low-carbon steel samples subjected to electrodeposition of gold with an applied potential of 3V for 60-90 seconds.

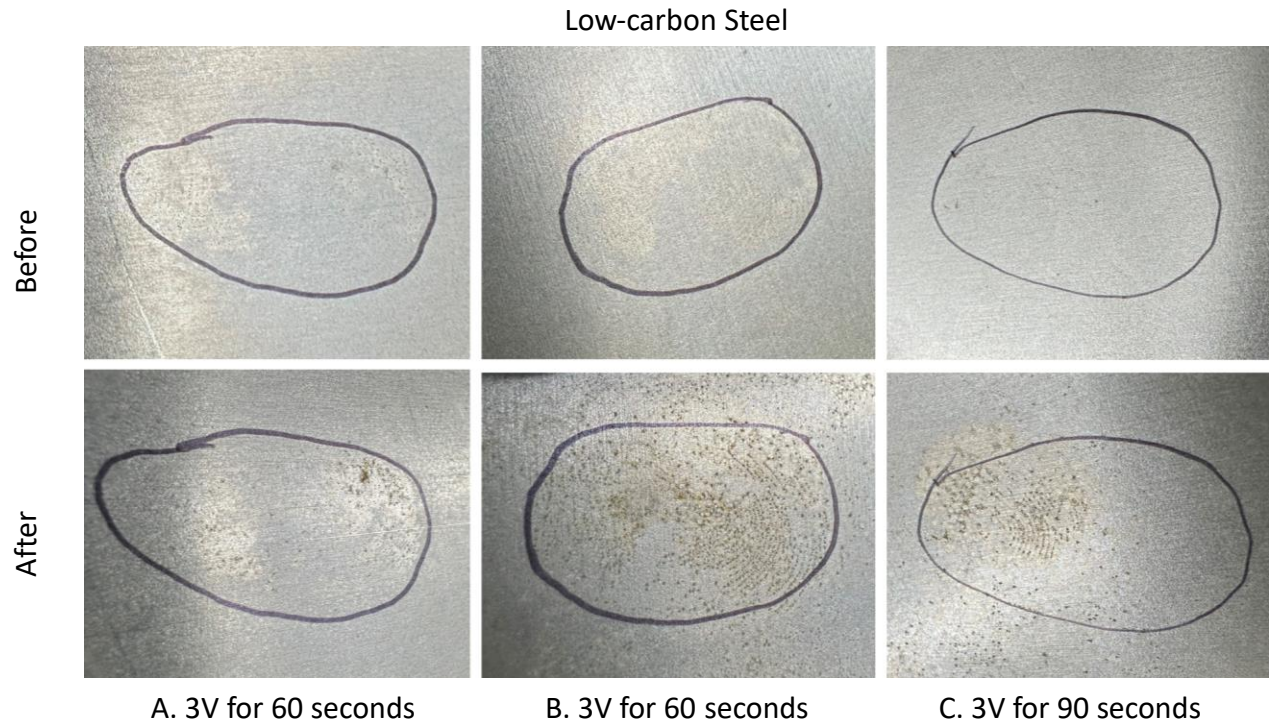


Figure 39: A and B represent before and after images of two of three trials of low-carbon steel samples subjected to electrodeposition of gold with an applied potential of 3V for 60 seconds. C represents before and after images of one of three trials subjected to an applied potential of 3V for 90 seconds

These images represent the three fingerprints with the highest grade of development after electrodeposition. Image sets A and B, two of three trials subjected to an applied potential of 3V for 60 seconds, demonstrate the level of inconsistency observed amongst trials subjected to the same applied potential for the same amount of time. Image set C, one trial subjected to the same applied potential of 3V but for a longer time frame of 90 seconds, is included to show that the results can overlap with one another in terms of development observed over different lengths of

time. This makes it challenging to distinguish specific optimal parameters for this particular method of latent fingerprint enhancement and should be considered prior to use.

### **5.3.2 Electrodeposition of Silver**

While other techniques typically reserve the application of silver or zinc until a base layer of another metal, such as gold, has been created, the electrodeposition of metals for latent fingerprint development is not well-explored or well-understood. For instance, the variations in fingerprint residue composition make it difficult to predict whether a given method will generate a regularly-developed or reverse-developed fingerprint in Vacuum Metal Deposition (VMD). Forensic scientists cannot visually distinguish primarily sebaceous residue from primarily eccrine and cannot be certain of composition without disturbing the residue and thus possibly destroying part of the fingerprint.

Given the inherent uncertainty in residue composition as well as the scope of this research, electrodeposition of silver is warranted, alone, onto metal substrates. Naturally, silver is also relatively inexpensive compared to gold, which makes it an alternative worthy of further exploration. Moreover, silver nitrate, a common reagent in forensic science, has been successfully used to develop fingerprints by reacting with chloride ions present in eccrine sweat to form silver chloride, a compound that darkens upon exposure to light, enhancing the fingerprint's visibility. This reaction underscores the potential utility of silver in forensic applications beyond its traditional use in argentation.

The exploration of electrodeposition of silver in this research could open new avenues for cost-effective and efficient fingerprint development methods, potentially offering a more straightforward and less material-intensive process compared to methods that require multiple layers of different metals. An innovative approach could involve the initial electrodeposition of metallic silver directly onto the latent fingerprints, followed by a targeted exposure to chloride ions. This method would exploit the natural presence of chloride in eccrine sweat residues found in fingerprints, or alternatively, a chloride-rich environment could be artificially created post-deposition.

This sequential process would involve two key stages. In the first stage, metallic silver would be deposited on the substrate where the latent fingerprints are located. The controlled application of an electric current would ensure that silver is deposited precisely in the regions where eccrine residues enhance electrical conductivity, thus mapping the ridge patterns of the fingerprints. Following the deposition of silver, the substrate could be exposed to a chloride solution or a chloride vapor. This exposure would facilitate the reaction between the deposited silver and the chloride ions, leading to the formation of silver chloride. The silver chloride, being light-sensitive, would darken upon exposure to light, thereby enhancing the visibility of the fingerprint ridges.

Such a method not only has the potential to streamline the fingerprint development process but also enhances the contrast and definition of the fingerprints. The formation of silver chloride directly on the fingerprint residues could provide dual benefits: strengthening the durability of the fingerprint image and increasing the contrast due to the photoreactive nature of silver chloride. This approach warrants further experimental validation to optimize the conditions



for silver deposition and subsequent chloride treatment to maximize the efficacy and reliability of this technique in forensic applications.

Building on these theoretical considerations, the experimental phase of this research sought to validate and refine the processes through practical applications. Similar to the electrodeposition of gold, which was methodically tested to establish optimal parameters, the experiments with silver aimed to mirror this rigor. Three trials were conducted at various applied potentials and durations to optimize fingerprint development for C260 brass and low-carbon steel samples. These experiments were designed to assess the practicality of the proposed silver electrodeposition method and its effectiveness in enhancing latent fingerprints under controlled conditions.

Table 23 below displays the average change in fingerprint grade after electrodeposition of silver onto C260 brass substrates at various potentials for various amounts of time.

Electrodeposition of silver onto C260 brass substrates was found to work best with an applied potential of 1V for 30 seconds which generated the highest average change in fingerprint grade of 1.3.

Table 23: Electrodeposition of silver onto C260 brass substrates and the average change in fingerprint grade for various applied potentials and time frames

|                      | <b>C260 Brass</b>                                    |
|----------------------|--|
|                      | <b>Average <math>\Delta</math> Fingerprint Grade</b> |
| <b>1V for 15 sec</b> | 0.3  |
| <b>1V for 30 sec</b> | 1.3  |
| <b>1V for 45 sec</b> | 0.7  |
| <b>1V for 60 sec</b> | 0.3  |

Figure 40 displays one of three trials held at an applied potential of 1V for 30 seconds which displays the most fingerprint development observed amongst all trials.

## C260 Brass



Figure 40: One of three trials of silver electrodeposited onto C260 brass held at an applied potential of 1V for 30 seconds

Comparing the highest average change in fingerprint grade of 1.3 obtained here to the 2.3 obtained with electrodeposition of gold and 3.0 achieved with targeted corrosion enhancement on C260 brass substrates continues to support targeted corrosion enhancement via potentiodynamic corrosion as the superior method of latent fingerprint development within the context of this research.

All twelve C260 brass samples displayed uneven corrosion throughout the surface and the developed areas of the fingerprint had lighter and darker portions making it challenging to discern friction ridges. Separately, the surface was completely coated with silver in approximately 5 seconds with the fingerprint beginning to appear around the 20 second mark. At approximately 45 seconds, the fingerprint begins to disappear. This may be due to the silver

coating becoming too thick for the fingerprint to be discernible from the substrate surface. Though one of the goals of this research was to shorten the 55-minute time frame of targeted corrosion enhancement, the 30-second time frame of these experiments could constitute a hindrance in terms of the overall resolution generated per fingerprint. The electrodeposition of silver onto C260 brass substrates appears to have an incredibly small window of time between the point of fingerprint development and the point at which the fingerprint has been destroyed by the development method, itself.

Electrodeposition of silver onto low-carbon steel samples presented its own unique challenges. Rather than an immediate coating appearing across the entire surface exposed to solution, agglomerations of silver appeared on the surface within 5 seconds. These agglomerations formed on each sample within the first 5 seconds, regardless of applied potential or length of time. Table 24 below displays the results of the average changes in fingerprint grade from the electrodeposition of silver on low-carbon steel samples over three trials at each applied potential and given time frame.

Table 24: Average change in fingerprint grade resulting from electrodeposition of silver onto low-carbon steel substrates for various applied potentials and lengths of time.

|                      | <b>Low-Carbon Steel</b>                              |
|----------------------|--|
|                      | <b>Average <math>\Delta</math> Fingerprint Grade</b> |
| <b>1V for 15 sec</b> | 0  |
| <b>1V for 30 sec</b> | 0.3  |
| <b>1V for 45 sec</b> | 0  |
| <b>1V for 60 sec</b> | 0  |
| <b>2V for 15 sec</b> | 0  |

The agglomerations of silver atoms made it challenging to discern fingerprint ridges and overall development. The highest average change in fingerprint grade of 0.3 was observed at an applied potential of 1V for 30 seconds. All measurements for longer lengths of time or higher voltages yielded more severe agglomeration resulting in no resolution of the fingerprint.

Figure 41 includes images from two separate low-carbon steel trials, both of which were subjected to an applied potential of 1V for a total of 30 seconds. Image A was taken at the 5 second mark when agglomerations of silver atoms began to form. Air bubbles were also observed on the substrate surface indicating an issue with hydrogen evolution as was previously observed in the initial characterization measurements in chapter 1. Image A also displays how rapidly the agglomerations begin to hinder discernment of ridges within the fingerprint. Image B was taken after the sample was subjected to silver electrodeposition at 1V for the full 30 seconds. It also represents the best results obtained with silver electrodeposition onto low-carbon steel

substrates. The agglomerations are not rinsed away by ultrapure water and remain present after being blotted dry with a KimWipe. These challenges may also be the product of lower conductivity in low-carbon steel samples. However, silver nitrate reagent also poses the challenge of darkening in short amounts of time, hindering fingerprint visibility. A similar unwanted effect may be occurring here. Naturally, these results suggest targeted corrosion enhancement would be more suitable in terms of latent fingerprint development on steel surfaces.

### Low-carbon Steel



A. Sample held at 1V, image taken at 5 second mark when agglomerations began to form on substrate surface submerged in solution.



B. Another sample held at 1V for 30 seconds. Sample removed from flat platform cell, rinsed and dried with KimWipe.

Figure 41: Images from two separate low-carbon steel trials subjected to electrodeposition of silver. Image A was taken looking down into the cell after 5 seconds of the measurement with the sample still submerged in solution. Image B is a separate trial that was completed, the sample was removed from the cell, rinsed and dried with a KimWipe

### 5.3.3 Electroless Deposition

Electroless deposition, as indicated by its name, does not require the application of an electrical potential to initiate and maintain electrochemical reactions. This characteristic fundamentally differentiates it from electrodeposition methods, offering distinct advantages in terms of operational simplicity and cost. In the context of this dissertation, the primary expenses in traditional electroanalytical methods often stem from the instrumentation, such as the potentiostat, and the specialized training required for personnel to operate and troubleshoot these devices effectively. By eliminating the need for complex equipment, electroless deposition significantly reduces both the cost and the level of training required, making it an attractive method for forensic applications, especially in environments with limited resources.

The exploration of electroless deposition as a method for enhancing latent fingerprints is driven by both the potential for cost reduction and the relatively unexplored nature of this technique in forensic science. Initial experiments focused on the use of gold, reflecting the discussions and findings from previous sections on electrodeposition. A commercially available solution, Transene bright electroless gold, was employed, which the manufacturer recommends maintaining at a temperature between 50-90°C. For the experimental setup, a beaker filled with this electroless gold solution was placed on a hot plate set to maintain a starting temperature of 50°C. A C260 brass sample was then submerged in the solution, covered with a watch glass to minimize evaporation and contamination.

Despite these initial setups, the first experiments with electroless gold deposition onto brass did not produce any results, which led to additional trials. Two more C260 brass samples underwent the same procedure, with the bath temperature eventually increased to 90°C, but still, no development was observed after the two- and three-hour marks. This lack of results prompted a shift to explore other, stronger reducing agents. The addition of sodium borohydride, a more potent reducing agent, was the next step; however, this too was unsuccessful in developing any observable fingerprint features on the brass samples.

Considering the next potential reducing agent, formaldehyde, its use was ultimately not pursued due to significant toxicity concerns. Formaldehyde is known to pose severe health risks, and heating solutions containing this chemical could release harmful gases, presenting unacceptable safety risks in a forensic or any laboratory setting.

A low-carbon steel sample was placed into a fresh solution bath at 60°C and the same procedure was followed. There was no observable development after 30 seconds, five minutes, two hours, or with the eventual increase of the solution bath temperature to 90°C. Two more low-carbon steel samples were subjected to the same procedural steps, all producing no observable development.

The absence of results from these experiments with safer alternatives highlighted the challenges and limitations inherent in adapting new forensic methods using electroless deposition for fingerprint enhancement. The experiments also underscored the importance of safety in selecting chemical processes for forensic applications. Given the severe toxicity risks associated with more effective but dangerous chemicals like formaldehyde, it remains crucial to prioritize operator safety and environmental health. This consideration steers the direction of forensic method development toward safer and equally effective alternatives.



## 5.4 Conclusions and Future Work

The evaluation of the electrodeposition of gold onto C260 brass substrates reveals a notable disparity in effectiveness when compared to more conventional methods. With an average change in fingerprint development grade peaking at 2.3, this method falls short of the 3.0 grade achieved through targeted corrosion enhancement via potentiodynamic corrosion. Although targeted corrosion enhancement emerges as the superior technique based purely on numerical grading, it is essential to consider the efficiency of these methods. The electrodeposition process requiring only 30 seconds is significantly faster than the 55-minute duration required for targeted corrosion enhancement. This time efficiency suggests that future research could focus on optimizing electrodeposition of gold as either a standalone technique or in conjunction with other established methods of fingerprint development. Given the fragile nature of fingerprints and their residues, investigating the potential of gold electrodeposition for preserving fingerprints—either before or after the application of other development methods—could provide valuable insights into enhancing forensic analysis.

The trials with electroless deposition did not fare any better. Initial attempts with electroless gold deposition on brass substrates failed to yield positive results, prompting experiments with stronger reducing agents like sodium borohydride, which also proved unsuccessful. The potential use of formaldehyde was considered; however, due to the severe toxicity risks associated with heating cyanide-based solutions containing formaldehyde, this line of investigation was deemed unsafe and not pursued further. This series of unsuccessful attempts

underscores the complexities and limitations of electroless deposition in forensic applications, highlighting the need for continued research into safer and more effective chemical formulations.

The application of gold electrodeposition to low-carbon steel substrates introduced several unique challenges, primarily due to the inconsistency and lack of repeatability in the results. Trials conducted at 3V for 60 and 90 seconds yielded overlapping results, with both durations achieving an average fingerprint development grade of 1.7—a significant reduction from the 3.4 grade obtained with targeted corrosion enhancement. The uneven adherence of gold atoms across the substrate surfaces can likely be attributed to the lower conductivity of low-carbon steel. This, combined with the 50% reduction in successful development and the challenges in determining an optimized timeframe, suggests a need for frequent interruption of the process to assess development. While this ability to pause and restart the development process is advantageous in techniques like cyanoacrylate fuming, it proves to be a limitation here due to the lower probability of successful development.

Exploration of silver electrodeposition on C260 brass as a standalone technique presented another set of challenges, despite the frequent practice of depositing silver and zinc after a gold layer. This approach achieved a modest average change in fingerprint grade of 1.3 when applying a potential of 1V for 30 seconds. A critical issue encountered was the narrow window between achieving optimal fingerprint development and completely obscuring the fingerprint under an excessive layer of electrodeposited silver. Additionally, the visual differences noted in Figure 40, where the core area of the fingerprint was most visible before electrodeposition, and the surrounding areas darkened post-electrodeposition, suggest an insulating effect of the residue on the brass surface. This differential development across the fingerprint warrants further investigation to quantify the electrodeposited layer's thickness over time. Finding an optimal

stopping point that enhances visualization without obliterating the fingerprint could significantly improve the efficacy of this method, either as a standalone approach or in combination with other techniques.

The attempt to employ silver electrodeposition on low-carbon steel was notably less successful, which is surprising given the proven effectiveness of silver nitrate as a fingerprint developing reagent. Like fingerprints developed with silver nitrate, which must be imaged immediately to prevent the background from darkening, a similar challenge may have affected these experiments. Further research should explore different concentrations of silver in the electrodeposition solutions to mitigate the rapid formation of silver aggregations that obscure the substrate surface. This adjustment could potentially refine the method's applicability and enhance its success in forensic applications.

## **Chapter 6: Comprehensive Conclusions and Synthesis of Research Findings**

### **6.1 Overview**

This dissertation has explored the use of electrochemical and electroanalytical methods for the forensic analysis of latent fingerprints on challenging metal substrates. Focusing on targeted corrosion enhancement, Inductively Coupled Plasma–Optical Emission Spectroscopy (ICP-OES), electrodeposition, and electroless deposition, the research aimed to enhance the reliability and effectiveness of latent fingerprint visualization under forensic conditions.

### **6.2 Analysis of Methods and Results**

The initial phases of this research investigated the effectiveness of targeted corrosion enhancement for latent fingerprints on various metal substrates including 6061-Aluminum, C260 Brass, low-carbon steel, and 400-Nickel. The study utilized potentiodynamic, potentiostatic, and galvanostatic methods to induce and control the corrosion processes that highlight latent fingerprints. Each method brought different insights into the corrosion behavior of these metals.

6061-Aluminum alloy and 400-Nickel alloy samples exhibited high variability and non-uniform corrosion patterns, significantly hindering the clarity and repeatability of latent fingerprint visualization. The unpredictable nature of the corrosion process in these materials made it difficult to use them reliably in forensic applications. However, C260 brass and low-

carbon steel samples demonstrated excellent results with all corrosion methods, showing consistent and predictable corrosion patterns that effectively enhanced the visibility of latent fingerprints. The stable corrosion characteristics of these substrates allowed for detailed and reliable fingerprint enhancement, making them ideal for forensic purposes. The repeatability and uniformity of C260 brass and low-carbon steel mirrored the findings from targeted corrosion enhancement, further confirming their suitability for forensic applications.

ICP-OES was instrumental in providing qualitative analysis of metal ion release during corrosion processes, offering a deeper understanding of the corrosion dynamics of different substrates. The findings from ICP-OES underscored the complex nature of interactions between metal surfaces and corrosive elements in eccrine secretions, helping to explain the varying degrees of success in fingerprint development across different metals. In 6061-Aluminum alloy samples, high levels of variability in aluminum ion release were observed, complicating consistent visualization of fingerprints. The substrate's propensity for uneven corrosion contributed to poor repeatability in fingerprint enhancement. C260 brass samples showed a controlled and uniform release of copper and zinc ions, facilitating the effective development of fingerprints. The process of dezincification was particularly beneficial, as it provided a gradual and predictable pattern of corrosion that enhanced fingerprint clarity. Low-carbon steel samples exhibited low variability in iron ion release, leading to high-quality fingerprint visualization. The predictable corrosion behavior made it an ideal candidate for forensic applications. The 400-Nickel alloy samples, similar to 6061-Aluminum alloy, faced significant challenges with uneven nickel and copper ion release. This led to non-reproducible results and made it less suitable for forensic methodologies that rely on corrosion-based enhancement.

Exploration into electrodeposition techniques, including the use of gold and silver, highlighted their potential in enhancing latent fingerprint visualization on metal substrates. Gold and silver were successfully deposited on C260 brass and low-carbon steel samples, enhancing the visibility and durability of fingerprints. The method allowed for precise control over the deposition process, which was critical in maintaining the integrity of the fingerprint ridges. Electroless deposition results were inconsistent and generally less effective in producing any discernible fingerprint ridge detail at all. This may be due to the potential for over-coating which could obscure fine details. The electroless deposition process involved significant safety concerns due to the use of hazardous chemicals like sodium borohydride and formaldehyde. These chemicals are strong reducing agents that can be highly toxic and reactive, posing risks of fire and chemical burns, as well as toxic exposure through inhalation or skin contact. Rigorous safety measures, including adequate ventilation, proper protective equipment, and strict handling procedures, are essential to mitigate these risks.

### **6.3 Summary of Novel Contributions**

The primary scientific contribution of this dissertation lies in the innovative application of electrochemical corrosion and electrodeposition methods to forensic science, particularly in latent fingerprint development. However, the significance of this work extends beyond forensic applications, offering valuable insights and advancements in the field of electrochemistry and materials science.

This research provides a fundamental understanding of how corrosion processes can be harnessed and controlled for specific applications. By investigating the corrosion potential and current of various metal substrates in the presence of eccrine and sebaceous fingerprints, this study elucidates the interactions between biological residues and metal surfaces, contributing to the broader knowledge of localized corrosion phenomena. The use of potentiodynamic, potentiostatic, and galvanostatic corrosion methods offers a comparative analysis of different electrochemical techniques, enhancing our understanding of their efficacy in targeted corrosion enhancement. This comparative approach is valuable for the broader corrosion science community, as it provides a framework for selecting appropriate corrosion methods based on specific applications and conditions.

Furthermore, the research demonstrates the utility of electroanalytical methods, such as open circuit potential (OCP) measurements, linear sweep voltammetry (LSV), and inductively coupled plasma-optical emission spectroscopy (ICP-OES), in real-time analysis and characterization of corrosion processes. These techniques are not only effective in forensic applications but also hold potential for broader use in materials science and engineering for monitoring and analyzing corrosion in various environments. The detailed analysis of electrolyte solutions and their impact on corrosion potential contributes to the optimization of electrochemical processes. This knowledge can be applied to other fields, such as battery technology, where electrolyte composition is critical for performance and longevity.

Additionally, the dissertation explores the electrodeposition of gold and silver onto metal substrates for enhancing fingerprint visualization. This technique, while innovative in forensic science, also offers broader implications for the field of surface engineering. The ability to deposit thin, uniform films of metals on various substrates can be applied to improve the

durability, conductivity, and corrosion resistance of materials used in electronics, aerospace, and automotive industries. The findings on the optimal conditions for electrodeposition, including applied potentials and durations, provide valuable data for industries that rely on precise surface modifications. This can lead to advancements in manufacturing processes where surface properties are critical for product performance.

The interdisciplinary nature of this research highlights the intersection of chemistry, materials science, and forensic science. By demonstrating the applicability of electrochemical methods to forensic investigations, this work encourages the integration of techniques from different scientific disciplines to solve complex problems. This approach can inspire further interdisciplinary research, fostering innovation and collaboration across fields. The techniques developed in this dissertation can be extended to other areas where surface interactions play a crucial role. For example, biomedical engineering can benefit from the insights gained in this research for developing better diagnostic tools and implants with enhanced biocompatibility and corrosion resistance.

In the forensic context, this dissertation addresses critical challenges faced by current fingerprint development techniques when applied to difficult substrates like fired shell casings and submerged weapons. By leveraging electrochemical corrosion methods, this research demonstrates how targeted corrosion enhancement can significantly improve latent fingerprint resolution while preserving fingerprint integrity. The application of potentiostatic, potentiodynamic, and galvanostatic corrosion methods showcases novel approaches to fingerprint visualization, providing forensic investigators with more reliable and effective tools. This research has notably increased the recovery rate from 1% to approximately 10% for all metal substrates tested, representing a significant improvement in the field.



Moreover, the exploration of electrodeposition techniques for latent fingerprint enhancement, such as the deposition of gold and silver, presents a creative application of electrochemical methods. These techniques not only improve fingerprint ridge contrast and durability but also offer potential solutions for forensic laboratories facing budget constraints and staffing limitations. By demonstrating the efficacy of these methods, this research paves the way for their adoption in forensic practice, ultimately contributing to public safety and the greater good.

While the primary focus of this dissertation is the advancement of latent fingerprint development through electrochemical methods, the broader scientific contributions cannot be understated. This work offers significant advancements in corrosion science, electroanalytical techniques, and electrodeposition, with wide-ranging implications for various scientific and engineering disciplines. By decoupling the forensic applications from the fundamental scientific contributions, this research stands as a valuable addition to the scientific community, paving the way for future innovations and interdisciplinary collaborations.

#### **6.4 Integration of Forensic Education and Research**

While this research stems from the need for novel latent fingerprint methods that can yield success on challenging substrates, the literature review (discussed in Chapter 1.1 Background and Literature Review) revealed that there are some novel methods that can yield success but are not widely used, or simply not used at all. A review of the literature does not, however, provide an answer for why this is the case.

The implementation of novel fingerprint development techniques in forensic labs can be significantly limited by rigorous quality assurance (QA) procedures, as detailed in Chapter 12 of *The Fingerprint Sourcebook* by the NIJ. Firstly, QA programs require comprehensive validation of new methods before they can be adopted, which involves thorough testing to ensure reliability and accuracy. This validation process is not only time-consuming but also resource-intensive, deterring frequent updates or quick adoption of innovative techniques.

Secondly, the quality assurance framework mandates extensive training and competency testing for examiners before they can undertake casework independently using new methodologies. This requirement ensures that all personnel are proficient with the latest techniques, but also slows down the integration of these methods into regular practice, as training programs need to be developed, implemented, and completed. The necessity for examiners to be verified by another competent examiner adds another layer of complexity and time to the process.

Lastly, the adherence to stringent quality controls and procedural documentation under a QA program adds another layer of complexity. Each step of the fingerprint development and analysis process must be meticulously documented and audited, ensuring that all procedures align with established quality standards. While this rigorous scrutiny upholds the integrity and accuracy of forensic results, it also constrains the flexibility to innovate and implement new techniques rapidly, as each change requires revision, approval, and documentation, further delaying their practical use [98].

Chapter 13 of *The Fingerprint Sourcebook* focuses on the legal aspects surrounding the admissibility of fingerprint evidence in court, particularly addressing the challenges faced when novel latent fingerprint methods are proposed [99]. The legal landscape, primarily shaped by the

pivotal *Daubert v. Merrell Dow Pharmaceuticals, Inc.* decision, sets a precedent for the stringent scrutiny of forensic evidence, including fingerprint analysis.

Novel fingerprint development methods face significant hurdles in being accepted in legal proceedings due to the necessity to meet rigorous admissibility standards established by federal and state courts. Under the *Daubert* standard, for a new method to be admitted into court, it must be shown to be scientifically valid and reliable, which requires substantial validation through peer-reviewed research, consistency with accepted principles, and potential error rates. This extensive validation process is both time-consuming and costly, often deterring the introduction of innovative methods that could potentially enhance forensic analysis.

The legal system demands that any novel method must not only withstand rigorous scientific scrutiny but must also be demonstrable and replicable in a legal context. Expert witnesses who advocate for new fingerprint techniques must be prepared to demonstrate their expertise, the scientific basis of their methods, and their practical applicability in forensic cases. This often involves a detailed explanation of the technology, methodology, and the scientific principles underlying these new techniques. Attorneys, often skilled in challenging the credibility and reliability of such evidence, can significantly impede the adoption of novel methods by casting doubts on their validity and applicability.

Courts are generally conservative and prefer relying on established methods with proven track records. There is a judicial reluctance to accept new forensic methods without overwhelming evidence of their reliability and effectiveness. This conservative approach is further reinforced by the potential risks associated with wrongful convictions or acquittals due to unreliable or unvalidated techniques. The judiciary's cautious stance is intended to preserve the

integrity of the legal process, ensuring that only the most rigorously tested and widely accepted methods are used in criminal proceedings.

The Fingerprint Sourcebook highlights the significant challenges in adopting new fingerprint technologies within forensic science and the judiciary. Chapter 12 discusses the rigorous quality assurance (QA) measures required to validate new methods, ensuring their reliability and consistency. Chapter 13 addresses the legal hurdles, where new techniques must withstand the strict scrutiny of the Daubert standard, demonstrating scientific validity and reliability through peer review and acceptance in the scientific community. This underscores the balance that must be struck between innovation and the meticulous standards needed for forensic practices and legal admissibility. The path to integrating new fingerprint technologies is fraught with obstacles, rooted in the need to maintain the highest levels of accuracy and dependability in forensic analysis and judicial processes. This careful vetting ensures that only thoroughly tested and proven methods are utilized, safeguarding the integrity of criminal investigations and trials.

Conversations with leaders at both the state and federal levels have shed light on the profound impact of budget restrictions and staffing limitations on the integration of new fingerprint technologies within forensic and legal frameworks. While quality assurance measures, the challenges of legal admissibility, and stringent legal scrutiny are significant, the practical realities of budget constraints and insufficient staffing emerge as even more critical hurdles. These financial and human resource limitations often dictate the pace and extent to which innovative technologies can be adopted and utilized effectively in forensic science.

Budget constraints directly affect the ability to purchase new equipment, train staff on emerging technologies, and conduct the extensive validation studies required for new methodologies to meet quality assurance standards. Without adequate funding, even the most

promising advancements in fingerprint technology cannot be implemented or sustained. Similarly, staffing limitations compound these challenges. Forensic departments frequently operate with fewer personnel than needed, which not only slows down the process of innovation but also places additional strain on existing staff to maintain the rigor of current operational standards.

Moreover, the intricate and often lengthy process of securing approval for new technologies within public agencies exacerbates these issues. The need for rigorous testing and peer review before a new method can be introduced—necessary to meet both scientific and legal standards—requires a level of staffing and expertise that is often beyond the capacity of underfunded forensic departments. Consequently, these budgetary and staffing issues not only impede the adoption of new technologies but also impact the overall efficacy and efficiency of forensic operations, ultimately affecting the justice system at large.

The importance of federal intervention in streamlining the implementation of novel fingerprint technologies cannot be overstated. By facilitating a smoother integration process, the federal government can ensure that these advanced methodologies are quickly and effectively put into use, thereby enhancing public safety. A focused federal effort to alleviate budget and staffing constraints would empower forensic departments to adopt cutting-edge technologies that improve the accuracy and speed of criminal investigations. This proactive approach is crucial in not only advancing forensic science but also in bolstering the justice system's capacity to protect citizens and deter crime.

## 6.5 Future Work

The findings of this research suggest several potential directions for future work to continue advancing the field of forensic fingerprint analysis. One significant area for further investigation is a comprehensive kinetics study for all four metal substrates examined in this dissertation: 6061-Aluminum alloy, C260 brass, low-carbon steel, and 400-Nickel alloy. The need for such a study arises from the observation that potentiodynamic corrosion consistently produced superior results compared to potentiostatic and galvanostatic corrosion, yet the underlying reasons for this remain relatively unclear.

A detailed kinetics study would help elucidate the electrochemical reactions and mechanisms occurring during the corrosion processes. This would involve examining the rates of anodic and cathodic reactions, the formation and dissolution of passive films, and the role of chloride ions and other components of eccrine sweat in these processes. By understanding the kinetics of these reactions, it would be possible to explain why potentiodynamic corrosion, which involves a continuously varying potential, is more effective in enhancing fingerprint visibility than the steady potentials used in potentiostatic and galvanostatic methods.

Relevant electrochemical reaction kinetics that should be considered in this study include the Tafel slopes for anodic and cathodic reactions, the exchange current density, and the diffusion coefficients of reactive species. For instance, the Tafel slopes would provide insights into the kinetics of the electron transfer reactions, while the exchange current density would indicate the inherent electrochemical activity of the metal substrates. Additionally, studying the diffusion coefficients would help in understanding the mass transport limitations and their impact on the corrosion processes.

Further research is also needed to optimize the parameters used in electrochemical methods like electrodeposition and potentiostatic corrosion. This includes exploring the effects of different electrical currents, voltages, and solution compositions to refine these methods for enhanced clarity and repeatability of fingerprints on various substrates. Conducting long-term stability studies on the corrosion patterns and the developed fingerprints could provide insights into the durability and permanence of these enhancements, which is crucial for the storage and archival of forensic evidence.

Another important direction is the development of safer and more effective chemical mixtures for electroless deposition. Future studies could focus on finding alternatives to hazardous chemicals like sodium borohydride and formaldehyde, which pose significant health and safety risks. Additionally, expanding the range of substrates studied to include newer alloys and metals commonly encountered in forensic scenarios could provide more comprehensive data and broaden the applicability of the techniques developed in this dissertation.

By addressing these areas, future research can continue to build on the foundation laid by this dissertation, pushing the boundaries of what is possible in forensic fingerprint analysis and helping to solve more cases effectively and efficiently.

## References

- [1] S. Johnson, "Development of latent prints on firearms evidence," *Journal of Forensic Identification*, vol. 60, no. 2, pp. 148-151, 2010.
- [2] A. Pratt, "Fingerprints and firearms," *Journal of Forensic Identification*, vol. 62, no. 3, pp. 234-242, 2012.
- [3] B. Maldonado, "Study on developing latent fingerprints on firearm evidence," *Journal of Forensic Identification*, vol. 62, no. 5, pp. 425-429, 2012.
- [4] M. Arne, Interviewee, *Deputy Laboratory Director - United States Secret Service - Forensic Services Division*. [Interview]. August 2021.
- [5] D. Wilkinson, D. Hockey, C. Power, R. Walls and J. Cole, "Recovery of fingermarks from fired ammunition and detonated improvised explosive devices using S2N2 - a proof of concept study," *Journal of Forensic Identification*, vol. 70, no. 1, pp. 59-88, 2020.
- [6] R. Lam, D. Hockey, J. Williamson and N. G. R. Hearn, "Latent fingermark development on fired and unfired brass ammunition under controlled and blind conditions," *Forensic Science International*, vol. 337, pp. 1-7, 2022.
- [7] S. M. Bleay, P. F. Kelly, R. King and S. Thorngate, "A comparative evaluation of the disulfur dinitride process for the visualisation of fingermarks on metal surfaces," *Science & Justice*, vol. 59, no. 6, pp. 606-621, 2019.
- [8] J. W. Bond and D. Phil, "Visualization of Latent Fingerprint Corrosion of Metallic Surfaces," *Journal of Forensic Science*, vol. 53, no. 4, pp. 812-822, 2008.
- [9] J. W. Bond, D. Phil and C. Heidel, "Visualization of Latent Fingerprint Corrosion," *Journal of Forensic Sciences*, vol. 54, no. 4, 2009.
- [10] G. Wightman and D. O'Connor, "The thermal visualisation of latent fingermarks on metallic surfaces," *Forensic Science International*, vol. 204, no. 1-3, pp. 88-96, 2011.
- [11] G. Wightman, F. Emery, C. Austin, I. Andersson, L. Harnus, G. Arju and C. Steven, "The interaction of fingermark deposits on metal surfaces and potential ways for visualization," *Forensic Science International*, vol. 249, pp. 241-254, 2015.
- [12] G. Williams and N. McMurray, "Latent fingermark visualisation using a scanning Kelvin probe," *Forensic Science International*, vol. 167, no. 2-3, pp. 102-109, 2007.
- [13] A. Nazarov and D. Theiry, "Application of Volta potential mapping to determine metal surface defects," *Electrochimica Acta*, vol. 52, no. 27, pp. 7689-7696, 2007.



- [14] C. Omek, C. Leygraf and J. Pan, "On the Volta potential measured by SKPFM – fundamental and practical aspects with relevance to corrosion science," *Corrosion Engineering, Science and Technology*, vol. 54, no. 3, pp. 185-198, 2019.
- [15] S.-M. Huang, S. Yee, R. T. Atanasoski, C. S. McMillan, R. A. Oriani and W. H. Smyrl, "Work Function Topography on Thin Anodic TiO<sub>2</sub>," *Journal of The Electrochemical Society*, vol. 138, no. 11, pp. 63-64, 1991.
- [16] H. Dafydd, G. Williams and S. Bleay, "Latent Fingerprint Visualization using a Scanning Kelvin Probe in Conjunction with Vacuum Metal Deposition," *Journal of Forensic Sciences*, vol. 59, no. 1, pp. 211-218, 2014.
- [17] A. L. Beresford and A. R. Hillman, "Electrochromic enhancement of latent fingerprints on stainless steel surfaces," *Analytical Chemistry*, vol. 82, no. 2, pp. 483-486, 2010.
- [18] R. M. Sapstead, N. Corden and R. A. Hillman, "Latent fingerprint enhancement via conducting electrochromic copolymer films of pyrrole and 3,4-ethylenedioxythiophene on stainless steel," *Electrochimica Acta*, vol. 162, pp. 119-128, 2015.
- [19] S. Valussi, "Microfluidics Systems for the Chemical Analysis of Fingerprint Residues," in *International Fingerprint Research Group Meeting*, St Albans, U.K., 2003.
- [20] J. S. Marshall, M. L. Sita and J. P. Landers, "Microfluidic Device for the Identification of Biological Sex by Analysis of Latent Fingermark Deposits," *Micromachines*, vol. 12, no. 4, p. 442, 2021.
- [21] M. Kucken and C. Champod, "Merkel cells and the individuality of friction ridge skin," *Journal of Theoretical Biology*, pp. 229-237, 2013.
- [22] W. J. Babler, "Embryologic development of epidermal ridges and their configurations," *Birth Defects Orig Artic Ser*, vol. 27, no. 2, pp. 95-112, 1991.
- [23] M. Kucken and A. C. Newell, "Fingerprint formation," *Journal of Theoretical Biology*, vol. 235, no. 1, pp. 71-83, 2005.
- [24] J. G. Barnes, "History," in *The Fingerprint Sourcebook*, Washington, DC: Office of Justice Programs, 2010.
- [25] A. V. Maceo, "Anatomy & Physiology of Adult Friction Ridge Skin," in *The Fingerprint Sourcebook*, Washington, DC: Office of Justice Programs, 2010.
- [26] K. Wertheim, "Embryology and Morphology of Friction Ridge Skin," in *The Fingerprint Sourcebook*, Washington, DC: Office of Justice Programs, 2010.
- [27] K. L. Monson, M. A. Roberts, K. B. Knorr, S. Ali, S. B. Meagher, K. Biggs, P. Blume, D. Brandelli, A. Marzioli, R. Reneau and F. Tarasi, "The permanence of friction ridge skin and persistence of friction ridge skin and impressions: A comprehensive review and new results," *Forensic Science International*, vol. 297, pp. 111-131, April 2019.

- [28] B. Yamashita and M. French, "Latent Print Development," in *The Fingerprint Sourcebook*, Washington, Office of Justice Programs, 2010.
- [29] S. Oden and B. Von Hofsten, "Detection of Fingerprints by the Ninhydrin Reaction," *Nature*, vol. 173, pp. 449-450, 1954.
- [30] F. Zampa, M. Hilgert, J. Malmberg, S. Maria, L. Schwarz and A. Mattei, "Evaluation of ninhydrin as a fingermark visualisation method – A comparison between different procedures as an outcome of the 2017 collaborative exercise of the ENFSI Fingerprint Working Group," *Science & Justice*, vol. 60, no. 2, pp. 191-200, 2020.
- [31] E. W. Yemm, E. Cocking and R. E. Ricketts, "The Determination of Amino-Acids with Ninhydrin," *The Analyst*, vol. 80, pp. 209-214, 1955.
- [32] D. A. Crown, "The Development of Latent Fingerprints with Ninhydrin," *The Journal of Criminal Law, Criminology, and Police Science*, vol. 60, no. 2, pp. 258-264, 1969.
- [33] A. Beaudoin, "New Technique for Revealing Latent Fingerprints on Wet, Porous Surfaces: Oil Red O," *Journal of Forensic Identification*, vol. 54, no. 4, pp. 413-421, 2004.
- [34] T. A. Trozzi, R. L. Schwartz and M. L. Hollars, "Processing Guide for Developing Latent Prints," U.S. Department of Justice, Quantico, 2000.
- [35] L. A. Lewis, R. W. Smithwick 3rd, G. L. Devault and S. A. Lewis Sr, "Processes involved in the development of latent fingerprints using the cyanoacrylate fuming method," *Journal of Forensic Sciences*, vol. 46, no. 2, pp. 241-246, 2001.
- [36] G. Singh Bumrah, "Cyanoacrylate fuming method for detection of latent fingermarks: a review," *Egyptian Journal of Forensic Sciences*, vol. 7, no. 4, 2017.
- [37] P. Theys, Y. Turgis, A. Lepareux, G. Chevet and P. F. Ceccaldi, "New Technique for Bringing Out Latent Fingerprints on Paper: Vacuum Metallisation," *Int Crime Police Review*, vol. 217, p. 106, 1968.
- [38] T. Kent, G. L. Thomas, T. E. Reynoldson and H. W. East, "A Vacuum Coating Technique for the Development of Latent Fingerprints on Polythene," *Journal of the Forensic Science Society*, vol. 16, no. 2, pp. 93-101, 1976.
- [39] N. Jones, D. Mansour, S. Milutin and C. Lennard, "The Influence of Polymer Type, Print Donor and Age on the Quality of Fingerprints Developed on Plastic Substrates Using Vacuum Metal Deposition," *Forensic Science International*, vol. 124, no. 2-3, pp. 167-177, 2001.
- [40] N. Jones, S. Milutin, C. Lennard and C. Roux, "Vacuum Metal Deposition: Factors Affecting Normal and Reverse Development of Latent Fingerprints on Polyethylene Substrates," *Forensic Science International*, vol. 115, no. 1-2, pp. 73-88, 2001.

- [41] G. Christofidis, J. Morrissey and J. W. Birkett, "Detection of Fingermarks-Applicability to Metallic Surfaces: A Literature Review," *Journal of Forensic Sciences*, vol. 63, no. 6, pp. 1616-1627, 2018.
- [42] R. G. Kelly, J. R. Scully, D. Shoesmith and R. G. Buchheit, "Introduction," in *Electrochemical Techniques in Corrosion Science and Engineering*, Boca Raton, CRC Press, 2002.
- [43] J. W. Bond and D. Phil, "The Thermodynamics of Latent Fingerprint," *Journal of Forensic Sciences*, vol. 53, no. 6, pp. 1344-1352, 2008.
- [44] R. G. Kelly, J. R. Scully, D. Shoesmith and R. G. Buchheit, "Passivity and Localized Corrosion," in *Electrochemical Techniques in Corrosion Science and Engineering*, Boca Raton, CRC Press, 2002.
- [45] ASM Handbook Committee, *Properties and Selection: Nonferrous Alloys and Special-Purpose Materials*, ASM International, 1990.
- [46] G. S. Frankel, "Pitting Corrosion of Metals: A Review of the Critical Factors," *Journal of the Electrochemical Society*, vol. 145, no. 6, pp. 2186-2198, 1998.
- [47] C. M. Girelli, B. J. Lobo, A. G. Cunha, J. C. Freitas and F. G. Emmerich, "Comparison of practical techniques to develop latent fingermarks on fired and unfired cartridge cases," *Forensic Science International*, vol. 250, pp. 17-26, 2015.
- [48] J. Morrissey, J. Larrosa and J. W. Birkett, "A preliminary evaluation of the use of Gun Bluing to enhance Friction ridge detail on Cartridge Casings," *Journal of Forensic Identification*, vol. 67, no. 3, pp. 313-322, 2017.
- [49] R. S. Ramotowski, A. A. Cantu, D. A. Leben, M. M. Joullie and G. C. Saunders, "Recent advances in latent print visualization techniques at the U.S. Secret Service," in *Forensic Evidence Analysis and Crime Scene Investigation*, Boston, 1997.
- [50] A. J. Bard and L. R. Faulkner, *Electrochemical Methods: Fundamentals and Applications*, 2nd Edition, Wiley, 2002.
- [51] R. G. Kelly, J. R. Scully, D. Shoesmith and R. G. Buchheit, "Development of Corrosion Models Based on Electrochemical Measurements," in *Electrochemical Techniques in Corrosion Science and Engineering*, Boca Raton, CRC Press, 2002.
- [52] J. E. Nutting, J. B. Gerken, A. G. Stamoulis, D. L. Bruns and S. S. Stahl, "'How Should I Think About Voltage? What is Overpotential?'" – Establishing an Organic Chemistry Intuition for Electrochemistry," *Journal of Organic Chemistry*, vol. 86, no. 22, pp. 15875-15885, 2021.
- [53] X. G. Zhang, "Corrosion Potential and Corrosion Current," in *Corrosion and Electrochemistry of Zinc*, New York, Springer Science + Business Media, 1996, pp. 125-156.

- [54] "Electrochemical Thermodynamics: The Gibbs Function, Electrochemical Reactions, and Equilibrium Potentials," in *Fundamentals of Electrochemical Corrosion*, ASM International, 2000.
- [55] F. E. Beamish, "Chapter 1 - The Action of Acids, Bases, Oxygen and Chlorine on the Noble Metals," in *The Analytical Chemistry of the Noble Metals*, Elsevier, 1966, pp. 1-38.
- [56] F. Zhang, Y. Zhu, Q. Lin, L. Zhang, X. Zhang and H. Wang, "Noble-metal single-atoms in thermocatalysis, electrocatalysis, and photocatalysis," *Energy & Environmental Science*, vol. 14, no. 5, pp. 2954-3009, 2021.
- [57] J. Wang, *Analytical Electrochemistry*, New Jersey: John Wiley & Sons, 2006.
- [58] S. W. Boettcher, S. Z. Oener, M. C. Lonergan, Y. Surendranath, S. Ardo, C. Brozek and P. A. Kempfer, "Potentially Confusing: Potentials in Electrochemistry," *ACS Energy Letters*, vol. 6, no. 1, pp. 261-266, 2021.
- [59] M. A. Prasad and M. V. Sangaranarayanan, "Current function for irreversible electron transfer processes in linear sweep voltammetry for the reactions obeying Marcus kinetics," *Chemical Physics Letters*, vol. 387, no. 4-6, pp. 317-321, 2004.
- [60] N. D. Greene, "Predicting Behavior of Corrosion Resistant Alloys By Potentiostatic Polarization Methods," *Corrosion: The Journal of Science & Engineering*, vol. 18, no. 4, 1962.
- [61] J. A. Gonzalez, A. Cobo, M. N. Gonzalez and S. Feliu, "On-site Determination of Corrosion Rate in Reinforced Concrete Structures by use of Galvanostatic Pulses," *Corrosion Science*, vol. 43, no. 4, pp. 611-625, 2001.
- [62] F. Mansfield, "Tafel Slopes and Corrosion Rates Obtained in the Pre-Tafel Region of Polarization Curves," *Corrosion Science*, vol. 47, no. 12, pp. 3178-3186, 2005.
- [63] E. J. Dickinson and A. J. Wain, "The Butler-Volmer Equation in Electrochemical Theory: Origins, Value, and Practical Application," *Journal of Electroanalytical Chemistry*, vol. 872, 2020.
- [64] S. Fletcher and T. S. Varley, "Beyond the Butler-Volmer equation. Curved Tafel slopes from steady-state current-voltage curves," *Physical Chemistry Chemical Physics*, vol. 13, no. 12, pp. 5359-5364, 2011.
- [65] G. S. Frankel and R. P. Frankenthal, "Wagner-Traud to Stern-Geary: Development of Corrosion Kinetics," in *Corrosion Science: A Retrospective and Current Status in Honor of Robert P. Frankenthal*, ECS, 2002, pp. 33-41.
- [66] U. Angst and M. Buchler, "On the applicability of the Stern-Geary relationship to determine instantaneous corrosion rates in macro-cell corrosion," *Materials and Corrosion*, vol. 66, no. 10, pp. 1017-1028, 2015.

- [67] F. Torabi and P. Ahmadi, "Chapter 2 - Fundamentals of Batteries," in *Simulation of Battery Systems*, Academic Press, 2019, pp. 55-81.
- [68] B. Sunden, "Chapter 2 - Electrochemistry and Thermodynamics," in *Hydrogen, Batteries, and Fuel Cells*, Academic Press, 2019, pp. 15-36.
- [69] Y. D. Gamburg and G. Zangari, "Introduction to Electrodeposition: Basic Terms and Fundamental Concepts," in *Theory and Practice of Metal Electrodeposition*, Springer Science + Business Media, 2011, pp. 1-14.
- [70] M. Paunovic and M. Schlesinger, "Metals and Metal Surfaces," in *Fundamentals of Electrochemical Deposition*, Wiley, 2005, pp. 25-40.
- [71] Y. Okinaka and T. Osaka, "Electroless Deposition Processes: Fundamentals and Applications," in *Advances in Electrochemical Science and Engineering*, New York, VCH Publishers, 1994, pp. 55-60.
- [72] O. Mallory and J. Hajdu, *Electroless Plating: Fundamentals and Applications*, Orlando, FL: AESFS, 1990.
- [73] Z. Bangwei, "History - From the Discovery of Electroless Plating to the Present," in *Amorphous and Nano Alloys Electroless Depositions: Technology, Composition, Structure and Theory*, 2017, Chemical Industry Press, 2017, pp. 4-40.
- [74] R. Mandal, M. Ghosh and A. Paul, "Electroless nickel coating on magnesium substrates: Fabrication method and applications," *Reference Module in Materials Science and Materials Engineering*, pp. 2-12, 2023.
- [75] S. S. Djokic, "Electroless Deposition of Metals and Alloys," in *Modern Aspects of Electrochemistry*, New York, Kluwer Academic/Plenum Publishers, 2002, pp. 51-133.
- [76] G. Tyler and J. Yvon, "ICP-OES, ICP-MS, and AAS Techniques Compared," *ICP Optical Emission Spectroscopy Technical Note*, 5, 1995.
- [77] J. W. Olesik, "Elemental analysis using ICP-OES and ICP/MS," *Analytical Chemistry*, vol. 63, no. 1, pp. 12a-21a, 1991.
- [78] C. G. Novaes, M. A. Bezerra, E. G. Paranhos da Silva, A. M. Pinto dos Santos, I. Lago da Silva Romao and J. H. S. Neto, "A review of multivariate designs applied to the optimization of methods based on inductively coupled plasma optical emission spectrometry (ICP OES)," *Microchemical Journal*, vol. 128, pp. 331-346, 2016.
- [79] H. L. Bandey and A. P. Gibson, "The Powders Process, Study 2: Evaluation of Fingerprint Powders on Smooth Surfaces," *Fingerprint Development and Imaging Newsletter: Special Edition*, vol. 8, no. 6, 2006.
- [80] D. Li, C. Lin, C. Batchelor-McAuley, L. Chen and R. G. Compton, "Tafel analysis in practice," *Journal of Electroanalytical Chemistry*, vol. 826, no. 1, pp. 117-124, 2018.

- [81] A. Atrens, G. L. Song, Z. Shi, A. Soltan, S. Johnston and M. S. Dargusch, "Understanding the Corrosion of Mg and Mg Alloys," in *Encyclopedia of Interfacial Chemistry*, 2018, pp. 515-534.
- [82] J. Zhang, M. Klasky and B. C. Letellier, "The aluminum chemistry and corrosion in alkaline solutions," *Journal of Nuclear Materials*, vol. 384, no. 2, pp. 175-189, 2009.
- [83] K. Khanari and M. Finsgar, "Organic corrosion inhibitors for aluminum and its alloys in chloride and alkaline solutions: A review," *Arabian Journal of Chemistry*, vol. 12, no. 8, pp. 4646-4663, 2019.
- [84] M. L. Doche, J. J. Rameau, R. Durand and F. Novel-Cattin, "Electrochemical behaviour of aluminum in concentration NaOH solutions," *Corrosion Science*, vol. 41, no. 4, pp. 805-826, 1999.
- [85] J. Skrovan, A. Alfantazi and T. Troczynski, "Enhancing aluminum corrosion in water," *Journal of Applied Electrochemistry*, vol. 39, pp. 1695-1702, 2009.
- [86] J. Mendoza-Canales and J. Marin-Cruz, "Corrosion Behavior of Titanium and Nickel-based Alloys in HCl and HCl + H<sub>2</sub>S Environments," *International Journal of Electrochemical Science*, vol. 3, no. 3, pp. 346-355, 2008.
- [87] R. Karimihaghighi and M. Naghizadeh, "Effect of alloying elements on aqueous corrosion of nickel-based alloys at high temperatures: A review," *Materials and Corrosion*, vol. 74, no. 8, pp. 1246-1255, 2022.
- [88] L. Kenworthy and W. G. O'Driscoll, "Dezincification of Brass," *Anti-Corrosion Methods and Materials*, vol. 2, no. 8, pp. 247-249, 1955.
- [89] S. Selvaraj, S. Ponmariappan, M. Natesan and N. Palaniswamy, "Dezincification of Brass and its Control - An Overview," *Corrosion Reviews*, vol. 21, no. 1, pp. 41-74, 2003.
- [90] H. Sugawara and E. Hideaki, "Dezincification of brass," *Corrosion Science*, vol. 7, no. 8, pp. 519-523, 1967.
- [91] A. Jain, S. P. Ong, G. Hautier, W. Chen, W. Davidson Richards, S. Dacek, S. Cholia, D. Gunter, D. Skinner, G. Ceder and K. A. Persson, "Commentary: The Materials Project: A materials genome approach to accelerating materials innovation," *APL Materials*, vol. 1, no. 1, 2013.
- [92] K. A. Persson, B. Waldwick, P. Lazic and G. Cedar, "Prediction of solid-aqueous equilibria: Scheme to combine first-principles calculations of solids with experimental aqueous states," *Physical Review B*, vol. 85, no. 23, 2012.
- [93] A. M. Patel, J. K. Norskov, K. A. Persson and J. H. Montoya, "Efficient Pourbaix diagrams of many-element compounds," *Physical Chemistry Chemical Physics*, vol. 21, no. 45, 2019.

- [94] A. K. Singh, L. Zhou, A. Shinde, S. K. Suram, J. H. Montoya, D. Winston, J. M. Gregoire and K. A. Persson, "Electrochemical Stability of Metastable Materials," *Chemistry of Materials*, vol. 29, no. 23, pp. 10159-10167, 2017.
- [95] C. Peng, G. Cao, T. Gu, C. Wang, Z. Wang and C. Sun, "The corrosion behavior of the 6061 Al alloy in simulated Nansha marine atmosphere," *Journal of Materials Research and Technology*, vol. 19, pp. 709-721, 2022.
- [96] H. Liu, F. Cao, G.-L. Song, D. Zheng, Z. Shi, M. S. Dargusch and A. Atrens, "Review of the atmospheric corrosion of magnesium alloys," *Journal of Materials Science and Technology*, vol. 35, pp. 2003-2016, 2019.
- [97] R. B. Rebak and P. Crook, "Nickel Alloys for Corrosive Environments," *Advanced Materials and Processes*, vol. 157, pp. 37-42, 2000.
- [98] M. L. Gray, "Quality Assurance," in *The Fingerprint Sourcebook*, National Institute of Justice, 2011, pp. 12-1 to 12-12.
- [99] A. A. Moenssens and S. B. Meagher, "Fingerprints and the Law," in *The Fingerprint Sourcebook*, National Institute of Justice, 2011, pp. 13-1 to 13-26.
- [100] I. Newton, *Newton's Principia : the Mathematical Principles of Natural Philosophy*, New York: Daniel Adee, 1846.
- [101] N. Craven, H. Youngling and T. Walthall, "Evaluation of the RECOVER LFT System: Experiments on Metal Plates," *Journal of Forensic Identification*, vol. 73, no. 4, pp. 357-382, 2023.
- [102] D. Johnson, Interviewee, *Forensic Scientist - Las Vegas Metropolitan Police Department Forensic Laboratory*. [Interview]. September 2021.

## Curriculum Vitae

**Crystal C. Kitanovski**

kotan@unlv.nevada.edu | c.kitanovski@proton.me

### **QUALIFICATIONS**

- Experienced researcher with 6 plus years working in Analytical Chemistry labs.
- Over 5 years of experience teaching general chemistry, organic chemistry, analytical chemistry, and instrumental analysis.
- Focused on electroanalytical chemistry applications in forensic science including targeted corrosion enhancement and electrodeposition onto latent fingerprints.
- Experience supervising and mentoring new graduate student teachers.
- Skilled in collaborating with government officials, project management principles, and effective communication.
- Monitored fellowship grant expenditures and ensured continued compliance with grant expectations and outcomes.

### **EDUCATION**

**Ph.D. | Chemistry**

**June 2024**

University of Nevada Las Vegas | Las Vegas, NV

- Dissertation: Evaluation of Electrochemical Corrosion, Electrodeposition and Other Electroanalytical Methods as Investigative Forensic Techniques for Advancing Metal Substrate Analysis

**B.S. | Biochemistry**

**May 2020**

University of Nevada Las Vegas | Las Vegas, NV

**A.A. | Natural Sciences**

**December 2016**

Moorpark College | Moorpark, CA

**A.A. | Behavioral Sciences**

**December 2016**

Moorpark College | Moorpark, CA



## **EXPERIENCE**

### **ORISE Research Fellow**

**September 2021 – October 2023**

Dept. of Homeland Security – United States Secret Service

- Successfully developed a novel latent fingerprint technique, targeted corrosion enhancement of latent fingerprints, to enhance recovery on fired shell casings.
- Investigated electrodeposition and electroless deposition as alternative electroanalytical methods to enhance latent fingerprint visibility on metals and alloyed materials.

### **Graduate Researcher**

**2020 – May 2024**

University of Nevada Las Vegas

- Developed pertechnetate sensor using activated carbon materials to be utilized in groundwater contamination monitoring near nuclear facility sites.
- Investigated electrochemical, spectroscopic, and other analytical methods to evaluate corrosion properties and parameters of electrode materials in molten salt and radioactive molten salt environments for future use in Molten Salt Reactor designs.

### **Graduate Teaching Assistant**

**August 2020 – May 2024**

University of Nevada Las Vegas

- Taught 4 sections of CHEM355L, Quantitative Analysis Laboratory, covering the following topics: statistics and measurements, calibration methods, gravimetric analysis, acid-base titration, complexometric titration, potentiometric titration, redox titration, cyclic voltammetry, and chloride sensors.
- Taught 4 sections of CHEM455L, Instrumental Analysis Laboratory, covering the following topics: absorbance vs fluorescence detection, radiation detection, voltammetry, atomic absorption spectroscopy, ion chromatography, and gas chromatography-mass spectrometry.
- Taught 2 sections of CHEM242L, Organic Chemistry II lab, an undergraduate course covering the following topics: infrared spectroscopy, nuclear magnetic resonance spectroscopy, Williamson ether synthesis, sodium borohydride reduction, Grignard reaction, Fischer esterification, preparation of alpha-beta unsaturated ketones, and condensation polymerization.
- Taught 2 sections of CHEM241L, Organic Chemistry I Laboratory, an undergraduate course covering the following topics: distillation, crystallization, extraction, chromatography, characterization by physical methods, purification, and characterization of products from microscale syntheses.

### **Undergraduate Researcher**

**January 2019 – August 2020**

University of Nevada Las Vegas

- Conducted evaluation of electrode materials, executed a variety of electro-analytical measurements, participated in electrode material development and characterization experiments.
- Responsible for fly care and breeding, data entry and behavioral video analysis.

## **Undergraduate Teaching Assistant**

**August 2018 – May 2019**

University of Nevada Las Vegas

- Worked under Dr Joseph Nika as a UTA for one section of BIOL351 of 60 students, covering the following topics: prokaryotic cell structure, function, genetics, diversity, ecology, and pathogenesis, with an emphasis on microbial metabolism, bacterial genetics, and molecular mechanisms.
- Worked under Nicole Espinoza as a UTA for one section of BIOL196 of 24 students, covering the following topics: structural and chemical nature of cells, complex organisms and cellular environments, transmission and molecular genetics, cell communication, reproduction, and energetics.
- Developed and proctored quizzes and exams

## **PRESENTATIONS AND PUBLICATIONS**

**International Association for Identification, National Harbor, MD**      **August 20<sup>th</sup>, 2023**

“Electrochemical Corrosion, Electrodeposition and Other Electroanalytical Methods as Forensic Investigation Techniques”

- Presented research done for ORISE Fellowship with United States Secret Service on novel latent fingerprint development.

**PNW International Association for Identification, Spokane, WA**      **June 8<sup>th</sup>, 2023**

“Targeted Corrosion Enhancement of Latent Fingerprints”

- Presented research done for ORISE Fellowship with United States Secret Service on novel latent fingerprint development.

**United States Secret Service, Forensic Services Division**      **September 1<sup>st</sup>, 2022**

State of the Lab Meeting

- Led meeting with updates on research conducted during fellowship on developing novel latent fingerprint enhancement techniques.

**International Association for Identification, Omaha, NE**      **August 2<sup>nd</sup>, 2022**

“Targeted Corrosion Enhancement of Latent Fingerprints”

- Presented research done for ORISE Fellowship with United States Secret Service on novel latent fingerprint development.

**Las Vegas Metropolitan Police Department, Las Vegas, NV**      **April 7<sup>th</sup>, 2022**

Seminar

- Participated in seminar on latent fingerprint recovery and presented research ideas on possible novel methods to elucidate what was most promising and worthy of further investigation.

## **TRAINING**

**Ron Smith & Associates**

**May 2023**

- Expert Witness Testimony for Laboratory Analysts (16 hours)

**Ron Smith & Associates**

**March 2023**

- Common Sense Digital Imaging for Latent Print Examiners (16 hours)

## **PROFESSIONAL AFFILIATIONS**

- **International Association for Identification** 2021 – Present
- **Women In Nuclear** 2020 – Present
- **American Chemical Society** 2019 – Present